TGF-β2 abundance in mice and men: A successful anti-TGF-β2 strategy in biliary-derived liver disease

PhD thesis

Presented by

Anne Dropmann

In July 2018

Supervisor

Prof. Dr. Steven Dooley

Dissertation

submitted to the

Combined Faculties for the Natural Sciences and for Mathematics

of the Ruperto-Carola University of Heidelberg, Germany

for the degree of

Doctor of Natural Sciences

Presented by
Anne Dropmann

Born in: Naumburg/Saale, Germany

Oral examination: 17.10.2018

TGF-β2 abundance in mice and men: A successful anti-TGF-β2 strategy in biliary-derived liver disease

Referees

Prof. Dr. Stefan Wölfl
Prof. Dr. Benito Yard

Summary

TGF-β1 is a key player in the onset, the progress, and end stages of CLD promoting fibrogenesis and tumorigenesis. To date, the expression and function of TGF-β2 have not been investigated thoroughly in liver disease. In this thesis, we provide evidence that TgfB2 and not, as formerly known, only TgfB1 correlate with fibrogenesis and liver cancer development.

In a comparative analysis, we analyzed TgfB2 and TgfB1 expression and secretion in murine and human HSCs, hepatocytes, and HCC/hepatoblastoma cell lines. In various mouse models reflecting regeneration, acute and chronic liver disease, and human HCC sample cohorts, we demonstrated that both isoforms are expressed in different types of liver cells and that expression is elevated during the progression of CLD in mouse models in most cases. Although TgfB2 is mostly secreted at lower levels than TgfB1, its expression patterns largely follow similar profiles. However, the secretion of TgfB2 exceeded that of TgfB1 in some HCC cell lines. Our data indicates a more prominent implication of TgfB2 in biliary-derived liver disease models.

In this thesis, the anti-fibrotic and immunoregulatory effects of TgfB2 silencing in cholestatic MDR2-KO mice have been delineated for the first time. TgfB2 silencing by AONs specifically reduced collagen deposition and αSMA expression, but induced anti-fibrotic PparG expression. Accumulation of TGF-β2-specific AON was detected in macrophage-activated fibroblasts, LSEC, and activated HSCs in mice. This was in accordance with TgfB2 expression in these cell types. CD45-positive immune cell infiltration was reduced upon TGF-β2-specific AON treatment in the livers of MDR2-KO mice. Furthermore, TGF-β2 levels were found to be elevated and correlated with CD45-positive immune cell infiltration in PSC and PBC patients.

In summary, the data presented, provides a strong rationale to examine anti-TgfB2-directed treatment in patients with cholestatic liver damage as PSC or PBC.

Taken together, this thesis points towards TGF-β2 as a promising therapeutic target in CLD especially of biliary origin. It provides a direct rationale for TGF-β2-directed drug development an further suggests to initiate a clinical trial testing TGF-β2 inhibition in PSC and PBC patients.

Zusammenfassung

TGF-β1 ist ein Hauptakteur, der an der Entstehung, der Entwicklung und an Endstadien von chronischen Lebererkrankungen beteiligt ist, in dem er den Prozess der Fibrogenese und der Tumorentstehung begünstigt. Bislang ist die Expression und Funktion von TGF-β2 in Lebererkrankungen weitgehend unerforscht. Diese Dissertation zeigt auf, dass auch TGF-β2 und nicht nur TGF-β1, wie bisher angenommen, an der Fibrogenese und Leberkrebsentstehung Anteil hat.

In einer vergleichenden Studie haben wir die Expression und Sekretion von TGF-β2 und TGF-β1 in murinen und humanen Sternzellen, Hepatozyten und HCC/Hepatoblaston-Zelllinien analysiert. In verschiedenen Mausmodellen für Regeneration, akute wie auch chronische Leberschädigung und in humanen HCC-Patienten-Kollektiven haben wir zeigen können, dass beide Isoformen in den verschiedenen Leberzelltypen exprimiert sind und das ihre Expression im Verlauf der chronischen Lebererkrankung in den meisten Mausmodellen zunimmt. Die Sekretion von TGF-β2 war in den meisten Fällen geringer im Vergleich zu TGF-β1, jedoch verhält sich die Expression beider Zytokine sehr ähnlich. In einigen HCC-Zelllinien überstieg die Menge an sekretiertem TGF-β2 sogar die von TGF-β1. Unsere Analysen zeigten, dass TGF-β2 in Mausmodellen mit biliärer Leberschädigung eine prominentere Rolle als TGF-β1 einnahm.

Mit dieser Arbeit wurden erstmalig die antifibrotischen und immunregulatorischen Effekte nach TGF-β2-Inhibition im cholestatischen MDR2-KO-Mausmodell beschrieben. Die Inhibition von TGF-β2 durch AONs verminderte besonders die Kollagenablagerung und die αSMA-Expression. Ebenso wurde der antifibrotische wie auch anti-inflammatorische Marker PparG induziert. Das TGF-β2-spezifische AON konnte in LSEC, durch Makrophagen-aktivierten Fibroblasten und in aktivierten Sternzellen von Mäusen nachgewiesen werden. Auch die Expression von TGF-β2 war in diesen Leberzelltypen entsprechend nachweisbar. Der Pan-Neutrophilmarker CD45 war nach Behandlung mit dem TGF-β2-spezifischen AON in MDR2-KO-Mäusen deutlich reduziert. In Patienten mit Primär sklerosierende Cholangitis (PSC) und Primär biliäre Cholangitis (PBC) waren die TGF-β2-Werte erhöht und korrelierten mit der Expression von CD45-positiven Immunzellen.

Zusammenfassend bieten die Daten dieser Dissertation vielversprechende Gründe, um eine anti- TGF-β2-gerichtete Behandlung in Patienten mit cholestatischer Leberschädigung wie PSC oder PBC zukünftig zu untersuchen. Mit dem Wissen, dass es bislang keine kurative Behandlung für Patienten mit dieser seltenen,

jedoch destruktiven Erkrankung gibt, zeigt sich TGF-β2 als eine aussichtsreiches therapeutische Zielstruktur für die Behandlung biliärer Leberschädigung.

Abbreviations

AFP-alpha-fetoprotein

AMA-Anti-mitochondrial antibody

AON-Antisense Oligonukleotide

ALT-alanine transaminase

AP-Alkaline Phosphatase

AST–aspartate-aminotransferase

BCLC-Barcelona Clinic Liver Cancer staging

BDECs-bile duct epithelial cells

BMP-bone morphogenic protein

CCC-Cholangiocarcinoma

cDNA-complementary DNA

CLD–Chronic Liver Disease

CCl_4-Carbon tetrachloride

CM-Collagen Monolayer

CS-Collagen Sandwich

ddH_2O-Double distilled water

DEN- Diethylnitrosamine

DNA-Deoxyribonucleic acid

ECM-Extracellular Matrix

EMT-epithelial mesenchymal transition

FCS-fetal calf serum

FXR-Farnesoid X receptor

GAPDH-Glyceraldehyde-3-phosphate dehydrogenase

HBV-Hepatitis B virus

HC-Hepatocyte

HSC-Hepatic Stellate Cell

HCC-hepatocellular carcinoma

HE-staining-hematoxylin and eosin stain

IF-Immunfluorescence

IHC-Immunohistochemistry

i.p.- intraperitoneally

KC-Kupfer Cells

KO-knockout

LSEC-Liver Sinusoidal Epithelial Cells

MDR2-$ABCB_4$ gene

MMP-matrix metalloproteinase

NorUDCA-Nor Ursodeoxycholic acid

PFA-Paraformaldehyde

PBC-Primary Biliary Cholangitis

PPARα-Peroxisome proliferator-activated receptor α

PSC-Primary Sclerosing Cholangitis

qPCR-quantitative polymerase chain reaction

RIPA buffer-Radioimmunoprecipitation assay buffer

s.c.-subcutaneous

SDS-PAGE-Sodium dodecyl sulfate-polyacrylamide gel electrophoresis

TGF-β-transforming growth factor beta

TGFβRII- transforming growth factor beta receptor II

TIMP-tissue inhibitors of metalloproteinases

UDCA-Ursodeoxycholic acid

YAP-Yes-associated protein

γGT- Gamma-glutamyltransferase

Table of Contents

1 Introduction

1.1 Transforming Growth Factor-β (TGF-β) in Chronic Liver Diseases (CLD) and Hepatocellular Carcinoma (HCC)

Currently, liver resection followed by a transplantation is the mainstay option for fighting terminal liver failure, yet the prognosis continues to be poor [1]. The demand for new therapies increases due to the lack of donor organs, which leads to a major medical problem. In chronic liver disease (CLD), tissue remodeling and wound healing are interrupted, resulting in complex modulation of the signaling processes at the cellular and molecular level. Subsequent fibrosis leads to the onset of hepatic disease development including cirrhosis, HCC, or hepatic failure. In this multi-step process, TGF-β plays a pivotal regulatory role, contributing to all stages of disease progression [2].

1.1.1 The TGF-β superfamily

The TGF-β superfamily is composed of about 33 structurally related secretory proteins. It includes groups of TGF-β isoforms, activins, nodals, as well as the larger group of bone morphogenetic proteins (BMPs) [3]. Originally, TGF-β was discovered as a transforming factor in cell-conditioned media from sarcoma mouse fibroblasts, which induced the growth of adherent cells [4]. Adhesion, differentiation, cell growth, migration, and embryonal development are regulated by TGF-β family members in a cell-type-specific and context-dependent manner. Their role is bidirectional, e.g., they are involved in both the promotion and inhibition of cancer progression [5]. They are also found in various other human diseases [6].

The three TGF-β isoforms (TGF-β1, TGF-β2, and TGF-β3) exist as homodimers in mammals. They are synthesized as precursors and then secreted as latent homodimeric complexes incorporated into the ECM. By proteolytic cleavage, they are activated and can then act on their target cells [2]. During secretion, the c-terminal TGF-β molecule remains bound to the N-terminus of the precursor, forming the latency-associated peptide (LAP). The LAP forms larger complexes with certain members of the latent TGF-β binding protein family (LTBP) that confer extracellular matrix interaction. Certain proteases, pH changes, competition of particular matrix components, and others induce the release of TGF-β isoforms from the LAP [7, 8]. Furthermore, TGF-β isoform activation requires integrin binding since it is expressed in an inactive or latent form [9].

Generally, TGF-β family members have about 66 to 80% sequence identity. The TGF-β1 and TGF-β2 isoforms are closely related and share about 70% of their amino acid sequence homology [10, 11]. All TGF-β ligands exert their effects on cells by signaling through a heterotetrameric receptor signaling system [12]. The complex of ligand–receptor interactions is able to initiate various downstream signaling pathways. The specificity of ligands at the receptor level is provided by a limited number of type II, type I, and accessory receptors (Figure 1). Various combinations occur at the level of ligand–receptor interactions and at the level of type II–type I receptor interactions [13, 14].The TGF-β receptors type I and II (TGFβRI, TGFβRII) are present in most mammalian cell types, including cancer cells [15]. TGFβR-I and -II are essential for provoking the biological response after the binding of a TGF-β ligand [8]. TGFβRII is activated via phosphorylation and subsequently phosphorylates TGF-β receptor type I. The TGF-β mediated activation of the ligand receptor complex signal through two autonomously working TGFβRI:TGFβRII pairs [16]; TGFβRI, in turn, phosphorylates intracellular mediators such as receptor (R)-Smads [17] and other effectors [18]. These complexes are translocated to the nucleus where they regulate the transcription of target genes [19]. The binding affinity of the TGF-β isoforms to the receptors differs. TGF-β3 and TGF-β1 bind TGFβRII with higher affinity [20-22], whereas Betaglycan and Endoglin (also known as TGFβRsIII) stabilize TGF-βs in a conformation optimal for binding to the signaling receptors. Betaglycan binds all TGF-β isoforms with high affinity [23] and significantly augments the binding efficacy of TGF-β2 to TGFβRII [24]. Its relative Endoglin only binds TGF-β1 and TGF-β3, but not TGF-β2 [25] . Thus, both co-receptors serve as modulators of the TGF-β isoform-receptor interaction and the responsiveness of the cells.

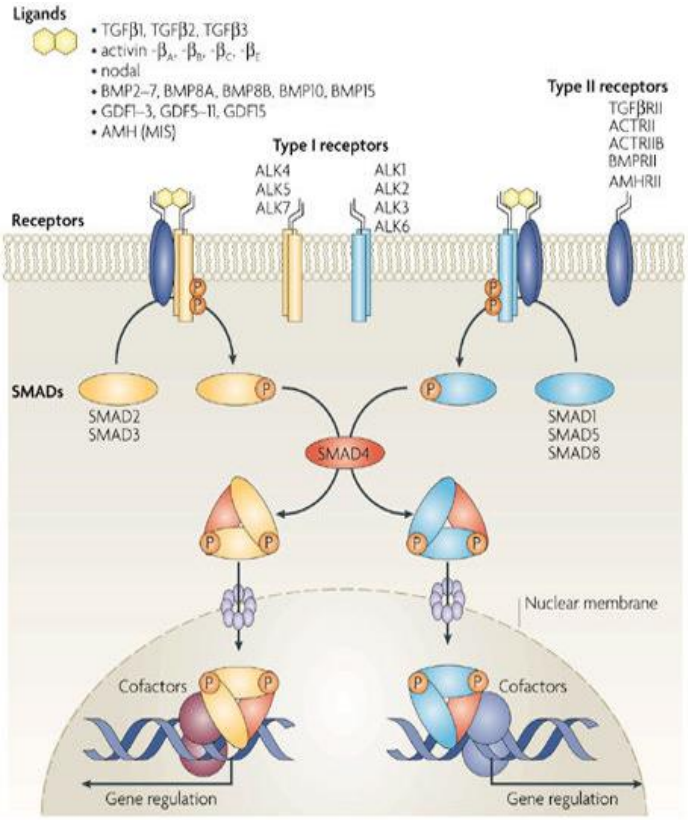

Figure 1 Schematic representation of the TGFβ-Smad signaling pathway [13] in mammalians.

1.1.2 Biological functions of the TGF-β isoforms

All three TGF-β isoforms modulate apoptosis, proliferation, differentiation, migration, and invasion and share partly overlapping but non-redundant functions.

1.1.2.1 The TGF-β1 isoform

Mouse models have been developed to unravel the functions of TGF-β. About 60% of homozygous TGF-$\beta1^{null}$ mice already die in utero due to deficient hematopoiesis and vasculogenesis, which underlines its function in embryogenesis and development. The other 40%, the surviving mice, develop multifocal inflammatory responses and tissue necrosis in the heart, liver, pancreas, and other organs, which leads to organ failure and death within less than one month. In the livers of these mice, altered phenotypes of hepatocytes and increased numbers of mitochondria in response to stress were found [26-29]. TGF-β1 is a multifunctional cytokine and plays a pivotal role in maintaining tissue homeostasis. It is involved in the

development of tissue fibrosis, where it is a strong stimulator of extracellular matrix (ECM) deposition. TGF-β1-mediated synthesis and accumulation of ECM components and the reduction of matrix metalloproteinases (MMPs) degradation [30] are common hallmarks of this isoform. In cancer, TGF-β1 has ambiguous functions: In early stages, it acts as a tumor suppressor, but in later stages it is often described as being a tumor promoter [5, 31, 32], with TGF-β1 being the most widely investigated isoform in many human cancers [33].

1.1.2.2 The TGF-β2 isoform

TGF-β2 also seems to be a mediator of developmental processes. TGF-$\beta2^{null}$ mice exhibit perinatal mortality and developmental defects in cardiac, lung, craniofacial, limb, spinal column, eye, inner ear, and urogenital tissues. Developmental defects of mice lacking TGF-β2 are mainly caused by altered epithelial-mesenchymal interactions, cell growth, extracellular matrix production, and tissue remodeling [34, 35]. Gremlin-mediated TGF-β2 expression was found to modulate the ECM of cells and tissue in glaucoma by increasing the expression of a variety of ECM proteins [36].Wick et al. [37] demonstrated that TGF-β2-mediated MMP-2 and MMP-9 expression induction along with suppressed tissue inhibition of metalloproteinase (TIMP)-2 expression facilitated invasion of cancer cells. In fibrosis-related cell types such as fibroblasts, TGF-β2 and TGF-β3 have shown profibrotic effects in vitro [38]. In view of that, TGF-β2 has been described as being involved in the activation of mesenchymal cells and in matrix production in fibrotic livers [39]. The role of TGF-β2 as an ECM modulator was strengthened by studies of glaucoma and mammary gland cells where its induction was accompanied by cell morphology changes and correlation with a mesenchymal phenotype [40]. Inhibition of microRNA-29, which is a negative regulator of ECM, led to TGF-β2 upregulation, where it contributed to the expression of several ECM components [41].

In cancer, there exists little information about TGF-β2. It was first described as a secreted peptide of human glioma cells suppressing the effects of interleukin 2-dependent T-cell growth [42]. Along with this finding, speculation about the immunosuppressive effects induced by TGF-β2 started. Its overexpression probably leads to a mechanism by which tumor cells can escape from immune surveillance. TGF-β2 is released by tumors of several origins, including glioblastomas, breast cancer, melanoma, and others [43]. In pancreatic cancer and high-grade glioma, TGF-β2 was found to be one key factor driving the immunosuppressive phenotype of patients and its overexpression correlated with poor clinical outcome [44, 45].

TGF-β3 knockout mice have shown defects in morphogenesis of the palate and the lungs, evidenced in mice by abnormal lung development and cleft palate and implicating the involvement of TGF-β3 in epithelial-

mesenchymal interactions [35, 46]. It seems that there are no or only a few phenotypic overlaps with all three-null mice, indicating numerous non-compensated functions [34].

1.1.3 TGF-β1 and TGF-β2 in liver and chronic liver disease (CLD)

TGF-β represents a key cytokine in liver, liver fibrosis, and subsequently in cirrhosis and HCC. Upon liver damage, TGF-β gets activated and mediates a series of cellular events during every progression stage of the disease, starting from hepatic stellate cell activation and ending with hepatocyte death and EMT (Figure 2).

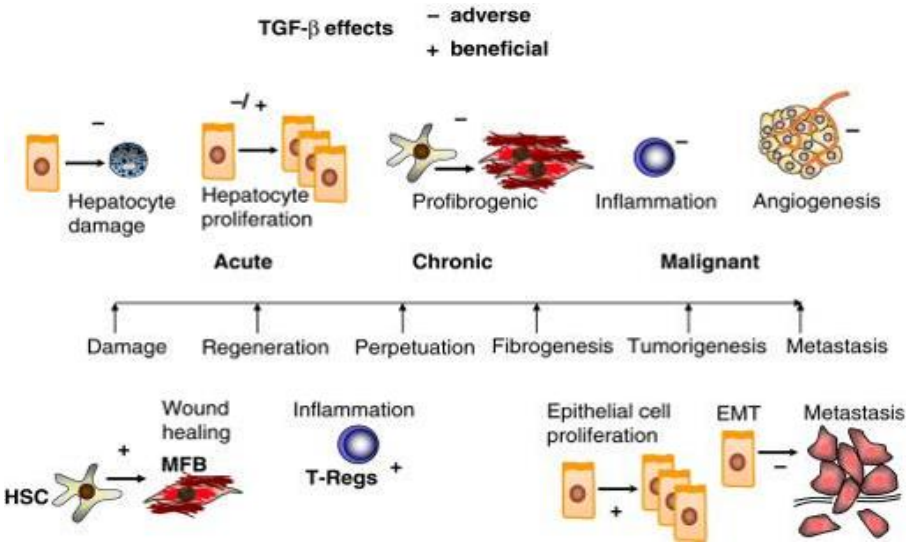

Figure 2 Adverse and beneficial impacts of TGF-β during the progression of chronic liver diseases [47].

All TGF-β isoforms are present in the liver, but their expression is not homogeneously distributed among all cell types. In the normal liver, expression of TGF-β1 and TGF-β2 was found enriched in isolated sinusoidal endothelial and Kupffer cells of rats [48]. Milani et al. [49] describe low expression of TGF-β1 solely in some portal tract stromal cells, and TGF-β2 mRNA was not detectable in normal human and rat livers as examined using in-situ hybridization and immunostaining. In human and rat fibrotic livers, TGF-β1 was detectable in portal tract cells, as well as in inflammatory and surrounding bile duct cells, whereas TGF-β2 showed a remarkably different pattern and was exclusively found in proliferation bile duct cells. In studies by De Bleser et al. [50], TGF-β1 was the most abundant isoform in normal and fibrotic rat livers, strongly expressed in Kupffer cells and moderately expressed by hepatic stellate cells. In the same context, TGF-β2 was highest in Kupffer cells and, to a minor extent, in stellate and endothelial cells, which confirms the results found in the studies of Bissell et al. and Milani et al. Examining two other liver injury models with

respect to TGF-β isoform expression, Bissel et al. [48] could confirm strong TGF-β2 expression in bile duct ligated rat livers, giving it a specific role in biliary-derived liver disease. Interestingly, although hepatocytes do not seem to synthesize TGF-β, significant amounts of latent TGF-β were found to be stored in their cytoplasm [51].

Chronic liver injury is characterized by continuous hepatocyte damage, death, and TGF-β1- driven stellate cell activation followed by myofibroblast transdifferentiation. Alterations of the extracellular matrix and thus the microenvironment are not only a hallmark of liver fibrogenesis but also a key event in liver cancer, as more than 80% of tumors arise from a background of chronic inflammation accompanied by liver fibrosis/cirrhosis [52]. Liver cancer comprises diverse primary hepatic neoplasms including hepatocellular carcinoma (HCC) and intrahepatic bile duct carcinoma (cholangiocarcinoma) (CCC). The expression of TGF-β isoforms is relevantly increased in hepatocellular carcinoma (HCC). All three TGF-β isoforms and their receptors in human HCC were found overexpressed in comparison to controls. Intense immunohistochemical staining of TGF-β isoforms was found in malignant hepatocytes and stromal cells, suggesting autocrine and paracrine pathways [53].

The molecular heterogeneity and thus the pathogenesis of HCC makes it very complex to generate suitable classifications and prognostic estimations for HCC patients. In Coulouarn et al. [54], a TGF-β-specific gene expression signature was defined and two homogeneous HCC groups were associated with so-called early and late TGF-β signatures. Increased invasiveness and recurrence appeared in tumors expressing late TGF-β-responsive genes. The expression signatures in HCC patients showed in most cases a more prominent role of TGF-β1 during disease development. Little is known, however, about TGF-β2 in this setting. The characterization of other intrahepatic malignant tumors such as cholangiocarcinomas (CC) or hepatocholangiocarcinomas (cHCC-CC), TGF-β2 comes to the mind. These tumors display biliary-derived perturbations and features of HCC formation. Gene analysis of hepatocholangiocarcinomas (cHCC-CC) has revealed various pro-fibrotic genes, including TGF-β1 and significantly upregulated TGF-β2. Further genes related to extracellular matrix (ECM) remodeling and biliary connection were found enhanced [55], which again indicates TGF-β-specific involvement in ECM rearrangements and biliary dysfunction. As a top-ranked gene, TGF-β2 has been described in high stromal expression along with poor prognosis in intrahepatic cholangiocarcinomas (ICC) [56]. In addition, a study from 2003 confirmed the overexpression of TGF-β2 and TGF-β3, but not TGF-β1 in cholangiocarcinoma [57].

Nevertheless, in human liver disease little is known about TGF-β2 and its functions in CLD. Research primarily focuses on TGF-β1, which is examined extensively in healthy liver and chronic liver disease. But

the abundance of TGF-β2 and the strong expression mainly cholestasis damaged livers makes it a druggable target, and only minor off-target effects are expected.

1.1.4 Therapeutic targeting of TGF-β signaling in CLD of mice and men

Once the role of at least TGF-β1 became clearer in cancer and fibrosis, great efforts have been undertaken to create sophisticated tools inhibiting the TGF-β pathway in disease. The number of possible compounds for treating chronic liver disease already at the onset of the disease using personalized approaches has increased in recent years [58, 59]. On the basis of observations, where TGF-β1 was found to act as a multifunctional cytokine, several strategies have been developed to block the TGF-β pathway. These include (1) ligand traps and peptides, (2) monoclonal antibodies, (3) antisense oligonucleotides, (4) small-molecule inhibitors, and (5) others [47, 59].

One of the best-studied approaches in regard to preclinical liver fibrosis is TGF-β inhibition using ligand traps and peptides, and in particular a soluble TβRII receptor fragment. This antagonist, which exerts the extracellular part of the TβRII receptor, interferes with ligand binding to the endogenous receptor complex and has been able to inhibit fibrotic markers in mice and rats with chemically induced fibrosis via CCl_4 and dimethylnitrosamine (DEN) or bile duct ligation. Interestingly, Nakamura et al. [60] were able to demonstrate inhibition of hepatic alterations via muscle-applied TβRII receptor compound delivery [60-63]. In liver disease, further experimental studies have been undertaken using galunisertib (LY2157299 monohydrate), a small molecule ALK5 inhibitor, in MDR2-KO mice with cholestatic liver damage. In this study, TGF-β inhibition by galunisertib did reduce CLD progression by modulating ECM components and not directly by reducing the stages of liver fibrosis [64]. Currently, a phase 1/2 dose escalation and safety/ tolerability trial in patients with advanced recurrent hepatocellular carcinoma, solid tumor and non-small cell lung cancer is ongoing (NCT02423343) in which the LY2157299 compound has been already tested for safety, tolerability, and efficacy in glioma [65].

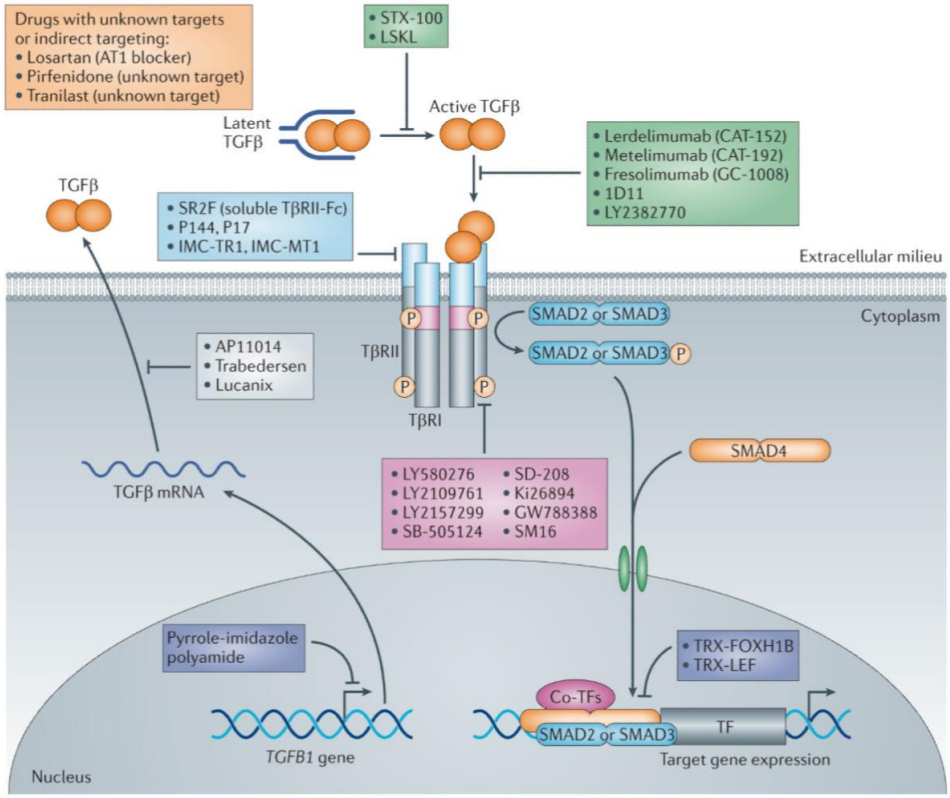

Figure 3 Scheme of therapeutic interventions for the TGF-β signal transduction pathway and targets [59].

In contrast to the promising anti-TGF-β treatment in preclinical disease models, only limited or even adverse results have been shown to date for human disease [47]. Some studies were stopped since patients died, e.g., due to application difficulties or incompatibility [66] (NCT00761280). Others are still ongoing and the results are pending. Multifarious tools for TGF-β ligand inhibition are available, among them several blocking antibodies, such as CAT-192 for TGF-β1 (NCT00043706) or CAT-152 for TGF-β2 [67, 68]. Trapping the TGF-β ligands TGF-β1 or TGF-β2 by using the aforementioned antibodies has been tested in renal fibrosis or systemic sclerosis in vivo, but none of them in liver-related diseases. Intriguingly, antisense oligonucleotides (AONs) have been progressed the furthest in terms of clinical testing and development and have shown successful anti-TGF-β2 inhibition when a specific AON (Figure 4) was used in the treatment of glioma [69] and cancers such as pancreatic carcinoma [70], colon carcinoma, and melanoma [71]. Other interesting anti-TGF-β2 antisense approaches are the generation of tumor vaccines by AON-transfected allogeneic non-small-cell lung cancer (NSCLC) cells, which are then injected into the subject. A study by Bazhenova in 2012 was able to show that TGF-β2-antisense gene-modified NSCLC cells helped patients acquire a significant dose-related survival difference, allowing the trial to progress to a phase III

clinical trial (NCT00676507) [72-74]. Drug delivery issues and application problems could be bypassed by using these TGF-β-inhibited, engineered tumor-specific cell lines.

Specific targeting of TGF-β members known to foster the complicated mechanism of liver fibrosis seems to be an important step forward in regard to treatment perspectives. Future aims may be the increase of drug efficacy and the avoidance of possible side effects due to systemic inhibition. Thus, a major therapeutic goal is the reduction, but not the complete ablation of TGFβ signaling in the body/organ/system, since TGF-βs have adverse as well as beneficial outcomes. The aforementioned issues may be the reason why many of the promising preclinical results from animal disease models could not be translated directly into clinical use.

Despite many unresolved questions, antisense oligonucleotides (AONs) present an eminent therapeutic potential. With the availability to a specific human and murine anti-TGF-β2-directed antisense oligonucleotide we aim to silence and investigate TGF-β2 in a mouse model for cholestatic liver disease.

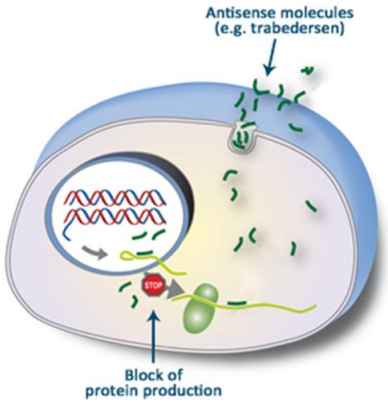

Figure 4 Schematic representation of the antisense oligonucleotides (AONs) mechanism of action in a mammalian cancer cell (Copyright, all rights reserved by Isarna Therapeutics, formerly Antisense Pharma).

1.1.5 TGF-β 2 in primary sclerosing cholangitis (PSC) and primary biliary cirrhosis (PBC)

Primary biliary cholangitis (PBC), formerly known as primary biliary cirrhosis, and primary sclerosing cholangitis (PSC) belong to the category of rare chronic autoimmune liver diseases initiated by inflammation that ultimately destroy the biliary system. The impaired bile formation results in parenchymal damage at the level of the hepatocytes or the cholangiocytes where intracellular accumulation of toxic bile components occurs and harms the hepatocytes. This bile duct damage in turn leads to cholestasis, from which it can further lead to fibrosis, cirrhosis, or even liver failure [75, 76]. The incidence rate of these autoimmune liver diseases is about 1-2 per 100.000 individuals per year [77].

PBC was first called primary biliary cirrhosis, but cirrhosis did not reflect the natural pathogenesis of the disease, which is rather an endpoint [78]. About 15-25% of PBC patients progress to liver failure and require transplantation. PBC occurs in small and intermediate intrahepatic bile ducts, where immunopathological alterations and injury by hydrophobic bile acids cause structural damage, ductopenia, and peri-biliary stromal propagation [75, 79]. Most of the patients are asymptomatic and nowadays diagnosed through serum measurements of cholestasis markers such as elevated alkaline phosphatase (AP) and gamma-glutamyl Transferase (γGT) serum levels, as well as anti-mitochondrial antibodies (AMA), since AMA is present in approx. 90% of all PBC patients and offers a 95% specificity in PBC [80]. Liver biopsy is no longer necessary to confirm the diagnosis of PBC.

Primary sclerosing cholangitis (PSC) appears in intra- and extrahepatic bile ducts. Half of the patients are symptomatic and display symptoms such as pruritus, abdominal pain, and hyperbilirubinemia, and show signs such as hepatomegaly in about 44% of the cases. Along with this, the levels of alkaline phosphatase (AP), gamma-glutamyl Transferase (γGT), and transaminases (AST, ALT) in a patient's serum can be elevated, although bilirubin levels are in the normal range in up to 70% of the patients. Early pathogenesis in PSC exists as a result of a peri-biliary inflammatory reaction and extinctive scars on the bile duct epithelium, which lead to atrophy, inflammation, or dilatation. Onion-like fibrosis is associated with progressive bile duct destruction [79, 81]. Unlike in PBC, further investigations such as cholangiography of the biliary tree or magnetic resonance cholangiopancreatography (MRCP) are essential to confirm the diagnosis and avoid biopsy.

Ursodeoxycholic acid (UDCA) is the first-line treatment so far for both diseases. Normalization of the liver serum parameters such as alkaline phosphatase (AP) and gamma-glutamyl Transferase (γGT) can be achieved and disease symptoms such as pruritus and hyperbilirubinemia can be alleviated. UDCA is a physiological component of the human bile and its therapeutic effect under cholestatic conditions comes from stimulation of the impaired hydrophobic bile acid secretion. Due to the lack of understanding of PSC and PBC pathogenesis, no curative treatment is available yet apart from liver transplantation. Since up to 40% of PBC patients do not respond to UDCA [82] and the use in PSC patients, where it can reach clinical endpoints if applied in high doses, is controversial [83], new therapy approaches are needed. Novel therapies are under evaluation and consider norursodeoxycholic acid (NorUDCA), which lacks a methylene group and facilitates passive transport into the cholangiocytes [84, 85]. Other approaches deal with nuclear receptor targeting such as the Farnesoid X receptor (FXR) or the peroxisome proliferator-activated receptor α (PPARα). Bile acids may serve as ligands for these nuclear hormone receptors, which are important in the expression regulation of hepatic transporters and bile secretion [75].

Studies by Voumvouraki et al. [86] investigated TGF-β serum levels in the blood of primary biliary cirrhosis (PBC) patients. While TGF-β2 was observed to be high in HCV-induced cirrhosis when compared to controls, it was not regulated in early or late PBC, indicating that its point of action is not systemic in the body. Not much information about TGF-β2 is known in PBC or PSC, but it was observed to be regulated in MDR2-deficient (Abcb4) mice. Here, TGF-β2 was strongly upregulated in mice with high disease activity [87]. MDR2-KO mice harbor reliably mimicking features of human cholestatic liver disease with various aspects of chronic portal inflammation, intrahepatic and extrahepatic fibrosis of bile ducts, making it a well-suited model for investigations of PBC and PSC [88-90].

1.1.6 Aims of this thesis

TGF-β deregulation is involved in the pathogenesis of several diseases, including cancer and fibrosis, making it an interesting druggable target. Our investigations focused on the role and druggability of TGF-β2 in CLD and the fact that TGF-β1 strategies have not yet led to any full therapeutic success in CLD. In detail, the following issues are investigated in this thesis:

1. TGF-β2 abundance in fibrogenesis and liver cancer development. To address this aim, the TGF-β1 and TGF-β2 isoforms and, in part, TGF-β receptors were analyzed using quantitative real-time PCR and ELISA in main non-malignant liver cells, e.g., primary hepatic stellate cells and hepatocytes, and in the human-derived HSC cell line LX-2.
2. In mouse models of liver regeneration, fibrosis upon CCl_4 challenge and in the case of biliary damage – here bile duct ligation and MDR2-KO – TGF-β isoform expression was examined at different stages and correlated with typical markers.
3. Eight human hepatocellular carcinoma (HCC)/hepatoblastoma cell lines and one animal model (TGFα/cMyc) were utilized to compare TGF-β1 and TGF-β2 expression in liver cancer.
4. Publically available microarray data using the Oncomine® database was searched in order to analyze TGF-β isoform expression in human HCC and cirrhosis collectives.
5. The effects of TGF-β2 silencing mediated by a TGF-β2-specific antisense-oligonucleotide were investigated in early biliary-derived liver damage using the MDR2-KO model on the molecular, cellular, and tissue level.

6 An analysis of TGF-β2 attenuation was performed in the context of the fibrotic and inflammatory niche.

7 The relevance of TGF-β2 expression in the tissues of patients with PSC and PBC was examined.

2 Materials and Methods

2.1 Materials

2.1.1 Chemicals

All general chemicals were purchased from Carl Roth GmbH, Karlsruhe, Germany, or from Sigma-Aldrich Co., St. Louis, MO, USA, unless otherwise stated, and were of the highest quality.

Acetone	Merck, Darmstadt, Germany
Acrylamide/Bis Solution, 37.5:1 (30% w/v)	Serva, Heidelberg, Germany
Ammonium persulfate (APS)	Sigma Aldrich, St. Louis, MO, USA
Chloroform	Sigma Aldrich, St. Louis, MO, USA
Chloramine-T hydrate (N-Chloro-p-toluenesulfonamide sodium salt hydrate)	Sigma Aldrich, St. Louis, MO, USA
DAPI	Roth, Karlsruhe, Germany
Desoxy nucleoside triphosphates (dNTPs)	Peqlab, Erlangen, Germany
Diethyl pyrocarbonate (DEPC), 99%	Sigma Aldrich, St. Louis, MO, USA
Dimethyl sulfoxide (DMSO)	Sigma Aldrich, St. Louis, MO, USA
Dithiothreitol (DTT)	Roche, Mannheim, Germany
3,3 -diaminobenzidine tetrahydrochloride (DAB)	Sigma Aldrich, St. Louis, MO, USA
DRAQ5	Cell Signaling Technology, Danvers, MA, USA
ECL substrate (electrochemiluminescence)	Amersham, Freiburg, Germany
Enzymes	Fermentas, St. Leon- Rot, Germany
EDTA, disodium salt	Merck, Darmstadt, Germany
Ethidium bromide	Sigma Aldrich, St. Louis, MO, USA
Ethanol, absolute or denatured	Merck, Darmstadt, Germany
Ehrlich Reagenz - 4-(Dimethyl-amino) benzaldehyde	Sigma Aldrich, St. Louis, MO, USA
Fetal Calf Serum (FCS)	Invitrogen, Karlsruhe, Germany
Fetal Bovine Serum (FBS)	Invitrogen, Karlsruhe, Germany
Fluorescent mounting medium	Dako, Hamburg, Germany

GelRed	GeneOne, Ludwigshafen, Germany
Glacial acetic acid	Merck, Darmstadt, Germany
Glycerol	Sigma Aldrich, St. Louis, MO, USA
Glycine	Merck, Darmstadt, Germany
Hank's Balanced Salt Solution (HBSS)	Thermo Fisher Scientific, Waltham, MA, USA
Hydrogen peroxide, solution 30% (w/w) in H_2O	Sigma Aldrich, St. Louis, MO, USA
Hydrochloric acid (HCl)	Merck, Darmstadt, Germany
Isopropanol	Merck, Darmstadt, Germany
Le-Agarose	Biozym Scientific, Hessisch Oldendorf, Germany
Luminol (3-aminophtolhydrazide)	Sigma, Munich, Germany
Mayer`s Haematoxylin	Sigma, Munich, Germany
Methanol	Merck, Darmstadt, Germany
β-Mercaptoethanol	Merck, Darmstadt, Germany
MOPS, buffer grade	AppliChem, Darmstadt, Germany
NaOH	Merck, Darmstadt, Germany
Nonident P40	Roche, Mannheim, Germany
O.C.T. Compound Tissue Tek	Sakura Finetek Staufen, Germany
Paraformaldehyde	Sigma, Munich, Germany
p-coumaric acid	Sigma, Munich, Germany
Penicillin/ Streptomycin	Invitrogen, Karlsruhe, Germany
Perchloric acid 60%	AppliChem, Darmstadt, Germany
Picrid Acid solution 1.3%	Sigma, Munich, Germany
Poly-D-Lysine (P6407)	Sigma, Taufkirchen, Germany
Phosphate buffered saline (PBS)	Invitrogen, Karlsruhe, Germany
Power SYBR Green PCR Mastermix	Thermo Fisher Scientific, Waltham, MA, USA
Protease inhibitor cocktail	Sigma, Munich, Germany
Phosphatase inhibitor cocktail	Roche, Mannheim, Germany
Roti®-Histofix 4 %	Carl Roth, Karlsruhe, Germany

Rat tail collagen I	Roche, Mannheim, Germany
SDS , Sodium dodecylsulfate	Carl Roth, Karlsruhe, Germany
Sirius Red	Sigma-Aldrich, St. Louis, MO, USA
Sodium chloride (NaCl)	Carl Roth, Karlsruhe, Germany
TaqMan Universal PCR Mix, no AmpErase UNG	Thermo Fisher Scientific, Waltham, MA, USA
TEMED (N,N,N′,N′-Tetramethylethylene-diamine)	Sigma-Aldrich, St. Louis, MO, USA
Transfer buffer solution 10x	Invitrogen, Karlsruhe, Germany
trans-4-Hydroxy-L-proline	Sigma-Aldrich, St. Louis, MO, USA
Tris, Tris(hydroximethyl)aminomethane	Carl Roth, Karlsruhe, Germany
Triton X-100	Sigma-Aldrich, St. Louis, MO, USA
TRizol	Invitrogen, Karlsruhe, Germany
Trypsin	Sigma-Aldrich, St. Louis, MO, USA
Trypanblue	Sigma-Aldrich, St. Louis, MO, USA
Tween-20	Carl Roth, Karlsruhe, Germany

2.1.2 Instruments

Agilent 2100 Bioanalyzer	Agilent Technologies, Santa Clara, CA, USA
autoMACS® Pro Separator	Milteny Biotec, Bergisch Gladbach, Germany
autoMACS® Columns	Milteny Biotec, Bergisch Gladbach, Germany
Cell culture incubator, HERA cell	Kendro Laboratory, Hanau, Germany
Chamber slides 8 wells	Becton Dickinson, Franklin Lakes, NJ, USA
Confocal microscope TCS SP8y	Leica, Wetzlar, Germany
Cryostat CM 3050S	Leica, Wetzlar, Germany
Dako Pen	Dako, Hamburg, Germany
Fusion SL Imaging system	Peqlab, Erlangen, Germany
Immobilon-P Transfer Membrane (PVDF)	Merck Millipore, Darmstadt, Germany

Intas Gel ix Imager	Intas, Göttingen, Germany
Inverted light-microscope, Leica DMi8	Leica Biosystems, Wetzlar, Germany
Laminar flow hood, HA 2472 GS	Heraeus Holding, Solingen, Germany
PeqStar Universal 96 well PCR cycler	Peqlab, Erlangen, Germany
PeqStar 48 well PCR cycler	Peqlab, Erlangen, Germany
PRECELLYS®EVOLUTION homogenizer	Peqlab, Erlangen, Germany
Realtime Stratagene MX 3005P	Agilent Technologies, Santa Clara, CA, USA
StepOne Plus Realtime PCR System	Thermo Fisher Scientific, Waltham, MA, USA
StepOne realtime PCR	Agilent Technologies, Santa Clara, CA, USA
Tecan infinite M200 mit Nano-Quant	Tecan, Männedorf, Germayn
Upright light-microscope, LAS X Widefield Systems	Leica Biosystems, Wetzlar, Germany

2.2 Cell Culture

2.2.1 Cell culture reagents and additives

William's E medium	Invitrogen, Karlsruhe, Germany
Dulbecco's Modified Eagle's Medium (DMEM) with 25nM Hepes, 4.5g glucose	Lonza, Basel, Switzerland
Dulbecco's Modified Eagle's Medium (DMEM) without phenol red	Lonza, Basel, Switzerland
RPMI 1640 medium	Lonza, Basel, Switzerland
L-Glutamine	PAA, Cölbe, Germany
Fetal bovine serum (FBS)	Invitrogen, Karlsruhe, Germany
Hank's Buffered Salt Solution (HBSS)	PAA, Cölbe, Germany
10x Trypsin (2.5% in PBS w/o calcium and magnesium	PAA, Cölbe, Germany
Dexamethasone	Sigma-Aldrich, St. Louis, MO, USA
Penicillin/Streptomycin	Lonza, Basel, Switzerland
Human recombinant TGF-β1	Peprotech, Hamburg, Germany
Human recombinant TGF-β2	Peprotech, Hamburg, Germany

2.2.2 Cell lines

Name	Description	Culture medium	Literature
HLE and HLF	HCC cell line derived from 68-year-old patient, poorly differentiated	DMEM supplemented with 10% FBS, 2 mM glutamine, 100 units/ml of penicillin, and 50 µg/ml of streptomycin	[91]
HuH7	Derived from liver tumor of 57-year-old Japanese male in 1982, HBV/HCV negative	DMEM supplemented with 10% FBS, 2 mM glutamine, 100 units/ml of penicillin, and 50 µg/ml of streptomycin	[92]
HuH6	Derived from human liver hepatoblastoma of Japanese infant, epithelial-like, HBV/HCV negative	RPMI 1640 medium supplemented with 10% FBS, 2 mM glutamine, 100 units/ml of penicillin, and 50 µg/ml of streptomycin	[92]
Hep3B	Differentiated human liver carcinoma-derived cell line from 8-year-old black American, tumor formation when injected into nude mice, HBV/HCV positive	DMEM supplemented with 10% FBS, 2 mM glutamine, 100 units/ml of penicillin, and 50 µg/ml of streptomycin	[93, 94]
HepG2	Derived from liver biopsy of 15-year-old male Caucasian, well differentiated HCC, epithelial, HBV/HCV negative	DMEM supplemented with 10% FBS, 2 mM glutamine, 100 units/ml of penicillin, and 50 µg/ml of streptomycin	[94]
FLC-4	Mutant of HCC cell line JHH-4, which was established from 51-year-old Japanese male with HCC of Edmondson's type III, well differentiated, HBV/HCV positive	DMEM supplemented with 10% FBS, 2 mM glutamine, 100 units/ml of penicillin, and 50 µg/ml of streptomycin	[95]

PLC/PRF/5 (Alexander)	Derived from a 24-year-old male patient from Mozambique, HCV positive, cirrhotic	DMEM supplemented with 10% FBS, 2 mM glutamine, 100 units/ml of penicillin, and 50 µg/ml of streptomycin	[93, 96]
LX-2 (Lieming Xu)	Human stellate cells, derived from collagenase/pronase perfusion of normal liver tissue, then spontaneously immortalized in low serum conditions LX-1	DMEM supplemented with 2% FBS, 2 mM glutamine, 100 units/ml of penicillin, and 50 µg/ml of streptomycin	[97]

Table 1 Cell lines

2.2.3 Cell culture and treatment

Human hepatocellular cancer cell lines HepG2, Hep3B, PLC/PRF, HLE, HLF, FLC-4, and HuH7, and the human HSC cell line Lieming Xu (LX)-2 were cultured in Dulbecco's modified Eagle's medium (Lonza, Basel) with 10% fetal bovine serum for HCC cell lines, respectively 2% for LX-2 cells, 1% penicillin (100 IU/ml)/streptomycin (100 µg/ml), and 2 mM glutamine. Human hepatoblastoma cell line HuH6 cells were cultured in RPMI 1640 medium (Lonza, Basel) with 10% fetal bovine serum, 1% P/S, and 1% glutamine. The cells were maintained in a 37°C humidified atmosphere containing 5% CO_2.

24 hours prior to the HCC cell line and the HSC line experiments, the medium was changed to 'starvation medium' with 0.5% FBS, and either 5 ng/ml or 10 ng/ml TGF-β (PeproTech GmbH, Hamburg) were used as indicated in the figures. For long-term storage, the cells were trypsinized and harvested through the addition of medium. Next, the cells were centrifuged, re-suspended in FCS containing 10% DMSO, and transferred as 1 ml aliquots into cryovials. The cells were stored at -80°C or in liquid nitrogen. To thaw the cells, the cryovials were kept for several minutes at 37°C and mixed with fresh medium to remove DMSO. After centrifugation for 3 minutes at 1000 rpm, the cells were re-suspended with new medium and re-plated in a petri dish.

Routinely, all cells were screened for mycoplasma contamination using the PCR Mycoplasma Test Kit I/C from PromoKine following the manufacturer's protocol.

2.2.4 TGF-β2 inhibition using antisense oligonucleotides (AONs)

Human LX-2, HuH7 cells were cultured at medium density to perform AON experiments. AON or scrambled oligonucleotide transfection was performed using RNAiMAX (Invitrogen, Darmstadt) according to the manufacturer's protocol. Briefly, the oligonucleotide and RNAiMAX were diluted in Opti-MEM (Life Technologies) and equal volumes were added to each other in a separate tube and then incubated for 20 min at room temperature. Subsequently, the DNA/RNAiMax solution was added dropwise to the medium, which was replaced after 6 hours of incubation. Knockdown efficiency was verified by quantitative real-time PCR. Two different AON and scrambled control concentrations were applied (1 nmol and 20 nmol). Knockdown was allowed to establish for 48h in medium supplemented with either 2% FBS for LX-2 or 10% FBS for HuH7. The TGF-β2 inhibition oligonucleotides (ASP_0047 and C3_0047) were provided by Isarna Therapeutics.

2.2.5 Primary murine hepatocyte isolation and culture

Primary hepatocytes were isolated from the livers of male C57BL/6 wild-type mice by collagenase perfusion [98]. The animals were handled and housed according to specific pathogen-free (SPF) conditions. Anesthesia was applied by intraperitoneal injection of a Ketamine/ Xylazine hydrochloride mixture. Liver perfusion was followed by liver removal and transfer to a petri dish in a sterile hood. Suspension of single cells was achieved by removal of the liver capsule and gentle shaking. The suspension was placed on a cell strainer (100 µm) and filtered through the mesh by gravity flow. After two further wash steps, the cells were centrifuged and then re-suspended in Williams E medium. Cell viability was determined by counting of Trypan blue-stained and unstained cells. The cells were plated on collagen-I-coated plates and cultured in Williams E medium supplemented with 10% fetal bovine serum, 1% penicillin (100 IU/ml)/streptomycin (100 µg/ml), 2 mM glutamine, and 0.1% Dexamethasone. After 4 hours of attachment, the cells were overlayed with Williams E medium for monolayer cultures or with collagen and medium for sandwich cultures. Collagen sandwich cultures were established as described in [99].

2.2.6 Isolation of primary mouse HSCs

Primary HSCs were isolated from female BALB/c wild-type mice by pronase/collagenase digestion followed by density gradient centrifugation and were cultured on plastic dishes in DMEM, supplemented with 4 mM L-glutamine, 10% FBS, and penicillin (100 IU/ml)/streptomycin (100 µg/ml) as described in [100]. The mice were anesthetized with an intraperitoneal injection of a Ketamine/ Xylazine hydrochloride mixture. The

livers were perfused through the inferior vena cava interior with EGTA solution (Sigma-Aldrich), followed by Pronase E solution (Sigma-Aldrich) and finally Collagenase D (Biochrom, Merk Millipore) solution. The livers were removed, placed into ice-cold DMEM, and the liver capsule was opened to obtain single cells. Cell debris and hepatocytes were removed through several wash and centrifugation steps. To separate stellate cells from the cell suspension, density gradient centrifugation was performed. In the resulting layers, stellate cells were located in the thin white layer below the clear HBSS solution. Then the cells were collected and, following two further wash steps, cell viability was determined by counting with Trypan blue and purity was assessed with UV light.

2.2.7 Simultaneous isolation of four liver cell types based on magnetic bead separation

Primary liver cells were isolated from BALB/c wild-type mice by collagenase perfusion followed by liver tissue separation with the autoMACS® Pro Separator (Milteny) and then cell-type-specific magnetic beads (Microbeads, Milteny). The mice were anesthetized with an intraperitoneal injection of a Ketamine/ Xylazine hydrochloride mixture. Liver perfusion started with insertion into the vena cava interior followed by a flow-through with EGTA solution and then Collagenase D solution. The liver was removed and placed in the autoMACS® Pro Separator (Milteny) for tissue dissociation. Hepatocyte separation was done before using low-speed centrifugation and later purification by Percoll (VWR). The single-cell suspension was then labeled with cell-type-specific MicroBeads for a certain incubation period (~15-30 min). The labeled cell suspension was then transferred to a MACS Column and placed in the MACS Separator, which induced a magnetic field and created a high gradient in the column. While positive-labeled cells were retained in the magnetic field, unlabeled cells passed through the column (negative fraction). This negative fraction was then used for the next cell-type-specific MicroBead labeling. These steps were performed until all cell-type-specific microbeads had been applied to the cell suspension. After the cells had been collected, and following further wash steps, cell viability was determined by counting with Trypan blue and purity was assessed either by immunofluorescence or qPCR. The following beads were used: for Kupfer cells (CD11b, Milteny), for LSEC (CD146, Milteny), and for stellate cells CD271 (Milteny).

2.3 Protein Biochemistry Methods

2.3.1 Cell lysates

Adherent cells were grown to confluency and then washed with PBS on ice. To lyse the cells, a RIPA buffer containing phosphatase and protease inhibitors was added and incubated for 10 to 20 minutes on ice. The

cells were then removed from the dish by scraping using a cell scraper, transferred to a collection tube, and spun down to remove cell debris (10 mins, 10000 rpm, 4 °C).

For tissue homogenization of the mouse livers, small liver pieces were placed in a 500 µl complete RIPA buffer in the provided tubes containing a mix of 1.4 mm & 2.8 mm ceramic beads, and followed by homogenization with the PRECELLYS®EVOLUTION homogenizer at 5000 rpm for 40 s. The samples were then placed on ice and incubated for 30 min, centrifuged at 10.000 rpm for 5 min, and then transferred into a new tube to remove the ceramic beads. With a second centrifugation step, cell debris was removed from the solution and the proteins were ready for further use.

The protein concentration was determined by performing the Lowry method (2.3.2) and then used directly for SDS-PAGE gel electrophoresis or stored at -20 °C.

2.3.2 Lowry method for determination of protein concentration

Protein concentration was determined by using a BCA protein assay (Pierce, Thermo Scientific) based on the Lowry method. For this purpose, 1 µl of protein sample or BSA standard (0-10 mg/ml) were transferred to a microtiter plate and supplemented with a 20 µl mix of solutions A and S (Pierce, Thermo Scientific). Each sample was then mixed with 200 µl of solution B and incubated for 15 min at room temperature on the shaker. Immediately, the absorption of all samples was detected at 690 nm using a microplate reader. Protein concentrations were calculated according to the BSA standard curve.

2.3.3 Protein sample preparation for SDS-PAGE

Equal amounts of protein (10-20 µg) were mixed with 4x loading buffer NuPAGE LDS Sample Buffer (Invitrogen) and 1 µl DTT (1M) and incubated at 95 °C for 5 min. The lysates were then briefly centrifuged and placed on ice, making them ready for SDS-PAGE gel protein separation (2.3.4).

2.3.4 SDS-PAGE gel protein separation

The proteins were separated electrophoretically on the basis of size as described in Laemmli [101]. Precasted NuPAGE 4-12 % Bis-Tris gel (1.5 mm x 15 wells) (Invitrogen) and an MOPS buffer were used as the standard protocol and electrophoresis was performed in an XCell II Mini Cell chamber (Invitrogen) for about 1 hour at a constant voltage of 150 V. Self-made gels were prepared (10-12 %) and ran in the Bio-Rad system for 1.5 hours at a constant voltage of 100 V in a Laemmli buffer.

Running gel: 7% Acrylamid; 0.375 M Tris pH 8.8; 0.1% SDS; 0.1% APS; 0.01% Temed

Stacking gel: 3% Acrylamid; 0.125 M Tris pH 6.8; 0.1% SDS; 0.1% APS; 0.01% Temed

Laemmli buffer: 25 mM Tris pH 8.3; 192 mM Glycin; 0.1% SDS

After the proteins had been separated by SDS-PAGE, they were electrically transferred onto a nitrocellulose membrane (0.45 micron, Pierce) encased by chromatography papers (3MM, Whatman) (sandwich blot) placed in an XCell II Blot module at 300 mA for 2-3 hours on ice. When the membrane transfer procedure was completed, the membrane was incubated with Ponceau Red solution to determine equal protein loading and to reduce unspecific binding of antibodies, then incubated with a blocking buffer at room temperature for 1 hour upon gentle shaking. Afterwards, the membrane was incubated with an appropriate primary antibody (following the manufacturer´s recommendations) at 4 °C overnight. After three washes in TBST buffer, the membrane was incubated with an HRP-conjugated secondary antibody in a 1:1000 dilution for 1 hour at room temperature and re-washed with TBST buffer. Finally, specific proteins were detected by enhanced chemiluminescence using ECL Western blotting detection reagents (SuperSignal West Dura, Pierce) following the manufacturer´s instructions. Chemiluminescence was detected using the Fusion SL Imaging system (Peqlab). The antibodies are listed in Table 2.

Antibodies used for Westernblot (WB) and Immunostaining (IHC) / Immunofluorescence (IF)				
Epitope	Species	Company	Cat No.	Dilution
pSmad3/1	rabbit	Abcam (formerly Epitomics)	1880-1	1:1000 (WB) 1:500 (IF)
pSmad2	rabbit	Cell signaling	3101	1:1000 (WB) 1:250 (IF)
GAPDH	rabbit	Santa Cruz	sc-25778	1:1000 (WB)
Smad2/3	rabbit	Cell Signaling	3102	1:1000 (WB)
Smad1	rabbit	Cell Signaling	9743	1:1000 (WB)
Digoxigenin	goat	Abcam	ab76907	1:300 (IF,IHC)
pp38	rabbit	Cell Signaling	9215	1:1000 (WB)
p38	rabbit	Cell Signaling	9212	1:1000 (WB)
Desmin	rabbit	Abcam	ab15200	1:200 (IF)
Alpha Smooth muscle actin	rabbit	Abcam	ab5694	1:200 (IF) 1:500 (IHC)
CD31	rabbit	Abcam	ab28364	1:200 (IF)
F4/80	rat	eBioscience	14-4801-85	1:200 (IF)
TGF-β2		Abcam	ab36495	1:1000 (IHC)
Goat anti-rabbit IgG-HRP	goat	Santa Cruz	sc-2301	1:10.000
Goat anti-mouse IgG-HRP	goat	Santa Cruz	sc-2005	1:10.000
Alexa 546 goat-anti-rat	rat	Invitrogen	A11081	1:200 (IF)
Alexa 488 goat-anti-mouse	mouse	Invitrogen	A11029	1:200 (IF)
Alexa 488 goat-anti-rabbit	rabbit	Invitrogen	A11008	1:200 (IF)
Alexa 555 goat-anti-rabbit	rabbit	Invitrogen	A21428	1:200 (IF)
Alexa 555 rabbit-anti-goat	goat	Invitrogen	A21431	1:200 (IF)
TO-PRO®-3	nucleic dye	Thermo Fisher Scientific	T3605	1:1000 (IF)

Table 2 Primary and secondary antibodies used for immunoblot, immunohistochemical, and immunofluorescence analysis

2.4 Enzyme-Linked Immunosorbent Assays (ELISA)

For the determination of secreted TGF-β1 and TGF-β2 in cell supernatants or lysates following conventional cell culture, ELISA was performed. For cell lysates, the cell culture medium was removed by centrifugation, Cell Lysis Buffer 1 (R & D Systems, Minneapolis) was added to the cell pellet, and the mixture was allowed to incubate for 60 minutes with gentle agitation. After activating TGF-β through acidification in the collected supernatants or lysates, ELISA was performed according to the manufacturer's instructions for Quantikine human TGF-β1 or murine TGF-β1 (R & D Systems, Minneapolis), respectively for Quantikine human TGF-β2 or murine TGF-β2 (R & D Systems, Minneapolis). Measurement of TGF-β1 and TGF-β2 secretion of murine HSCs was performed using the ELISA-based system Luminex (BioRad, Munich).

2.5 DNA and RNA Methods

2.5.1 RNA isolation and reverse transcription

The total RNA was extracted from cells or tissue according to the manufacturer's instructions using either the InviTrap Spin Universal RNA Mini Kit (Stratec, Birkenfeld) or the TRizol reagent (Invitrogen, Karlsruhe), with subsequent chloroform extraction as described in [102]. The RNA concentration was determined with the help of the Tecan infinite M200 Microplate reader (Tecan, Switzerland). Reverse transcription to cDNA was performed with cDNA synthesis reagents (Thermo Scientific). cDNA was synthesized using 0.5–1 µg of the total RNA. For quantitative real-time PCR or conventional PCR, the samples were diluted with ddH_2O at a ratio of 1:5 to 1:10.

2.5.2 Polymerase Chain Reaction (PCR)

To amplify specific DNA fragments, PCR was performed using the Taq DNA Polymerase and dNTPack system (Roche, Mannheim). In order to separate DNA fragments according to their size, a 1-2% agarose gel with 1xTAE buffer was prepared. GelRed (GeneOn, Ludwigshafen) or Ethidiumbromide was added to visualize the DNA on a UV transilluminator. The primers are listed in Table 4.

TAE buffer: 40 mM Tris Base; 20 mM glacial acidic acid; 1 mM EDTA pH 8.0

2.5.3 Quantitative real-time PCR

Real-time polymerase chain reaction (qPCR) was carried out with Power SYBR Green (Life Technologies) or TaqMan Universal Master Mix II (Life Technologies) using the Stratagene MX 3005 P or StepOne Plus Realtime PCR system. Gene expression was analyzed using 2 µl of each diluted sample and a mix containing 10 µl of SYBRGreen (2x), 1µl of forward and reverse primer (10µM), and 6 µl of ddH2O in a total

volume of 20 µl. For the performance with TaqMan probes, only 1 µl of probe was used. After centrifugation, qPCR was started and the samples were amplified with the following program: 40 cycles from step 2 to 4.

1) 95 °C – 10 min, 2) 95 °C – 15 sec, 3) 60 °C – 1 min, 4) 72 °C – 1 min

Each sample was analyzed either in duplicates or triplicates and evaluated as follows. The threshold of fluorescence above the background of fluorescence was defined as the point at which the fluorescence increases significantly and was measured by the real-time qPCR device. The results were displayed as the CT values at which the fluorescence of a sample crossed the threshold. The relative quantity of target genes was determined according to the ΔΔCt ("delta-delta") method [103]. To compensate for the variation between qPCR runs, the target gene expression was normalized to the expression of the endogenous, unregulated reference gene rS18, HPRT, or PPIA. To ensure that the primers produced specific PCR amplification products, a dissociation curve was analyzed to guarantee specificity. (Only primers with a unique dissociation peak were used).The primers and probes are listed in Table 3 and Table 4, respectively.

$$R = \frac{(2)^{\Delta Ct\ [target]\ (control-sample)}}{(2)^{\Delta Ct\ [ref]\ (control-sample)}}$$

R – relative ratio

ΔCt – deviation of Ct values

[104] – gene whose relative expression ratio between control and sample is measured

Gene Name	Assay ID	Species	qPCR Type
Endoglin	HS00923996_m1	human	Taqman
TGF-βRI	HS00610320_m1	human	Taqman
TGF-βRII	HS00947893_m1	human	Taqman
TGF-βRIII	Hs01114253_m1	human	Taqman
rS18	Hs03003631_g1	human	Taqman
TGF-β2	Mm00436955_m1	mouse	Taqman
TGF-β1	Mm01178820_m1	mouse	Taqman
PPIA	Mm02342430_g1	mouse	Taqman

Table 3 qPCR primer sets based on Taqman assays.

Gene Name	Forward	Reverse	Species
rS18	AAACGGCTACCACATCCAAG	CCTCCAATGGATCCTCGTTA	human
HPRT	CCTGGCGTCGTGATTAGTGA	CGAGCAAGACGTTCAGTCCT	human
TGF-β1	TGGTGGAAACCCACAACGAA	GAGCAACACGGGTTCAGGA	human
TGF-β2	GCAGATCCTGAGCAAGCTG	GTAGGGTCTGTAGAAAGTGG	human
PCNA	CTGAGGGCTTCGACACCTAC	TCACTCCGTCTTTTGCACAG	human
CD45	CCCCGGACTCTTTGGATAAT	AGGGTTGAGTTTTGCATTGG	human
PPARg	GTGGCCGCAGAAATGACC	CCACGGAGCTGATCCCAA	human
Ppia	GAGCTGTTTGCAGACAAAGTC	CCCTGGCACATGAATCCTGG	mouse
TgfB1	AGGGCTACCATGCCAACTTC	CCACGTAGTAGACGATGGC	mouse
TgfB2	GCAGATCCTGAGCAAGCTG	GTAGGGTCTGTAGAAAGTGG	mouse
Col1a1	ACGTGGAAACCCGAGGTATG	TTGGGTCCCTCGACTCCTAC	mouse
Col3a1	ACGTAAGCACTGGTGGACAG	GGAGGGCCATAGCTGAACTG	mouse
smaA	TTCGCTGTCTACCTTCCAGC	GAGGCGCTGATCCACAAAAC	mouse
PparG	TCCAGCATTTCTGCTCCACA	ACAGACTCGGCACTCAATGG	mouse
TnfA	CCCTCACACTCACAAACCAC	ATAGCAAATCGGCTGACGGT	mouse
Timp1	CGAGACCACCTTATACCAGCG	ATGACTGGGGTGTAGGCGTA	mouse
Il-6	TAGTCCTTCCTACCCCAATTTCC	TTGGTCCTTAGCCACTCCTTC	mouse
Il-1B	CCCAACTGGTACATCAGCACCTC	GACACGGATTCCATGGTGAAGTC	mouse
Ctgf	AGATTGGAGTGTGCACTGCCAAAG	TCCAGGCAAGTGCATTGGTATTTG	mouse
Muc	CCAAGCGTAGCCCCTATGAG	GTGGGGTGACTTGCTCCTAC	mouse
Tff2	CTTGGTGTTTCCACCCACTT	CACCAGGGCACTTCAAAGA	mouse
Cd45	TGTACCACCAGGGACTGACAAG	TCTGGCTCACAGTGGAGTACATATG	mouse

Table 4 qPCR primer sets based on the SybrGreen approach.

2.6 Immunohistochemistry (IHC) and Immunofluorescence (IF)

2.6.1 Immunofluorescence

2.6.1.1 Cryosections of liver tissue

After liver resection, a fresh part of the right liver lobe was placed in a cryomold, embedded in Tissue-Tek® O.C.T. (Sakura, Germany), and gently frozen on dry ice. The frozen blocks were cut into 5 µm sections with the Cryostat CM 3050S (Leica) and were dried overnight at room temperature. The sections were stored for direct use at -20 °C or for future use at -80 °C.

2.6.1.2 Immunofluorescence staining

The slides were fixed either with cold 4% paraformaldehyde or ice-cold acetone at room temperature for 10 minutes. The tissue was rinsed in PBS pH 7.0 and surrounded with a hydrophobic barrier using a barrier pen (DAKO). The specimens were blocked and permeabilized for 60 minutes with a blocking buffer containing 0.3% Triton X-100. Afterwards, a primary antibody solution was applied to each slide according to the manufacturer's recommendations and incubated at 4 °C overnight in the dark. The next day, the sections were washed three times with PBS pH 8.0 and an appropriate secondary antibody was applied and incubated for 1-2 hours at room temperature. For nuclear counterstaining, TO-PRO®-3 (dilution 1:1.000 in PBS) was added to the slides for 15 minutes. The sections were then washed three times in PBS, mounted with aqueous Fluorescent Mounting Medium (S3023, Dako), and examined with a confocal microscope (TCS SP8y, Leica). As negative controls, sections were incubated with secondary antibodies only.

2.6.2 Immunohistochemistry (IHC)

2.6.2.1 Paraffin sections

The tissues were fixed with Roti®-Histofix 4 % (Roth) or other fixatives for 24-48 hours at room temperature. The fixed tissues were placed in embedding cassettes and processed for paraffin embedding as follows:

70% ethanol, two changes, 1 hour each

80% ethanol, one change, 1 hour

95% ethanol, one change, 1 hour

100% ethanol, three changes, 1.5 hour each

Xylene, three changes, 1.5 hour each and then

paraffin wax (58-60 °C), two changes, 2 hours each.

Paraffin blocks were then used to generate 4-6 µm tissue sections. These sections were dried either overnight at 37 °C or for 1 hour at 60 °C.

2.6.2.2 Immunohistochemical staining

Immunohistochemical staining was performed using sections of 4-6 µm thickness and were de-paraffinized in xylene, and rehydrated in decreasing concentrations of alcohol. Antigen retrieval was achieved in either EDTA buffer (1mM, pH 8.0) or Tris-NaCitrate-Dihydrate buffer (0.01M, pH 6) by microwave treatment. To block endogenous peroxidase activity, the slides were treated with 10% H_2O_2 for 15 min at room

temperature followed by incubation with the primary antibody (see Table 2) at 4 °C overnight. After rinsing with PBS, the sections were incubated with horseradish peroxidase conjugated secondary antibody for 30-45 min and visualized with 3,3-diaminobenzidine tetrahydrochloride (DAB) (D5905, Sigma) staining. The samples were then counterstained with hematoxylin and examined under a light microscope.

2.6.2.3 Picro Sirius Red staining and quantification

For the detection of collagen, the paraffin sections were de-waxed and hydrated and the nuclei were stained with hematoxylin for 8 min. The slides were washed under running tap water for 10 min and then stained with Picro Sirius Red solution (Sigma) for 1 hour at room temperature. In two changes, the samples were washed with acidified water (0.5% acetic acid), dehydrated with ethanol, and cleared in xylene [105, 106]. The quantification of Picro Sirius Red staining was achieved from nine non-overlapping 10x magnified fields of each liver sample and displayed in percentages of the total liver area using the software ImageJ 1.49v. Regions of large centrilobular veins and large portal tracts were excluded from the calculation.

2.7 Hydroxyproline Assay

Liver collagen content was quantified colorimetrically as total hydroxyproline as described in [107, 108]. One snap frozen liver specimen from the caudate lobe, weighing between 50 and 100 mg, was incubated in 2 ml of 6N HCl (Sigma) for 30 min at 110 °C, then briefly homogenized , followed by a 16 h hydrolysis at 110 °C. The solution was then filtered to remove solids and the supernatant was collected. Triplicates of 15 microliters of the supernatant were placed into Eppendorf tubes and mixed with 15 µl of methanol, then dried at 75-80 °C; the resulting crystals were dissolved in 0.5 ml 50% isopropanol. In the next step, 100 µl of Chloramine-T solution was added and incubated for 10 min. Then 0.5 ml of freshly prepared Ehrlich´s reagent was added to the reaction mixture and incubated at 50 °C for 90 min. Absorbance was measured at 558 nm in a Tecan infinite M200 Microplate reader (Tecan, Switzerland). Total hydroxyproline (µg/liver weight) was calculated on the basis of the individual liver weights, the corresponding relative hydroxyproline content, and the liver lysate dilution factors.

2.8 Animal Models for Liver Fibrosis and Carcinogenesis

2.8.1 Mice and animal husbandry

Wild-type mice were obtained from Charles River or Jackson Laboratory and MDR2-KO (Mdr2−/−) mice were kindly provided by F. Lammert, Saarland University Medical Center. The animals were housed under

specific-pathogen–free conditions in the animal facility of the Medical Faculty Mannheim, Heidelberg University. They received human care and all animal protocols were in full compliance with the guidelines for animal care and approved by the government's Animal Care Committee. For all experiments, the mice were between 10 and 20 weeks old. Genotyping of all transgenic mice was performed by conventional PCR.

2.8.2 Plasma liver function parameter analysis

Whole blood was obtained via retrobulbar blood draw from the mice. The blood samples were collected in Lithium-Heparin microvettes, incubated for 5 min at room temperature on a roll shaker, and then centrifuged at 2.000×g for 5 min at 4 °C. Supernatant (plasma) was transferred to a new Eppendorf tube and either stored at −80 °C or used directly for analysis. The plasma concentrations of alanine aminotransferase (ALT), aspartate aminotransferase (AST), alkaline phosphatase (AP), glucose, cholesterol, triglycerides, proteins, bilirubin, and glutamate dehydrogenase (GLDH) activities were measured with the Cobas® 8000 analyzer (Roche, Mannheim).

2.8.3 Biodistribution of a labeled antisense oligonucleotide (AON) in vivo

Sixteen-week-old Balb/c wild-type mice were injected either intraperitoneally (i.p.) or subcutaneously (s.c.) with a single dose of 10 mg/kg of body weight FAM-labeled AON (ASP_0047). The hepatotropic efficiency of the application method and the AON content in the liver were decisive for the choice of the application method. 24 h and 5 days after AON administration, the mice were sacrificed; blood was taken, and liver, spleen, kidney, and lungs were resected. The FAM-labeled AON (ASP_0047) content was then determined in cryosections using a confocal microscope (2.6.1.1).

After the precondition definition of the AON application, the AON biodistribution was determined in two mouse models of chronic liver diseases. In a model for biliary fibrosis, MDR2-KO mice were subcutaneously (s.c.) injected with a single dose of 10 mg/kg of body weight Digoxigenin-labeled AON (ASP_0047). All mice were sacrificed 72 h after AON administration and liver samples were immediately snap-frozen in liquid nitrogen according to standard operating procedures. Specimen sampling was performed for RNA, protein, plasma, and immunohistochemical analyses. Female and male mice were included in order to observe any gender-specific differences.

2.8.4 Acute and chronic CCl_4-induced liver damage

In eight-week-old C57BL/6 mice (4 animals per group), acute liver damage was induced by a single intraperitoneal injection of 1 ml/kg per body weight CCl_4 (mixed 1:8 with mineral oil). At 0 h, 3 h, 6 h, day

1, day 2, day 3, or day 6 post injection, the mice were sacrificed and liver and blood specimens were obtained according to standard operating procedures.

Chronic liver damage mRNA samples were kindly provided by S. Weber (Homburg). C57BL/6 or Balb/c mice received intraperitoneal injections of CCl_4 (0.7 ml/kg per body weight in mineral oil) twice a week for six weeks. Liver samples were taken from untreated mice, 24 h after a single CCl_4 injection, after three CCl_4 injections, and after 6 weeks of two CCl_4 injections per week ($n_{ut} = 12$; $n_{24h} = 12$; $n_{3x} = 13$; $n_{6wk} = 12$ animals per group). Untreated animals or animals treated with mineral oil served as controls for the gene expression analysis.

2.8.5 MDR2-KO – a model for cholestatic fibrosis

RNA samples of age-matched male MDR2-KO (Mdr2−/−) and control C57BL/6 wild-type mice were kindly provided by P. Angel and J. Hess (Heidelberg). The mice were sacrificed at the age of 3, 6, 9, and 15 months and liver and blood samples were obtained according to standard operating procedures. RNA samples were used for gene expression analysis (Fluidigm).

2.8.6 Systemic AON treatment in MDR2-KO mice

14-week-old sex-matched Mdr2-/- mice (MDR2-KO) and control Balb/c wild-type animals received in the first week either 15ml/kg of body weight C3_0047 (control oligo) or ASP_0047 (AON) every day for five consecutive days (oligo push). The following treatment was then applied once per week for another three weeks. Six groups of animals were included as follows:

Balb/c untreated group (n=6, untreated for 4 weeks);

Balb/c control group (n=10, received 15ml/kg of body weight of C3_0047 (control oligo));

Balb/c AON group (n=10, received 15ml/kg of body weight of ASP_0047 (AON));

MDR2-KO control group (n=10, untreated for 4 weeks);

MDR2-KO control oligo group (n=10, received 15ml/kg of body weight of C3_0047 (control oligo)); and

MDR2-KO AON group (n=9, received 15ml/kg of body weight of ASP_0047 (AON)).

The mice were sacrificed 72 h after the last treatment and specimens were sampled according to standard operating procedures for further analysis. The study design is displayed in Figure 5.

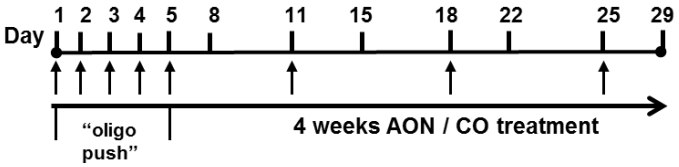

Figure 5 AON application scheme in MDR2-KO mice

2.8.7 Bile duct– ligation (BDL) induced cholestatic liver damage

RNA samples from bile-duct-ligated mice over the course of 14 days were kindly provided by K. Abshagen (Rostock). The surgical procedure was carried out as previously described by Abshagen et al. [109, 110]. Male Balb/c mice (n = 3–5) were anesthetized with isoflurane (1.5 vol%) and midline laparotomy was performed. Then the common bile duct was ligated three times using non-resorbable sutures (polyester 5–0; Catgut, Markneukirchen), and cut between the two gut-near ligatures. The sham-operated mice underwent a laparotomy with exposure but no ligation of the bile duct (0h). The animals were allowed to recover from anesthesia and surgery under a red warming lamp and received drinking water containing Metamizole as an analgesic. The mice were held in single cages and were sacrificed after 0, 6, 12, 18, or 30 hours, respectively after 2, 5, or 14 days. Blood and liver samples were preserved (n =3–5). Sham-operated animals without BDL served as controls (n = 5). RNA samples were used for gene expression analysis performed with quantitative real-time PCR (qPCR).

2.8.8 TGFα/cMyc transgenic mouse model for hepatocarcinogenesis

Liver tissue of double transgenic TGFα/cMyc mice was kindly provided by A. Piiper (Frankfurt). The mice were generated by crossing c-Myc mice with TGF-α mice as described in [111]. Hepatocarcinogenesis in male TGFα/cMyc mice was induced by the addition of $ZnCl_2$ to the drinking water. The development of liver tumors was monitored by Gd-EOBDTPA-enhanced magnetic resonance imaging [112]. Liver tumors and normal liver tissue were then resected and snap-frozen at –80 °C for further analysis. For quantitative real-time PCR, RNA was extracted as described in 2.5.1.

2.9 Human Patient Collectives

Publicly available databases such as Oncomine® Research Edition and Arrayexpress, and data from collaborative collaborative projects (GSE7980, Mannheim, Frankfurt and Regensburg), were used to analyze TGF-β isofom isofom expression in human patient samples. The data was analyzed with the GraphPad Prism 6 tool. The expression values were referred to normal liver samples and/or to surrounding non-cancerous tissue of the same same patient. In total, seven HCC collectives and seven cirrhosis/precancerous stage collectives were analyzed analyzed using Oncomine® Research Edition. Different criteria were applied for the analysis of TGF-β isoform isoform expression in HCC vs normal, in cirrhosis/precancerous stages vs normal, and in HCC vs cirrhosis/ precancerous stages when the p-value was ≤ 0.05. For the data retrieved from Arrayexpress (GSE7980), the the following criteria were used: (1) significance below 0.05 (p-value < 0.05), (2) number of cohorts with significant significant differences in TGF-β1 and TGF-β2 expression (≥ 3), and (3) tendency of TGF-β1 and TGF-β2 expression expression within different cohorts (up- or down-regulated). In two cohorts (GSE7980 and Regensburg), the the clinicopathological parameters were correlated with TGF-β2 expression (

Table 7). An overview of all patient cohorts used in this study is listed in Table 5 and Table 6.

2.10 Statistical Analysis

Error bars represent standard d to the mean and were used unless described otherwise; two-tailed Student-t tests or one-way ANOVA were used to calculate the p-values. Additionally, Pearson correlation was performed. Differences were considered to be significant if the calculated p-value was *p ≤ 0.05, **p≤ 0.01, ***p≤ 0.001; the p-values were not significant if not indicated. GraphPad Prism (GraphPad Software, Version 6) was used unless described otherwise.

3 Results

3.1 TGF-β2 Incidence in Mice and Men

3.1.1 TGF-β2 expression in murine primary hepatocytes and hepatic stellate cells

Hepatocytes represent the major cell type of the liver and account for 80% percent of the liver mass. They are involved in metabolic, endocrine, and secretory processes and therefore widely used for hepatic toxicology and drug metabolism studies. Isolated hepatocytes are known to lose their specific functions and dedifferentiate when cultured on a normal plastic or collagen monolayer [113]. Hepatocytes cultured in a collagen sandwich maintain stable differentiated functions and hepatic polarity. As part of this work, freshly isolated hepatocytes were cultured either on collagen sandwich (CS) or on collagen monolayer (CM) and *TgfB1* and *TgfB2* mRNA expression was determined (Figure 6A). In both settings, the expression of *TgfB1* and *TgfB2* increased with culture duration after 24 and 48 hours and induction was higher in CS for both cytokines. Secretion of TGF-β2 was lower, but induction of TGF-β2 secretion after 48 h on CM was stronger compared to TGF-β1 (Figure 6B). Stimulation of CM-cultured hepatocytes with TGF-β1 led to increased TGF-β1 secretion up to 4700 pg/ml after 2 h, plateauing at constant levels of approximately 2000 pg/ml after 10 h. In contrast, TGF-β2 secretion constantly increased over time but to a lesser extent (Figure 6C).

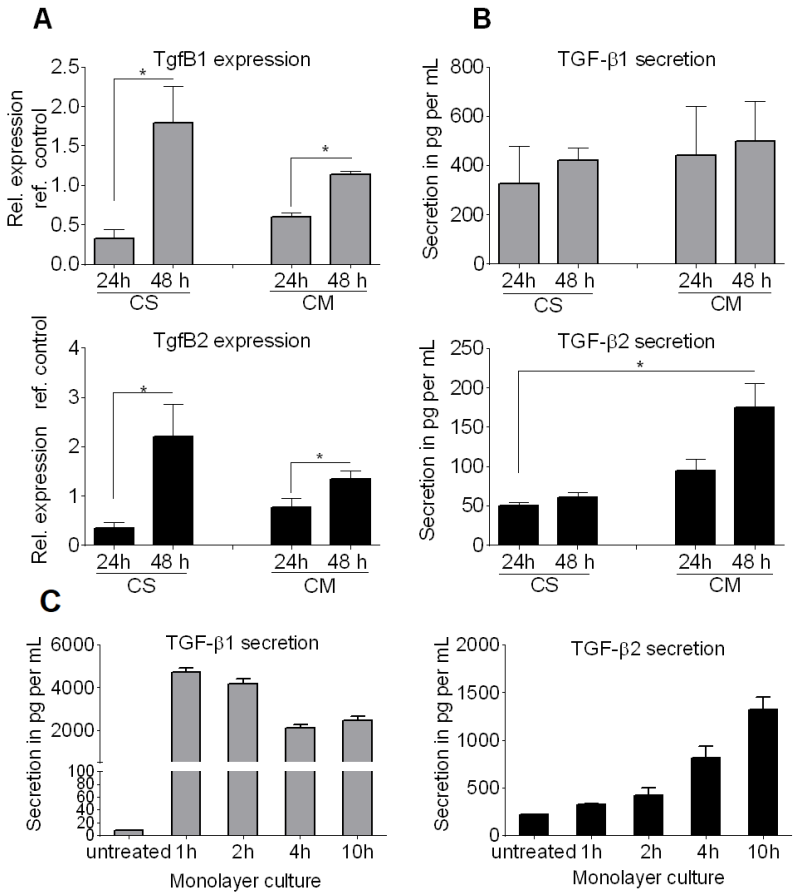

Figure 6 Expression and secretion of TGF-β1 and TGF-β2 by primary mouse hepatocytes after 24 and 48 hours of culture on collagen monolayer (CM) or collagen sandwich (CS). (A) Relative expression of TgfB1 (upper panel) and TgfB2 (lower panel) was analyzed using Sybrgreen-based qPCR. (B) Secretion of TGF-β1 and -β2 by hepatocytes was measured using Quantikine ELISA. (C) Hepatocytes were stimulated with 1 ng/mL TGF-β1 cytokine and secretion was measured at the indicated time points using Luminex assay. The data represents the summary of 3-4 independent experiments and the error bars represent the standard error. Adapted and modified according to [114].

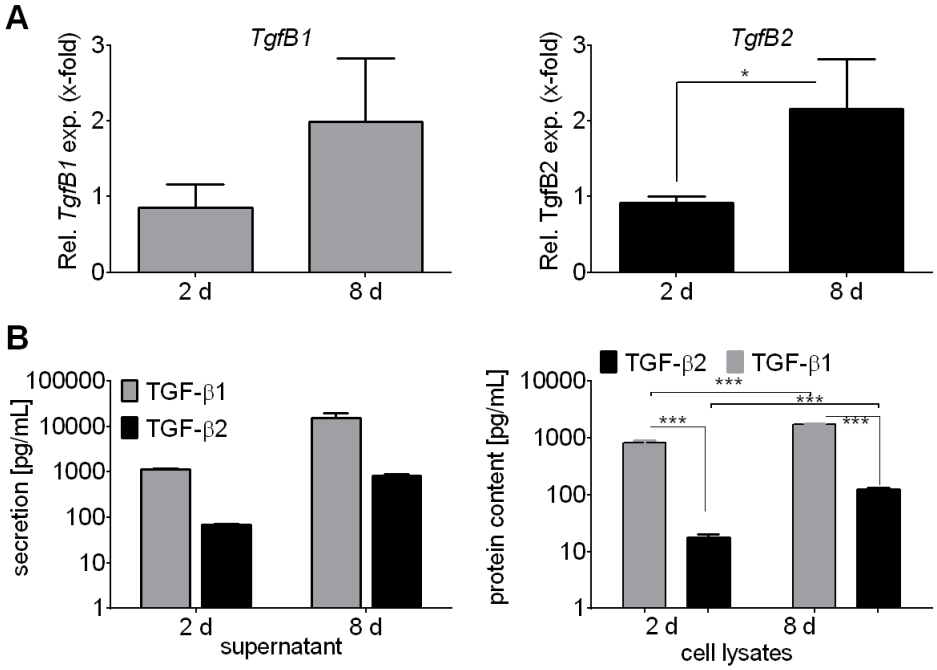

Figure 7 TGF-β isoform expression and secretion by quiescent (2 days) and culture-activated (8 days) primary mouse hepatic stellate cells (HSCs). After 2 and 8 days, (A) relative TgfB1 and TgfB2 expression was determined by qPCR and referred to HSCs cultured for 2 days, and (B) secretion of TGF-β1 and TGF-β2 was measured without stimulation using a Luminex ELISA (left panel). The protein content of the HSC lysates was quantified using Quantikine ELISA. The data is presented as the mean of 3 independent experiments and the error bars represent the standard deviation. Adapted and modified according to [114].

Hepatic stellate cells are described as the main fibrogenic cell type and as extracelluar matrix producers in the liver. HSCs are located in the Space of Disse between sinusoids and hepatocytes. Upon liver damage, HSCs express and secrete TGF-β1, which in turn activates paracrine signaling and affects all other cell types. In this study, *TgfB2* mRNA expression and TGF-β2 secretion were compared in quiescent (2 days) and activated (8 days) primary mouse HSCs. Expression of both cytokines increased within 8 days during cell culture activation (Figure 7A). Mainly TGF-β1 (~16,000 pg/mL) was secreted after 8 days, while only about 850 pg/ml of TGF-β2 were detected at that time point. Furthermore, the secretion of both TGF-β isoforms was demonstrated to be increased ~10-fold after 8 days when compared to the 2-day time point (Figure 7B) (left panel). The ELISAs of total cell lysates revealed different TGF-β protein amounts in the cells than the measured secreted amounts. Intracellular TGF-β2 (day 2: ~200-fold, day 8: ~10-fold) levels increased about 10-fold between 2 and 8 days, while TGF-β1 content remained stable but markedly higher (Figure 7B (right)). This fact suggests the assumption that there is a cytokine-specific maximum protein

level in the cells, which is reached for TGF-β1 already on day 2. All produced cytokines passed the limit and were then secreted continuously. Thus, 8- to 10-fold levels of both cytokines were found in the supernatant compared to the cell lysates on day 8.

It is well known that TGF-β1 signaling plays a pivotal role in HSCs and in their transdifferentiation to myofibroblasts [47]. TGF-β1 treatment of quiescent HSC leads to Smad phosphorylation. Related to this, and to examine whether TGF- β2 has the same effect, freshly isolated primary HSCs were treated separately with both cytokines over the course of 24 h. TGF-β2 could induce Smad phosphorylation (up to 6 h), although it was not persistent up to 24 h (Figure 8).

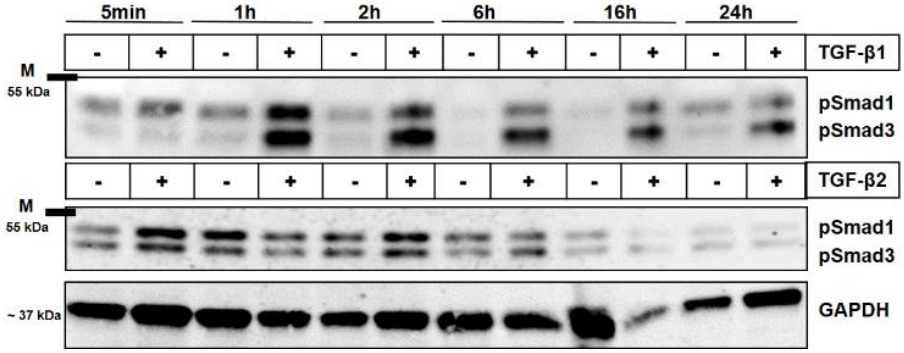

Figure 8 Immunoblot of murine primary HSCs for phospho-Smad 1/3. Immunoblot analysis of Smad1, 2, and 3 phosphorylation upon stimulation with 10 ng/ml TGF-β1 or TGF-β2 recombinant protein. Stimulation time and cytokines were used as indicated in the figure.

3.1.2 TGF-β2 in human liver cell lines

3.1.2.1 Human LX-2

To translate our findings to the human system, we examined the human HSC cell line LX-2, which retains key features of human primary HSCs. First, the expression of TGF-β1 and -β2 was examined, revealing no change from day 2 to day 4 (Figure 9A). Secretion of TGF-β1 was found to be about 1.5 times higher than that of TGF-β2 after 4 days (Figure 9B). Next, the impact of secreted TGF-β isoforms on TGF-β receptor expression in HSC was investigated by stimulating HSCs with either 10 ng/ml TGF-β1 or TGF-β2 recombinant protein. Since it is known that TGF-β1 can influence the expression of its signaling receptors, the TGF-β receptor expression in LX-2 cells was then analyzed [115]. Stimulation with 10 ng/ml TGF-β1 for 1 and 24 hours either decreased or did not alter TGF-β receptor expression, while stimulation with TGF-β2 decreased receptor expression after 1 h, but notably induced TGF-β receptor expression after 24 h ($p_{endoglin} \leq 0.027$) (Figure 9C). These mRNA results suggested a different impact of TGF-β2 on HSC signaling and thus Smad phosphorylation was investigated. After 1 or 24 hours of TGF-β1 and -β2

treatment, phosphorylation of Smad1, 2, and 3 was found to be similar, whereas 24h TGF-β2 pretreatment of LX-2 cells led to sensitization of the cells towards subsequent cytokine stimulation. Here, phosphorylation of Smad1 was seen to be induced, which could be in line with the receptor upregulation seen on the mRNA level (Figure 10).

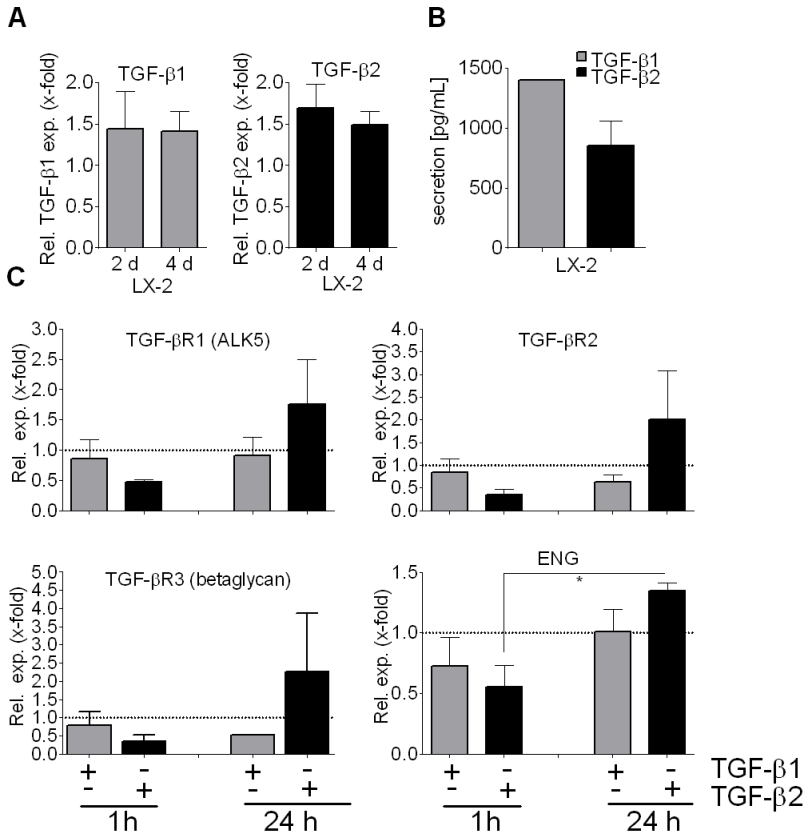

Figure 9 mRNA expression and secretion of TGF-β1, TGF-β2, and TGF-β-receptors in LX-2 cells. (A) Gene expression of TGF-β1 and -β2 after 2 and 4 days and (B) secretion after 4 days of cell culture. (C) Stimulation of TGF-β1 or TGF-β2 with 10 ng/ml recombinant protein and subsequent qPCR analysis of TGF-β receptor expression. The levels of TGF-β receptors in unstimulated cells at the time points indicated served as references. Adapted and modified according to [114].

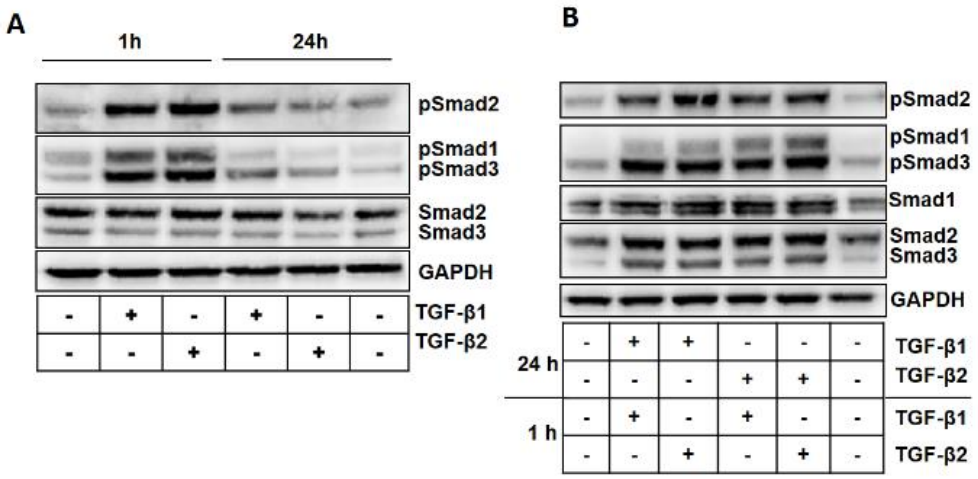

Figure 10 Immunoblot analysis of Smad1, 2, and 3 expression and phosphorylation upon stimulation with either 10 ng/ml TGF-β1 or TGF-β2 cytokine. (A) Stimulation time and cytokines were used as indicated in the figure. (B) LX-2 cells pretreated for 24 h with TGF-β2 are sensitized towards subsequent cytokine-induced Smad1 signaling. The first treatment lasted for 24 hours as indicated and was followed by a 1-h treatment. Adapted and modified according to [114].

3.1.2.2 Human HCC cell lines

TgfB2 and TgfB1 mRNA expression levels in seven different hepatocellular carcinoma cell lines and one hepatoblastoma cell line (HuH6) were investigated to get an insight into TGF-β2 involvement in late-stage CLD. While very low amounts of TgfB2 were expressed in HuH6, PLC, and HepG2 cells, TgfB2 expression was higher in FLC-4, Hep3B, HLF, HLE, and HuH7 cells with decreasing extent in the respective order (Figure 11A). After 4 days of culture, secretion of TGF-β2 was low in PLC, HLE, HepG2, and HuH6 cells, but high and in a similar range as TGF-β1 in Hep3B, HuH7, HLF, and FLC-4 cells (Figure 11B). Interestingly, in Hep3B and HuH7 cells, TGF-β2 secretion even exceeded TGF-β1 secretion significantly ($p_{Hep3B} \leq 6E{-}05$; $p_{HuH7} \leq 0.0024$). TgfB1 and TgfB2 expression correlated well in HCC cell lines ($R_{TGF\text{-}\beta1\text{-}/TGF\text{-}\beta2} = 0{,}811$, $p = 0{,}015$) (Figure 11C), and mRNA expression of TgfB1 and TgfB2 correlated with secretion of the respective TGF-β isoform. Interestingly, TGF-β1 and TGF-β2 secretion did not coincide (Figure 11D).

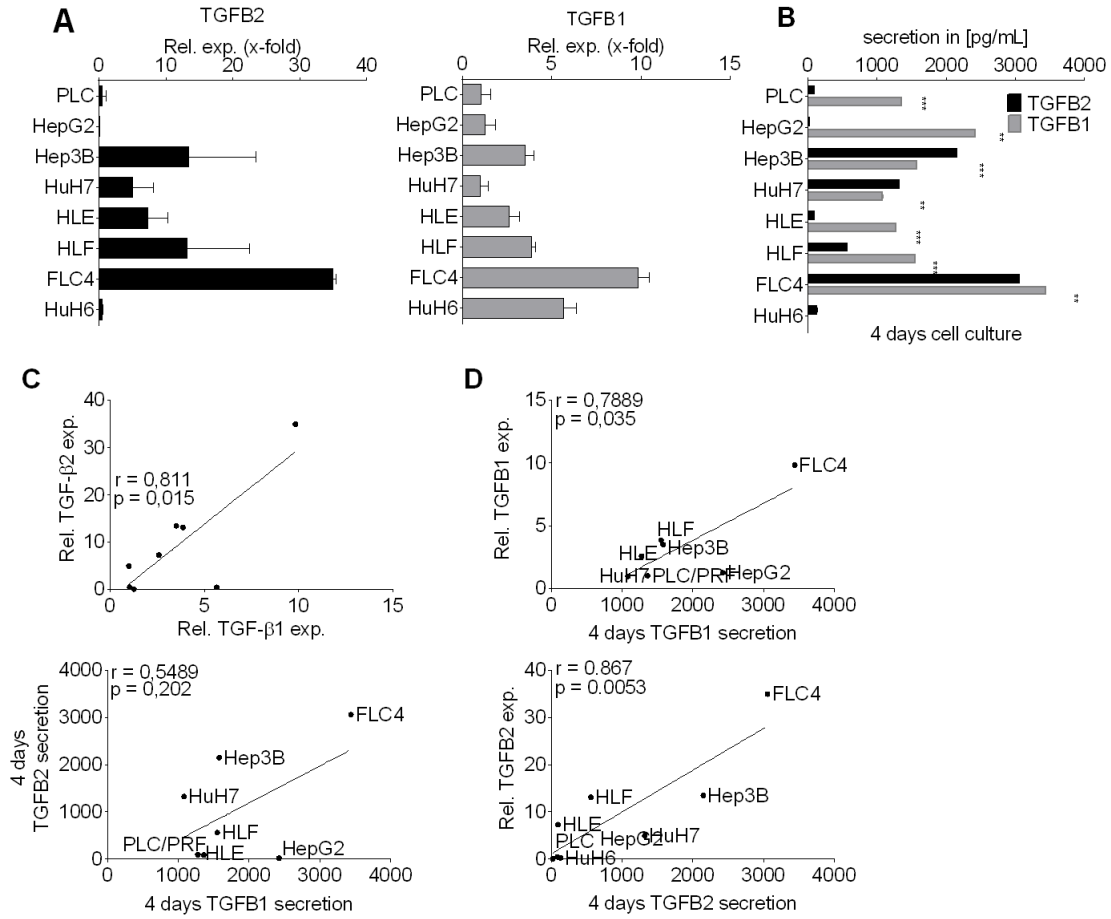

Figure 11 Different appearance of TGF-β1 and TGF-β2 expression in human HCC cell lines and one hepatoblastoma cell line. (A) TGFB1 and TGFB2 expression analysis by qPCR in 7 HCC cell lines and one hepatoblastoma cell line. (B) After 4 days in culture, TGF-β isoform secretion was determined by performing ELISA. (C) Pearson correlation of TGF-B1 versus TGFB2 expression and (D) TGFB isoform expression versus TGFB secretion in all HCC cell lines. *$p \leq 0.05$, **$p \leq 0.01$, ***$p \leq 0.001$. Adapted and modified according to [114].

3.1.2.3 TGF-β2 knockdown in human HuH7 and LX-2 cells using a TGF-β2-specific anti-sense oligonucleotide (AON)

A TGF-β2 knockdown experiment using an isoform-specific antisense oligonucleotide (AON) was performed in one HCC cell line (HuH7) and one human hepatic cell line (LX2) presenting high TGF-β2 expression. Successful downregulation of TGF-β2 in both cell lines (Figure 12 (A) revealed the suitability of TGF-β2 AON as a functional tool for studying the role of TGF-β2 in vitro.

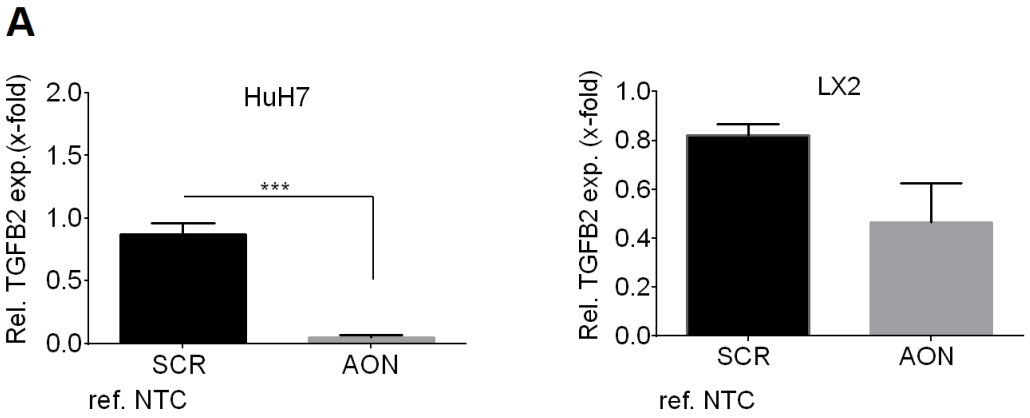

Figure 12 AON-mediated TGF-β2 knockdown in HuH7 and LX-2 cells. (A) Validation of knockdown efficiency in HuH7 (left panel) and LX-2 cells (right panel) analyzed by qPCR after 48 h and referred to non-treated cells. For both cell lines, an AON concentration of 20 nmol was used. Adapted and modified according to [114].

3.1.3 TGF-β2 expression in animal models of chronic liver disease

To confirm our findings, TGF-β1 and -β2 expression was analyzed in different animal models of chronic liver disease, each presenting distinct attributes of the disease process.

3.1.3.1 Expression of TgfB1 and TgfB2 in chemically induced fibrosis of CCl_4-challenged mice

A widely used model for studying liver regeneration and fibrosis is hepatic intoxication with carbon tetrachloride (CCl_4). A single CCl_4 dose leads to acute, but reversible liver damage followed by regeneration. Within 6 days, similar dynamics of TgfB2 and TgfB1 expression were shown by quantitative real-time qPCR (Figure 13). Two days after CCl_4 administration, the expression of both isoforms was at maximum (Figure 13A). Interestingly, collagen 1A expression consistently peaked on day 2. The study was then extended to chronic CCl_4 treatment. The mice received either one CCl_4 injection or three CCl_4 injections within one week, or, for chronic treatment, twice per week for six weeks. In all setups, CCl_4 treatment significantly enhanced the expression of TgfB1 and TgfB2, but the highest expression of both isoforms was observed after six weeks of chronic treatment (Figure 13B). Performing Pearson correlation analysis in individual mice that had been treated for six weeks with CCl_4, positive correlation of collagen 1A1 expression with both TGFB isoforms was visible (Figure 13C).

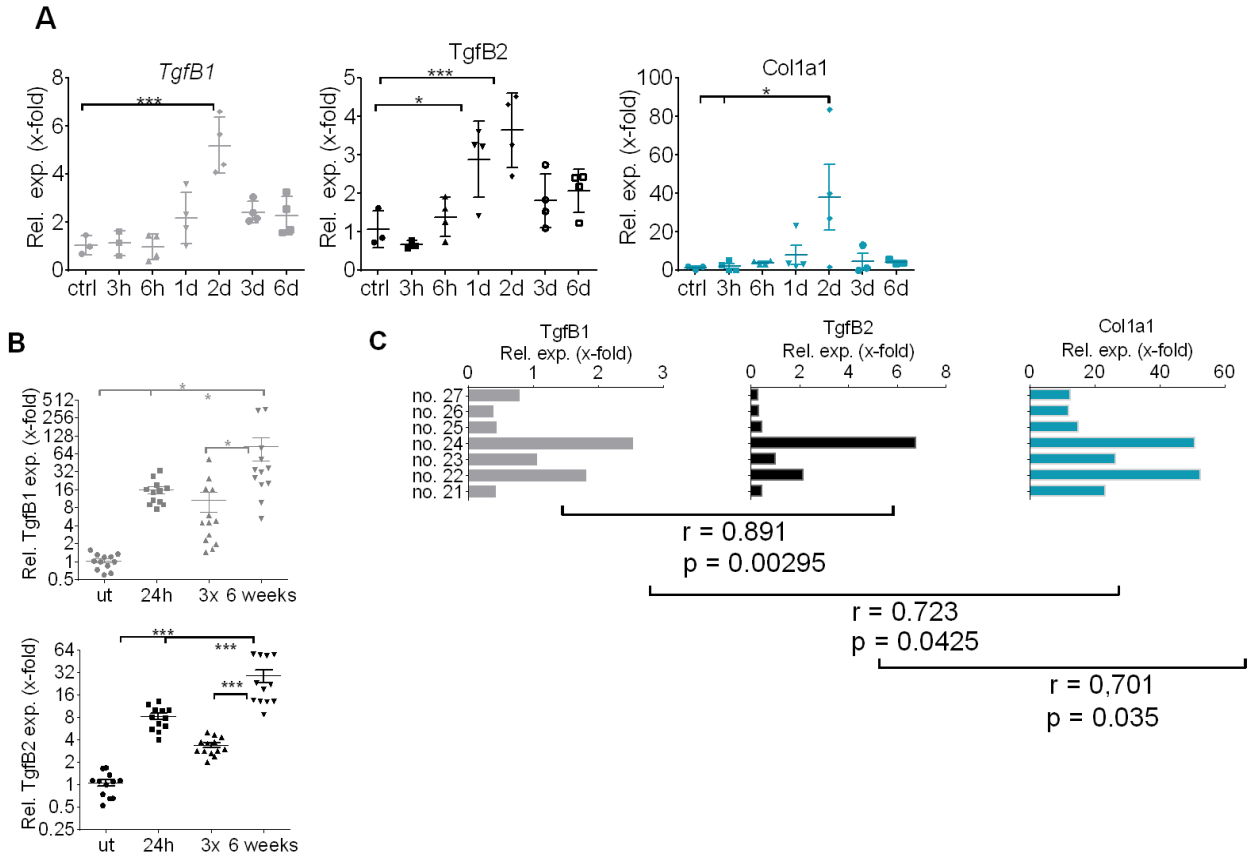

Figure 13 Expression of TgfB1, TgfB2, and Collagen 1a1 upon acute and chronic CCl_4-induced liver damage. (A) The dynamics of TgfB1, TgfB2, and Collagen 1a1 expression over the course of six days were determined by qPCR in comparison to untreated animals. (B) Examination of TgfB1 and TgfB2 mRNA expression 24 h after 1 CCl_4 injection, 3 injections within one week, or two injections per week for six weeks as indicated. (C) In 7 individual mice harboring chronic liver damage, TgfB1 and TgfB2 expression correlated with Collagen 1a1 expression (6 weeks of treatment). The Pearson coefficients were $r_{TGF\text{-}\beta_1/TGF\text{-}\beta_2}$ = 0.891, $r_{TGF\text{-}\beta_1/Col_1A}$ = 0.723, and r = 0.701, respectively. Adapted and modified according to [114].

3.1.3.2 TGF-β isoform expression in models of biliary-derived liver disease

Liver fibrosis comprises different etiologies; among these, cholestatic liver disease and biliary fibrosis account for a considerable part. An established animal model for studying cholestasis is ligation of the common bile duct (BDL). The expression patterns of TgfB1 and TgfB2 were analyzed over the course of up to 14 days after BDL and revealed an elevation of TgfB1 and TgfB2 expression. Only a slight induction of TgfB1 expression (~4-fold as compared to 0 h) was found in this time period, while TgfB2 was strongly induced after 14 days (~155-fold as compared to 0 h) (Figure 14A). Time-resolved high-throughput

quantitative Taqman qRT-PCR (Fluidigm) [114] analysis revealed parallel induction of TgfB2 and different fibrosis markers such as TgfB1, Acta2, Col1a1, Col4a3, Col8a1, and Timp1 (Figure 14B).

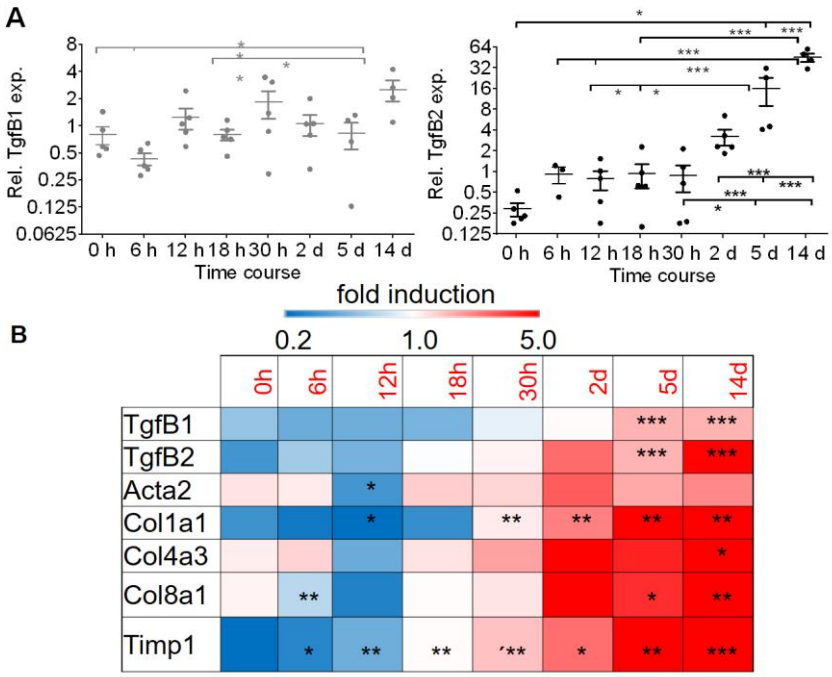

Figure 14 Expression patterns of TgfB1, TgfB2, and fibrotic markers in bile-duct-ligated mice (BDL). (A) TgfB1 and TgfB2 expression were determined over the course of 14 days after bile duct ligation (BDL). Relative expression was normalized to expression of GAPDH and referred to the mean ΔCt of all samples. (B) Fluidigm-based gene expression analysis of typical fibrosis markers displayed in a heat map. The color represents the expression level of the gene. Red represents high expression, while blue represents low expression. *p < 0.01; **p < 0.005; ***p < 0.001. Adapted and modified according to [114].

To confirm a potential involvement of TGF-β2 in the cholestasis process, TgfB1 and TgfB2 expression was additionally determined in MDR2-KO (Abcb4-/-) animals, a reproducible mouse model of chronic biliary liver disease. MDR2-deficient mice spontaneously develop progressive biliary damage resembling human primary sclerosing cholangitis (PSC). MDR2-KO animals showed significant TgfB2 upregulation in early stages (3 months) and at late time points (15 months) over the course of 3 to 15 months compared to the correspondingly aged wild-type mice, while TgfB2 was significantly increased at 3 months and 9 months (up to 10-fold). TgfB1 expression was notably weaker than TgfB2 expression (up to 2.5 times) (Figure 15A). To visualize the change of TGF-β isoform expression over time, line graphs of fold change expression were generated using 3-month old wild-type animals as a reference for all time points (Figure 15B). Interestingly, TgfB2 expression in wild-type and MDR2-KO animals seemed to increase over time, while expression of TgfB1 was consistent and lower than TgfB2 in both mice groups at all time points. As the MDR2-KO model

covers a progression of biliary disease from early precancerous stages to cancerous stages, such as HCC, tumors derived from MDR2-KO animals and their corresponding surrounding tissue were analyzed for TgfB1 and TgfB2 expression. No further increase in the expression of both TgfB isoforms could be shown in tumors when compared to the corresponding surrounding tissue (Figure 15C). The highest TgfB expression for both cytokines had already taken place in the surrounding tissue.

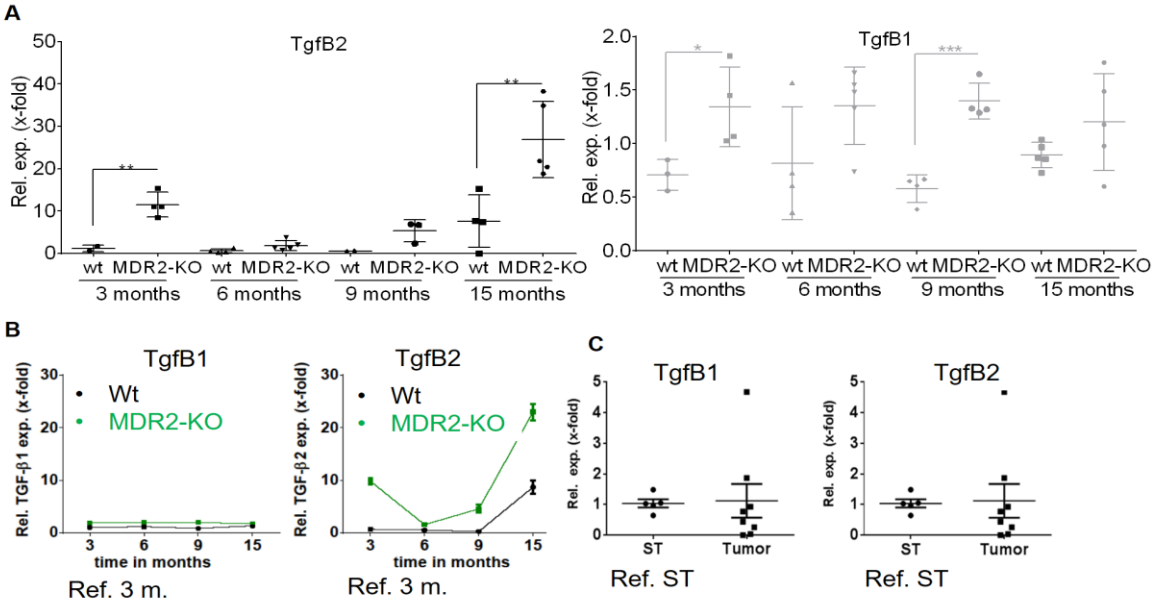

Figure 15 Expression levels of TgfB1 and TgfB2 in MDR2-KO mice. (A) TgfB1 and TgfB2 mRNA expression in MDR2-KO mouse livers after 3, 6, 9, and 15 months was referred to the liver tissue of wild-type animals of the same age. (B) TgfB isoform expression over time. (C) Comparison of TgfB1 and TgfB2 expression in the surrounding tissue and the respective tumor tissue of MDR2-KO mice aged 80-86 weeks. Adapted and modified according to [114].

3.1.3.3 Characterization of TgfB1 und TgfB2 expression in murine HCC models

As expression of TgfB2 was upregulated in aged MDR2-KO mice, another experimental liver carcinogenesis model was investigated. Overexpression of c-myc in the liver leads to constant hepatocyte proliferation and eventual HCC. Epithelial hyperplasia in the liver and even neoplastic transformation is reached when TGF-α is overexpressed, which leads to a high incidence of tumor development over time. In the TGF-α and c-myc animal model applied here, c-myc and TGF-α are co-expressed and therefore the development of liver tumors is very likely. The expression of TgfB2 and TgfB1 in tumors of TGF-α/c-Myc mice was higher than in normal tissue of the same animals, but overall TgfB2 mRNA expression was significantly elevated in tumors of TGF-α/c-Myc animals (Figure 16A).

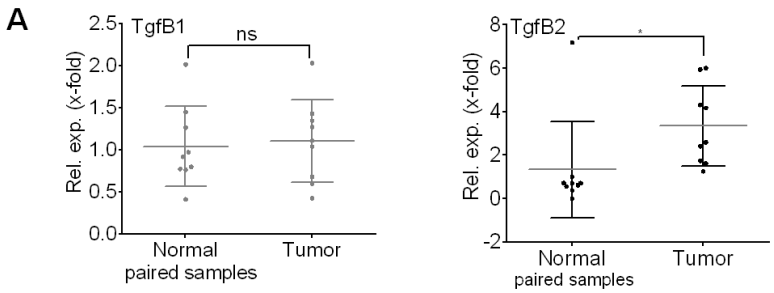

Figure 16 TGF-β isoform expression in TGFα/cMyc, a murine HCC model. (A) qPCR for TgfB1 and TgfB2 expression in paired samples of TGFα/cMyc mice. Adapted and modified according to [114].

3.1.4 Expression data and correlations of human specimens from microrarray data analysis

Animal models provide several advantages when it comes to studying target expression and function, including the study of the liver as a whole organ and the ability to study the mechanistic background of disease development. Nevertheless, no mouse model exactly reflects the complex human liver and human liver diseases with all variables and features. Hence, we aimed to translate our findings to the patient's situation.

3.1.4.1 TGFB1 and TGFB2 expression in human HCC and cirrhosis patients based on Oncomine® Research Edition analysis

Publicly accessible microarray repositories were searched for human HCC and cirrhotic patients(

Table 6). The expression data of the TGF-β isoforms was then analyzed. In four out of seven studies, TGFB2 upregulation was reported, independent of etiology, whereas only one dataset described TGFB2 downregulation (Figure 17). In the former collectives, TGFB2 was one of the top 5–10% of upregulated genes, while downregulation was less remarkable (in 25% of downregulated genes). Investigating TGFB1 expression in the same cohorts, two studies reported upregulation (in 25% of the most upregulated genes) and another two reported downregulation (in 25% of the top downregulated genes) (Table 6). To underline a potential role of TGFB2 in human hepatocarcinogenesis, the survival analysis and the clinicopathological parameter of the GSE1898/4024 collectives were correlated with TGFB2 regulation. Groups with high and low TGFB2 expression were defined. Notably, high TGF-β2 expression correlated with a poorer survival rate ($p < 0.01$) (Kaplan-Meier-plot), but not with other clinical features like AFP levels, tumor size, differentiation grade, cirrhosis, and hepatoblast vs. hepatocyte subtype (data not shown; published in [114]).

No. of Cohort in Figure 17	Publication	Reference Tissue
8	Mas Liver, Mol Med. 2008 [116]	Cirrhosis vs. normal
9	Wurmbach Liver, Hepatology 2007 [117]	Cirrhosis vs. normal
10	Wurmbach Liver, Hepatology 2007 [117]	Dysplasia vs. normal
11	Chiang Liver 2, Cancer Res.2008 [118]	HCC vs. Liver Cancer Type: Liver Cancer Precursor
12	Mas Liver, Mol Med. 2008 [116]	HCC vs. Liver Cancer Type: Liver Cancer Precursor
13	Archer Liver, Cancer Epidemiol Biomarkers Prev .2009 [119]	HCC vs. Liver Cancer Type: Liver Cancer Precursor
14	Chen Liver. Mol Biol Cell. 2002 [120]	HCC vs. Liver Cancer Type: Liver Cancer Precursor

Table 5 Liver cancer precursor and cirrhosis cohorts used for the analysis of TGFB1 and TGFB2 expression based on Oncomine® Research Edition. Adapted and modified according to [114].

				Overexpression			Underexpression		
TGFB2	Publication	Samples	Total no. of measured genes	TGFB2 gene rank	Fold change (median centered ratio)	p-value	TGFB2 gene rank	Fold-change (median centered ratio)	p-value
1	Chen Liver. Mol Biol Cell. 2002 [120]	197	10.802	5239 (in top 49%)	1.107	0.221	2569 (in top 24%)	-1.258	0.006
2	Guichard Liver. Nat Genet. 2012 [121]	185	18.823	838 (in top 5%)	1.114	1.08E-14	17148 (in top 92%)	1.114	1.000
3	Guichard Liver 2. Nat Genet. 2012 [121]	52	18.823	787 (in top 5%)	1.103	4.32E-6	17195 (in top 92%)	1.103	1.000
4	Mas Liver. Mol Med. 2008 [116]	115	12.603	890 (in top 8%)	1.191	1.56E-6	3547 (in top 29%)	-1.076	0.003
5	Roessler Liver. Cancer Res. 2010 [122]	43	12.603	4250 (in top 34%)	1.194	0.046	5540 (in top 44%)	-1.029	0.118
6	Roessler Liver 2. Cancer Res. 2010 [122]	445	12.624	5015 (in top 40%)	1.053	0.001	5115 (in top 41%)	-1.034	0.004

7	TCGA Liver. No Associated Paper. 2012	212	18.823	792 (in top 5%)	1.233	3.40E-15	ND	ND	ND
TGFB1	**Publication**	**Samples**	**Total no. of measured genes**	**TGFB1 gene rank**	**Fold change (median centered ratio)**	**p-value**	**TGFB1 gene rank**	**Fold change (median centered ratio)**	**p-value**
1	Chen Liver. Mol Biol Cell. 2002 [120]	197	10.802	10452 (in top 97%)	-1.557	1.000	512 (in top 5%)	-1.557	1.56E-12
2	Guichard Liver. Nat Genet. 2012 [121]	185	18.823	5712 (in top 31%)	1.013	0.060	12282 (in top 66%)	1.013	0.940
3	Guichard Liver 2. Nat Genet. 2012 [121]	52	18.823	ND	ND	ND	11608 (in top 62%)	1.007	0.820
4	Mas Liver. Mol Med. 2008 [116]	115	12.603	1784 (in top 15%)	1.513	1.40E-4	X	X	X
5	Roessler Liver. Cancer Res. 2010 [122]	43	12.603	1836 (in top 15%)	2.225	3.09E-4	5267 (in top 42%)	-1.071	0.093
6	Roessler Liver 2. Cancer Res. 2010 [122]	445	12.624	5677 (in top 45%)	1.098	0.043	3088 (in top 25%)	-1.111	3.69E-7
7	TCGA Liver. No Associated Paper. 2012	212	18.823	5854 (in top 32%)	1.027	0.021	12130 (in top 65%)	1.027	0.979

Table 6 HCC sample cohorts used for the analysis of TGFB1 and TGFB2 expression based on Oncomine® Research Edition. Total number of samples, total number of genes measured, *p*-values, gene ranks, and fold change are given for TGFB1 and TGFB2 as indicated. Additionally, the table summarizes in which range of differentially expressed genes the respective gene was found in the study (top %). ND = not detected in the study. Adapted and modified according to [114].

Given the downregulation of TGFB2 in HCC compared to surrounding liver tissue (Figure 17C), which is usually cirrhotically dearranged, TGFB1 and TGFB2 expression was also evaluated in pre-neoplastic stages, such as cirrhosis, using the Oncomine® database. In precancerous and cirrhotic stages in human patients, both isoforms were found to be upregulated compared to normal liver tissue (Figure 17B). A continuous increase of TGFB1 expression from healthy tissue via cirrhosis and further to HCC was noticed (Figure 17

A-C, right panel). In contrast, in cirrhotic tissue, TGFB2 expression was higher than in the normal liver and even stronger than in HCC. This dissimilar expression of the two isoforms in precancerous and cirrhosis stages compared to HCC hints at contradirectional regulation of TGFB1 and TGFB2 in the progression from cirrhosis to HCC (Figure 17D).

Similar to our results in liver tissue, serum analysis of human cirrhosis and hepatocellular carcinoma patients in comparison to healthy donors revealed a tendency towards higher TGFB2 levels in cirrhotic sera. Intriguingly, the TGFB2 amounts were found to be the lowest in sera of HCC patients compared to patients with cirrhosis and even compared to healthy patients. This data is consistent with the Oncomine® gene expression data showing higher TGFB2 expression in precancerous and cirrhotic stages and lower expression in HCC (Figure 18).

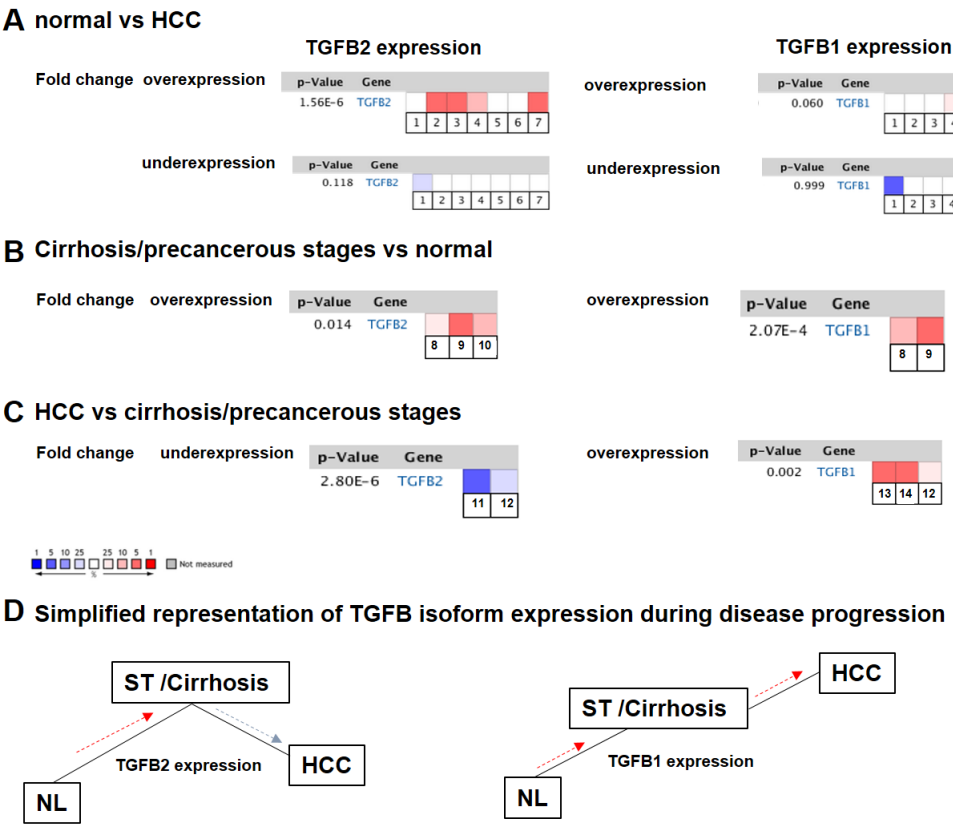

Figure 17 TGFB1 and TGFB2 expression in human HCC, cirrhosis, and precancerous stages using the Oncomine® Research Edition database. (A) TGFB1 (right panels) and TGFB2 (left panels) expression in human HCC versus normal stages were examined using in silico analysis on the Oncomine® database platform. (A) Gene expression in HCC vs. normal liver was analyzed. The numbers correspond to the list of references in Table 6. (B-C) Gene expression in precancerous stages/cirrhosis vs, normal or cancer vs. precancerous stages/cirrhosis was analyzed. The numbers correspond to the list of references in Table 5. (D) Scheme for potential TGFB1 and TGFB2 regulation during disease progression. p-values of < 0.05 were set and the p-value for a given gene is its p-value for the median-

ranked analysis. Note: In the Mas Liver data (collective numbered with 8), TGF-β2 was also downregulated significantly (p = 2.54E-5, top 23%, median rank 2790) in cirrhosis vs. normal tissue. Adapted and modified according to [114].

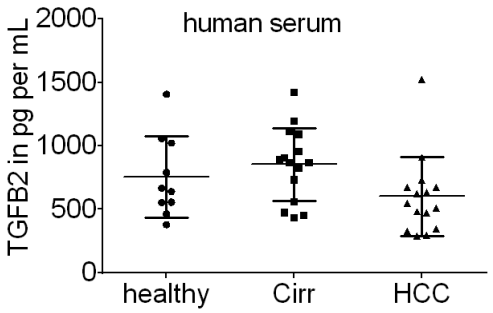

Figure 18 TGFB2 levels in human sera of different entities: Systemic TGFB2 levels in sera of healthy, cirrothic, and HCC patients using a specific TGFB2 enzyme-linked immunosorbent assay. Each single dot represents an individual patient.

3.1.5 In vivo targeting of TgfB2 using antisense oligonucleotides (AONs)

Our findings regarding TgfB2 expression in mice and human so far indicate that TgfB2 might represent a potentially relevant target in CLD. To test this hypothesis, TGFB2 was specifically silenced in vivo in the MDR2-KO mouse model, which represents biliary and other inflammation-associated liver damage. TGFB2 mRNA was specifically targeted using antisense oligonucleotides (AONs). Their simple generation and design as well as their various application opportunities make them an attractive tool for gene function investigations and a therapeutic agent. Antisense-based therapies are actually in use in many preclinical and clinical trials for various types of disease and have been shown to be well-tolerated by patients.

3.1.5.1 Antisense oligonucleotides (AONs) as a tool in vivo

To analyze the effect of TGFB2 silencing on liver fibrosis and inflammation, the TGFB2-specific antisense oligonucleotide (ASP0047) was used. ASP0047 represents a 17-mer full phosphorothioate Locked Nucleic Acid (LNA)-modified antisense oligodeoxynucleotide '4+4' gapmer that selectively targets TGFB2.

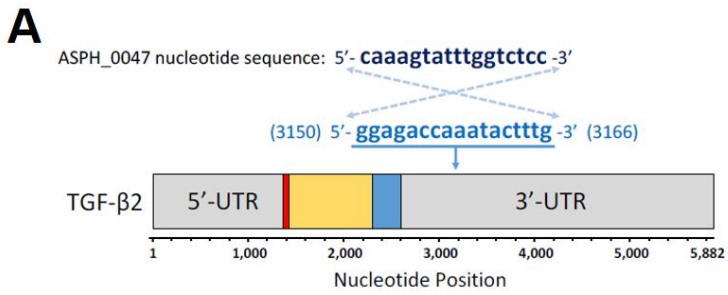

Figure 19 Sequence of the TGFB2-directed AON ASPH0047. The TGF-β2-directed AON ASPH0047 was engineered as a 17-mer full phosphorothioate LNA-modified antisense oligodeoxynucleotide '4+4' gapmer. A scramble control oligo C30047 (C0) was used to control for non-sequence-specific biological effects of oligonucleotides.[123]

3.1.5.2 Biodistribution and physiological compatibility of AONs

The hepatotropic efficiency of the TGFB2-targeting AON for the liver was determined after subcutaneous (s.c) or intraperitoneal (i.p.) injection into Balb/c wild-type mice (Figure 20A). The liver toxicity of ip and sc AON application in wild-type Balb/c mice was analyzed using a standard liver plasma parameter. No negative effects of the AON at a concentration of 10 mg/kg of body weight was recorded after 24 h or 5 days following application (Figure 20B). The body weight as well as the liver/body weight ratio were not affected by the AON treatment (Figure 20C). In the liver tissue of Balb/c mice, an AON labeled Digoxigenin was visualized by performing immunohistochemistry. The AON accumulated in the Space of Disse, but was not detectable in hepatocytes (Figure 21A). Similar observations were made in MDR2-KO mice. In cholestatic mice, the AON accumulated along the bile ducts and portal areas. Livers of Balb/c wild-type

and MDR2-KO animals were then co-stained for specific liver cell type markers such as CD31 (LSEC), Desmin (HSC), αSMA (aHSC),S100A4 (FSP1) (KC) Elastin (PF), and the AON (Digoxigenin) by means of immunofluorescence. Interestingly, in MDR2-KO animals the AON accumulated in LSECs, hepatic stellate cells (HSC), and Kupffer cells (Figure 21B), whereas in Balb/c mice, it was solely found in CD31-positive cells, a marker for liver sinusoidal endothelial cells (LSEC).

To investigate whether TgfB2 expression and TgfB2-silencing AON accumulation are localized in same cell types, a magnetic-bead-based simultaneous four liver cell type isolation for hepatocytes (HC), liver sinusoidal endothelial cells (LSEC), Kupffer cells (KC), and hepatic stellate cells (HSC) was performed in 6 Balb/c mice following qPCR for TgfB2 mRNA expression. Noticeably, TGF-β2 mRNA expression was found to be the highest in non-parenchymal cells by qPCR, e.g., in KCs, LSEC, and HSCs (Figure 21c), thus showing a similar distribution as the AON in MDR2-KO mice.

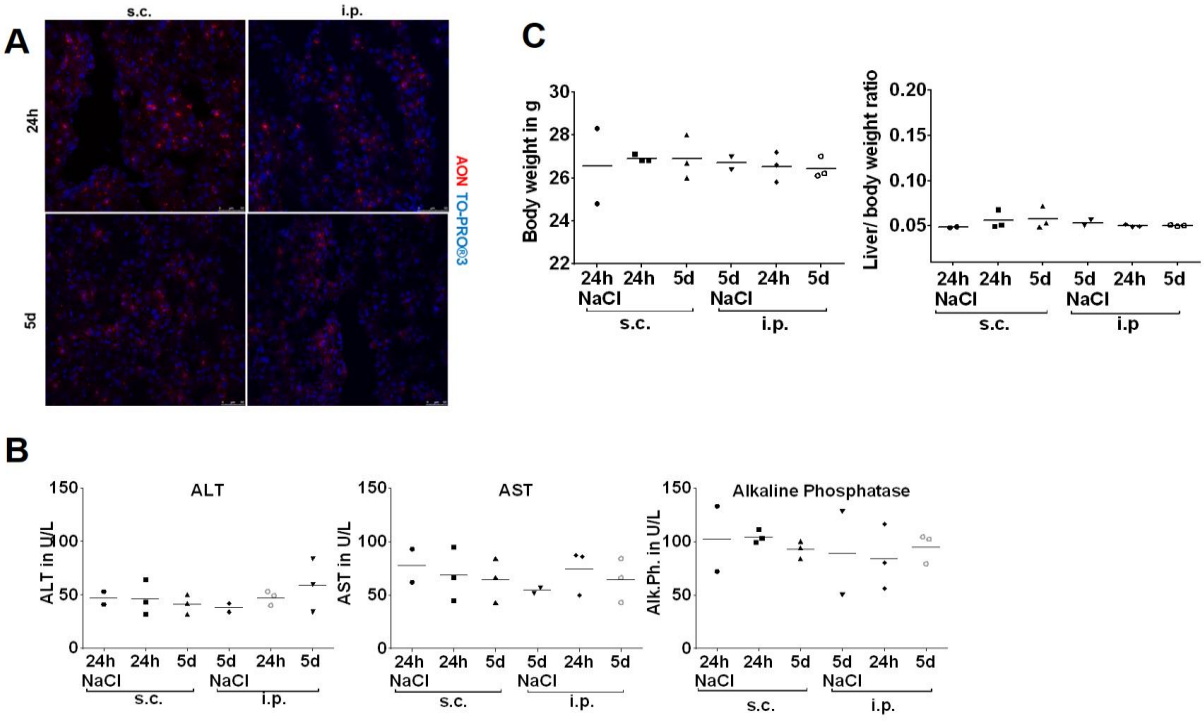

Figure 20 AON biodistribution and safety tolerability. (A) Subcutaneous (s.c.) and intraperitoneal (i.p.) TgfB2-directed AON application in Balb/c mice did not alter (B) liver parameters such as AST and ALT nor (C) the body weight or liver/body weight ratio of the respective animals. Each dot represents one animal.

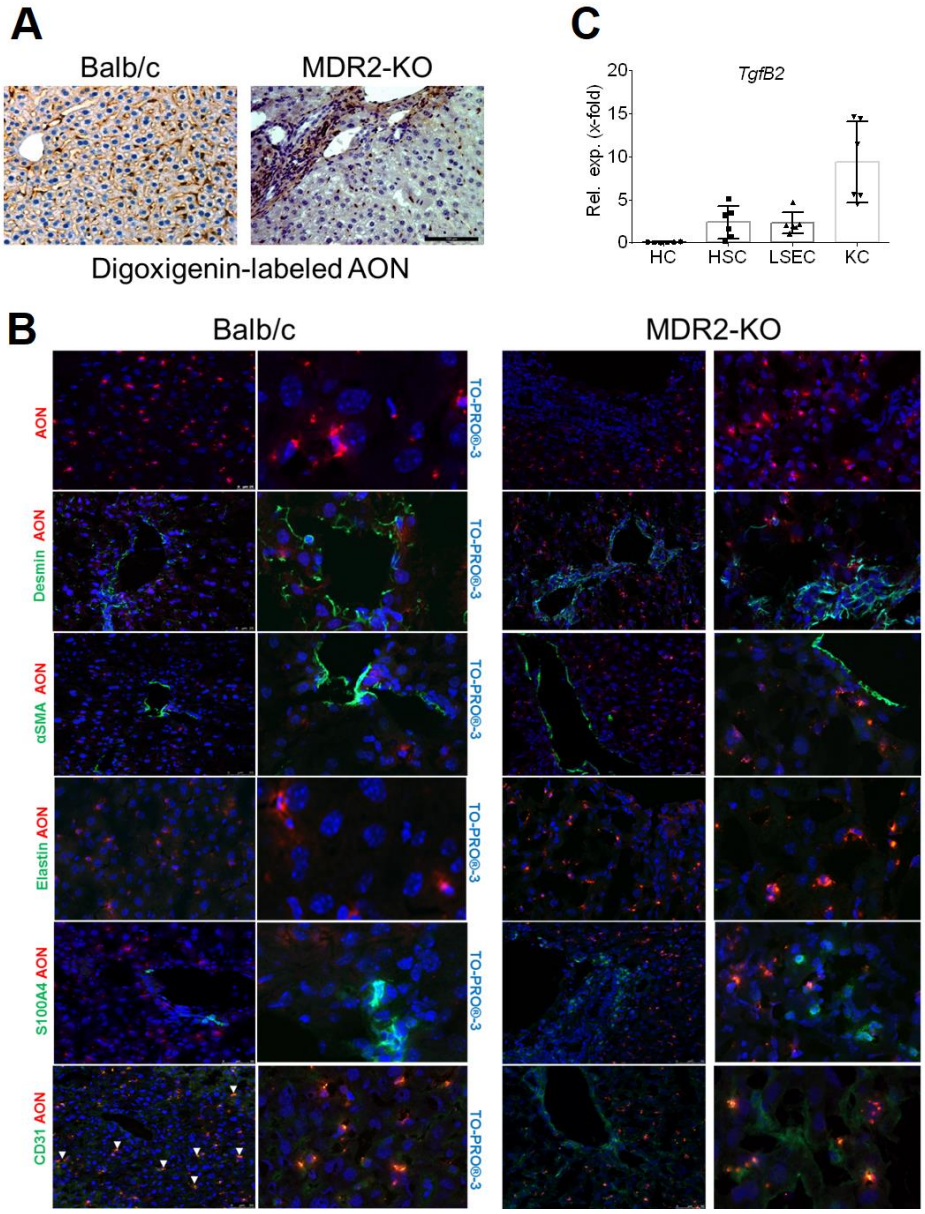

Figure 21 Cell-type-specific localization of TGF-β2-directed AONs by means of immunohistochemistry.TgfB2 expression after 4 liver cell type isolation and AON co-immunofluorescence with cell type markers. (A) In wild-type Balb/c and MDR2-KO mice, the TGF-β2-specific AONs were enriched in sinusoidal areas of the liver tissue as confirmed by immunohistochemical staining of labeled AONs. (C) Magnetic-bead-based 4 liver cell type isolation following qPCR for TGFB2 expression displayed TGF-β2 abundance in the non-parenchymal compartment, in particular in Kupffer cells (n=6). (B) Immunofluorescence revealed co-localization of the AONs (red) with non-parenchymal cell markers, i.e., αSMA, desmin, elastin, S100A4, and CD31 (each green). Hepatocyte nuclei are stained in blue by TO-PRO®-3.

3.1.6 Efficient TgfB2 downregulation in cholestatic MDR2-KO mice and its impact on fibrosis and inflammation

3.1.6.1 Fibrosis

With the intention of ameliorating or even blocking fibrogenesis and inflammation in cholestatic liver disease through downregulation of TGFB2, MDR2-KO mice were treated for four weeks with the AON, starting with an oligo push in the first week. No impact was detected on body weight and liver/body weight ratio nor on liver function parameters; thus no toxicity for the liver was ensured (Figure 22A-B). Remarkably, TgfB2 mRNA levels were efficiently decreased in MDR2-KO mice after AON application (~12.7-fold), characterizing the AON as an effective tool for silencing TGFB2 expression. In addition, systemic TGFB2 plasma levels were also found to be reduced in MDR2-KO mice treated with the AON compared to untreated and control oligo-treated animals (Figure 22C-D).

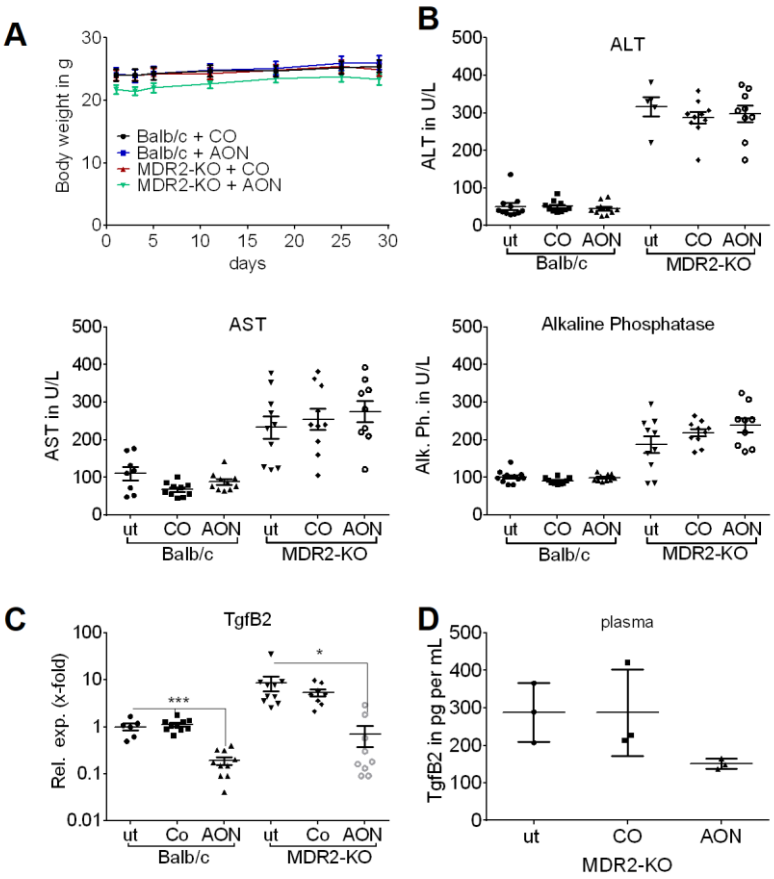

Figure 22 TgfB2-specific AON treatment of cholestatic MDR2-KO mice. (A) Treatment with control or TgfB2-specific AONs did not alter the body weight of any of the animals. (B) Liver parameters of Balb/c and MDR2-KO mice after administration of control oligos (Co) and TGF-β2-specific AONs. ALT, AST, and Alkaline phosphatase plasma levels

were higher in MDR2-KO mice than in Balb/c wild-type animals. Treatment with specific or control AON did not alter the liver parameters. (C) *TgfB2* was significantly downregulated in Balb/c and MDR2-KO animals treated with AON. * $p \leq 0.05$, *** $p \leq 0.001$. (D) After AON application, the TgfB2 level in plasma was reduced compared to control oligo-treated and untreated MDR2-KO mice.

In order to detect the impact of the TgfB2-targeting AON on fibrogenesis, multiple common fibrosis markers were examined. Since excessive accumulation of extracellular matrix, in particular collagen, is a hallmark of fibrosis, the hydroxyproline content in the livers of MDR2-KO mice was determined quantitatively. No difference was observed in AON or control oligo-treated wild-type animals compared to untreated Balb/c mice. Significant hydroxyproline reduction was achieved in MDR2-KO mice upon AON application in comparison to non-treated and control oligo-treated MDR2-KO mice. The hydroxyproline content and the Col1a1/Col3a1 mRNA level of MDR2-KO mice were generally higher than those of Balb/c wild-type animals, while no difference was detected between the treated and non-treated groups (Figure 23A-B). Collagen deposition was then analyzed by performing Sirius Red staining. Compared to untreated MDR2-KO mice, AON-treated mouse livers showed significant downregulation (~56%) of collagen accumulation while wild-type animals showed no differences in collagen deposition between the untreated and treated groups (Figure 23C). To further examine the anti-fibrotic potential of TgfB2, some typical fibrosis markers were investigated on the mRNA expression level. Unlike TgfB2, TgfB1 expression was not elevated in MDR2-KO animals. When comparing MDR2-KO mice with wild-type animals, TgfB1 and Ctgf expression was similar in all tested livers. Timp1 and α-SMA expression were slightly increased in MDR2-KO mice, but AON treatment showed no significant impact on their expression (Figure 24A). Since α-SMA mRNA expression appeared very divergent, α-SMA protein expression was further analyzed by means of immunohistochemistry and immunoblot. Positive α-SMA staining was significantly reduced (~35%) upon AON treatment of MDR2-KO mice. This effect was confirmed by immunoblot of MDR2-KO total liver lysates (Figure 24 B-D).

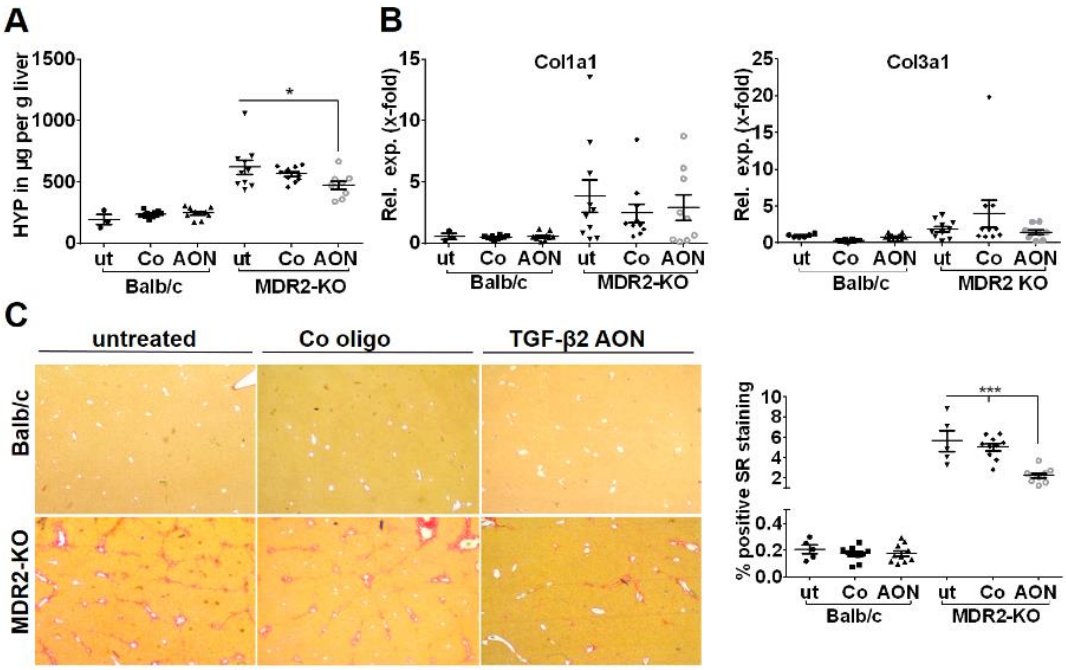

Figure 23 Collagen expression and deposition after AON-mediated TgfB2 silencing in MDR2-KO mice. (A) AON-treated MDR2-KO mice showed significantly downregulated hydroxyproline content in the liver compared to untreated and control oligo-treated animals. (B) mRNA expression of two collagen types showed no regulation after AON or control oligo treatment. (C) Sirius Red staining revealed significant downregulation (~56%) of collagen deposition in the tissue of AON-treated MDR2-KO mice compared to untreated MDR-KO mice. * p ≤ 0.05, **p ≤ 0.01, ***p ≤ 0.001

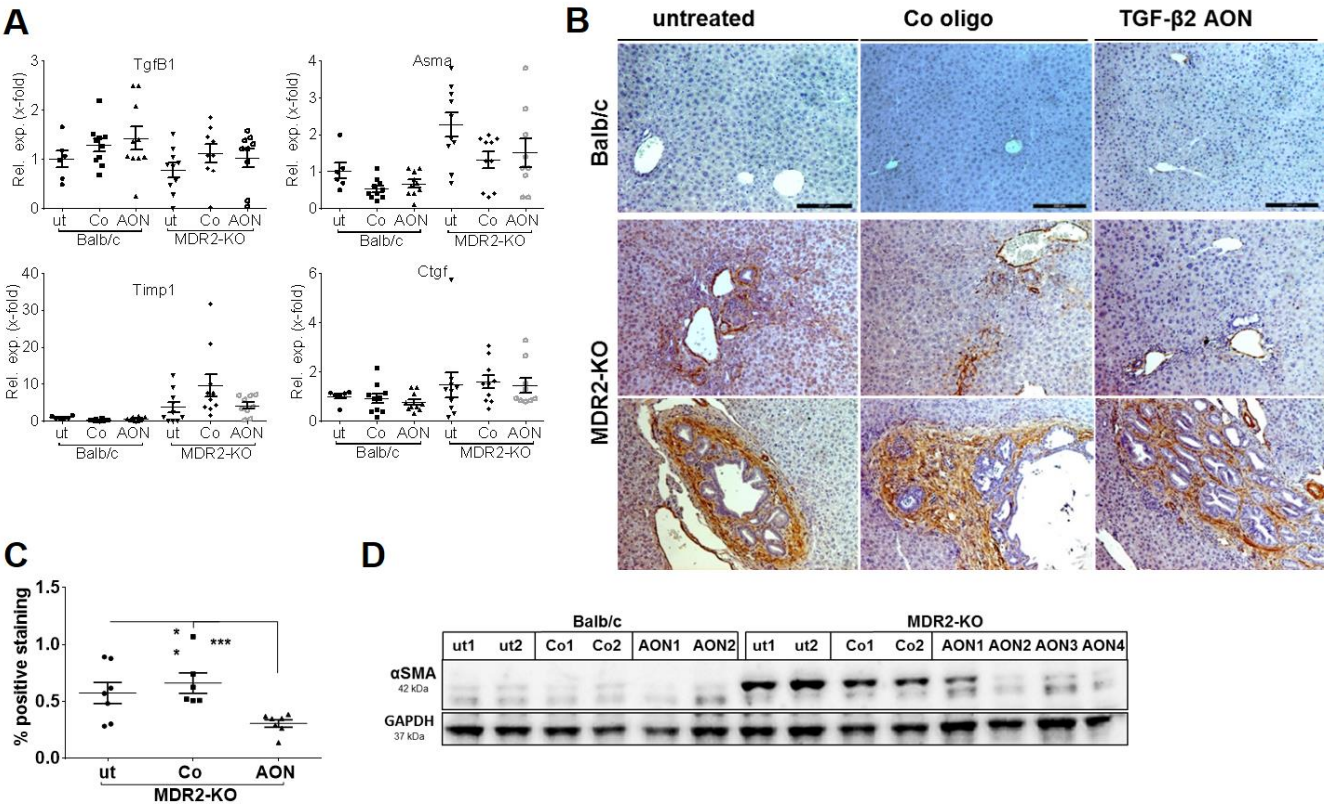

Figure 24 Impact on fibrotic marker expression after AON administration in MDR2-KO mice. (A) TgfB1, Timp1, and Ctgf mRNA expression was not changed considerably by TgfB2-directed AON treatment verified by qPCR. (B-C) Immunohistochemical staining and quantification demonstrated a decrease of αSMA expression of 35% in AON-treated animals compared to untreated animals and of 43% compared to animals treated with control oligos. (D) Reduction of the αSMA protein level was verified by immunoblot analysis. * p ≤ 0.05, **p ≤ 0.01, ***p ≤ 0.001.

3.1.6.2 Biliary damage: MDR2-KO mouse model of sclerosing cholangitis and biliary fibrosis

MDR2-KO mice lack the Mdr2 gene, which encodes for a phospho flipase. Therefore, they must sufficient excretion of phospholipids into the bile canaliculus. The external appearance of MDR2-KO mice shows no difference compared to age-matched wild types in the course of the first year. Already a few weeks after birth, an irregular canaliculi phenotype is visible and the livers of MDR2-KO mice have altered immune responses, such as neutrophil-granulocytic infiltrates, proliferating fibroblasts, and ductular reaction (DR) in larger portal tracts, in comparison with age-matched control animals. Likewise, these mice develop periductal onion-skin fibrosis between bile ducts at an early age [124]. Since histological and macroscopic features found in MDR2-KO are similar to human PSC, these mice represent a suitable model for mimicking PSC in mice and make it possible to study inflammation-driven fibrosis.

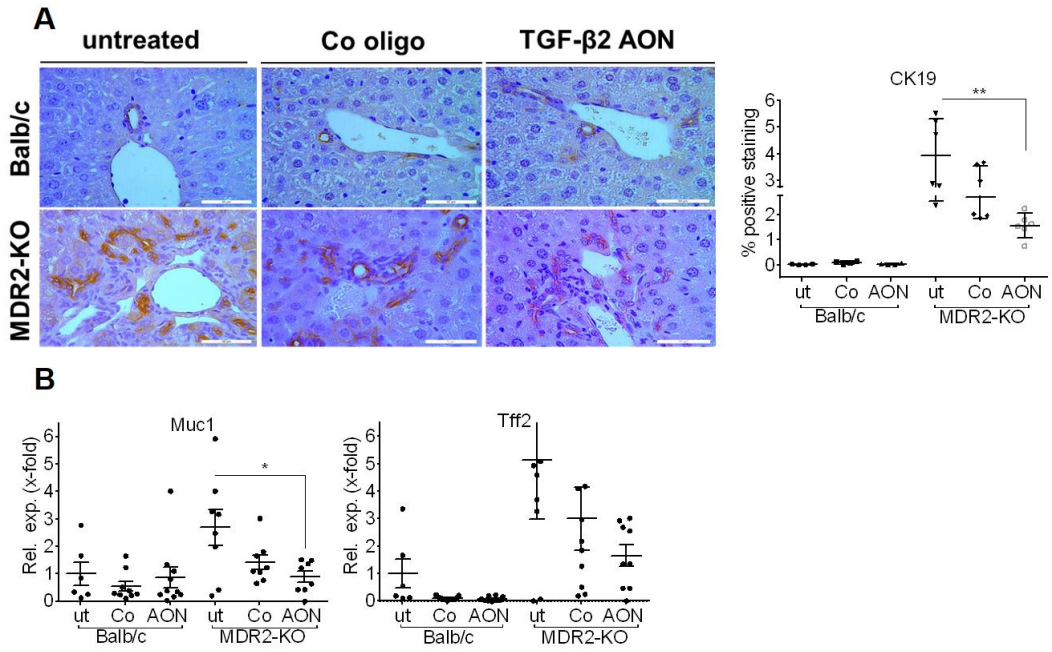

Figure 25 Impact of AON treatment on biliary damage and ductular reactions (DR). TgfB2 silencing by AON reduced biliary damage and ductular reactions (DR). Using qPCR and immunohistochemical staining, significant downregulation of Muc1 as a marker of biliary damage and CK19 as a marker of DR, respectively, was detected in AON-treated MDR2-KO mice. * p ≤ 0.05, ***p ≤ 0.001.

As shown in Figure 24 and Figure 25, MDR2-KO mice exhibit fibrogenic liver rearrangements, periductular onion-skin fibrosis, and pronounced ductular reaction (DR) at the age of 18 weeks. AON treatment of MDR2-KO mice improved biliary damage and reduced DRs, as demonstrated by CK19 staining of the liver tissue (Figure 25A). Analyzing the effect of AON application with respect to biliary damage, Muc1 and Tff2 expression was investigated in all groups of MDR2-KO animals and the corresponding wild-type animals. Muc1, which has been reported to be a marker for biliary disease stages, was downregulated by AON treatment. Another marker, Tff2, showed a similar trend, but only in treated mice (Figure 25B).

3.1.6.3 Inflammation

Cholestatic liver disease of MDR2-Ko mice is known to be associated with increased bile duct proliferation, biliary fibrosis, and pronounced inflammation. Interestingly, staining of the panleukocyte marker CD45 (Figure 27) and portal area assessment of H&E stained tissue sections (Figure 26) verified a significant decrease in the number of infiltrating inflammatory cells in AON-treated MDR2-KO mice. To assess the inflammatory status of the mice in more detail, prominent targets such as TnfA, Il6, and Il1B were investigated in AON-treated and untreated mice. These targets are known to be induced by M1-type

macrophages, which exhibit an inflammatory phenotype. The expression of TnfA, Il6, and Il1B did not significantly change between the treated and untreated groups (Figure 27). Remarkably, significantly increased expression of PparG, an indicator for reduced liver fibrosis and an affector for macrophages [125, 126] ,was found in AON-treated MDR2-KO mice. Taken together, these findings point towards ameliorated inflammation in the livers of these animals.

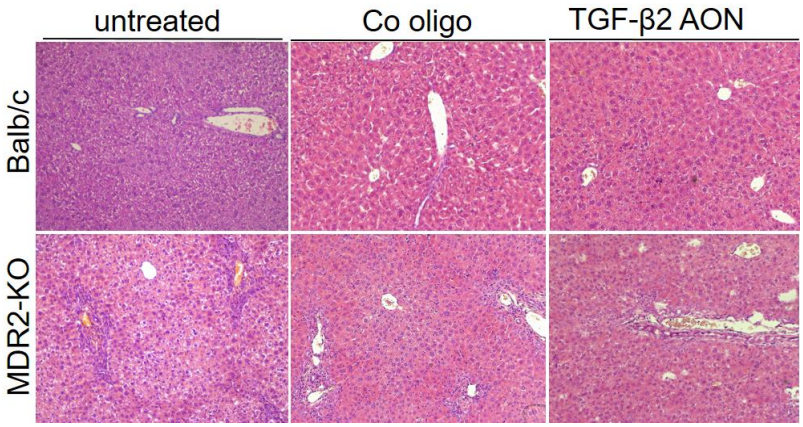

Figure 26 Representative H&E images of all mouse groups. H&E staining confirmed inflammation reduction through TgfB2-silencing AON treatment in MDR2-KO mice compared to untreated or control oligo-treated MDR2-KO mice. All Balb/c mice groups did not show any significant inflammatory infiltration before or after any of the treatments.

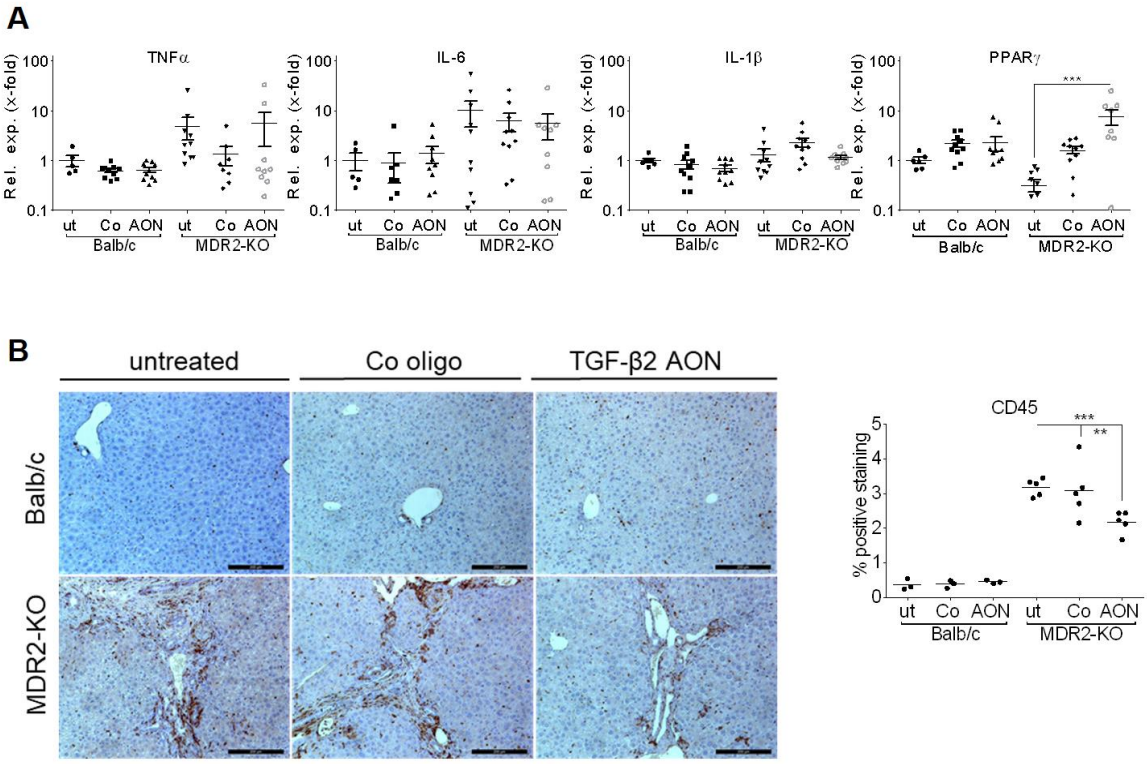

Figure 27 Immune cell detection in the liver tissue of AON-treated MDR2-KO mice compared to controls. (A) The expression levels of *TnfA*, *Il6*, and *Il1B* as typical M1 markers were not elevated in AON-treated groups compared to Balb/c mice. The expression of PparG showed significant upregulation in AON-treated mice (right plot). (B) Immunohistochemical staining and quantification of CD45 revealed significant downregulation in AON-treated MDR2-KO mice. *$p \leq 0.05$, **$p \leq 0.01$, ***$p \leq 0.001$.

The inflammatory niche of the mouse model was further characterized by staining the monocyte macrophage marker F4/80 and the neutrophil marker myeloperoxidase (MPO). Untreated Balb/c and MDR2-KO mice as well as control oligo-treated groups showed no remarkable F4/80+cell infiltration. MDR2-KO animals treated with TGF-β2-silencing AON instead showed significant attraction of F4/80-positive macrophages, predominantly around portal tracts (Figure 28 A). Similar levels of MPO-positive cells were observed in all control groups of Balb/c and MDR2-KO mice. In AON-treated animals, a significant increase of MPO-positive cells was visible compared to untreated or control oligo-treated animals, suggesting enhanced infiltration of macrophages and neutrophils, although typical inflammation parameters were found to be reduced (Figure 28B).

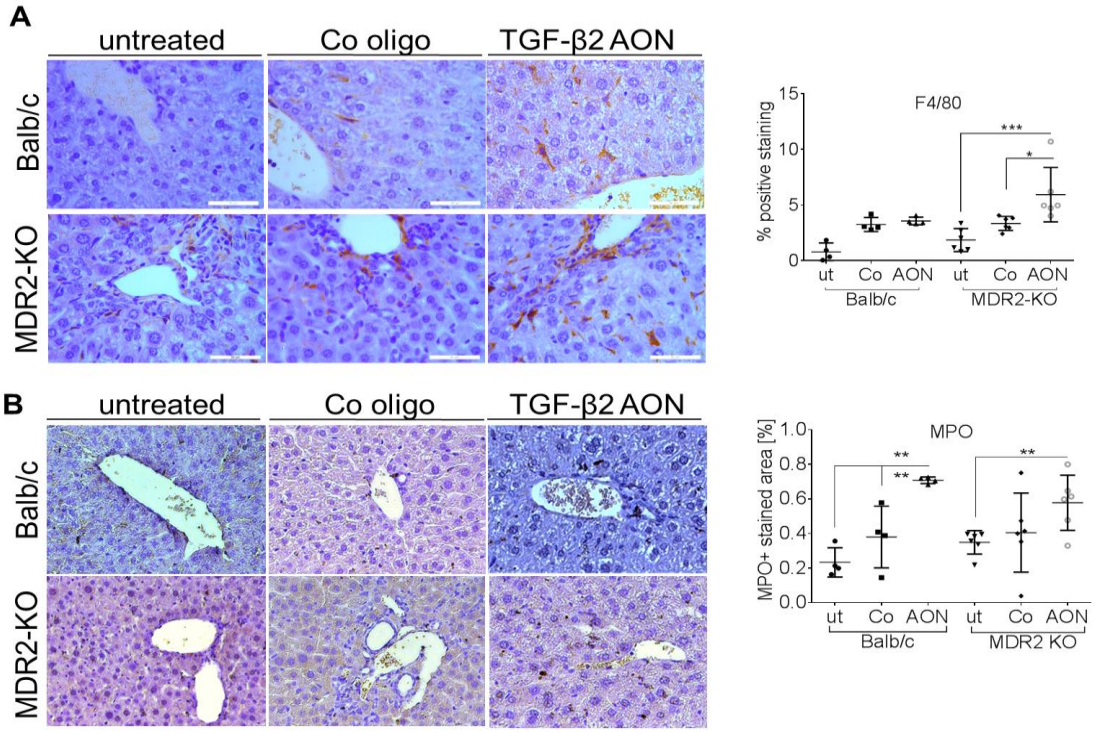

Figure 28 Immune cell infiltration into the liver tissue of AON-treated MDR2-KO mice and corresponding controls. (A) In AON-treated MDR2-KO mice, liver-resident F4/80-positive macrophages were detected. Immunohistochemical staining and quantification of F4/80-positive cells revealed significant upregulation in AON-treated MDR2-KO mice. (B) In AON-treated Balb/c and MDR2-KO mice, significant MPO upregulation was observed, as shown by immunohistochemical staining and quantification. *p ≤ 0.05, **p ≤ 0.01, ***p ≤ 0.001

3.1.7 From mice to men: TGFB2 in human primary sclerosing cholangitis (PSC) and primary biliary cholangiopathy (PBC) patients

Cholestatic liver diseases, including primary biliary cholangiopathy (PBC) and primary sclerosing cholangitis (PSC), belong to the category of rare diseases. While PBC occurs more often in intrahepatic bile ducts and primarily affects women, PSC is more prevalent in men and appears in the intra- and extrahepatic bile ducts. Both diseases are characterized by inflammation, portal fibrosis, and strictures of the above-mentioned bile ducts, which leads to a chronically progressing disease and further to biliary cirrhosis and end-stage liver disease [127, 128]. Since biopsies and human material are not taken routinely from these patients, they are not commonly available and hence poorly studied.

In terms of the results found in animal models of biliary-derived liver disease such as BDL and MDR2-KO mice mice described in 3.1.3.2, liver tissue samples of PSC and PBC patients (collectives from Regensburg, Mannheim,

Mannheim, and Frankfurt) were investigated for their TGFB2 mRNA expression and two cohorts (GSE7980 and and Regensburg) were correlated with clinicopathological data. Comparing the expression data of these patients patients to normal liver tissue, TGFB2 showed significant upregulation in PSC and PBC patients and significant significant correlation with the inflammation grade of both collectives (

Table 7). Consistently, in another cohort (GSE79850) comprising nine high-risk patients who ultimately needed liver transplantation and seven low-risk patients who responded to UDCA treatment, upregulated TGFB2 expression was found in the high-risk patient group. High TGFB2 expression was significantly associated with a high Scheuer grade (III and IV). Additionally, high TGFB2 expression correlated well with the diagnosis of ductopenia, but not with the inflammation grade of the patients in this group.

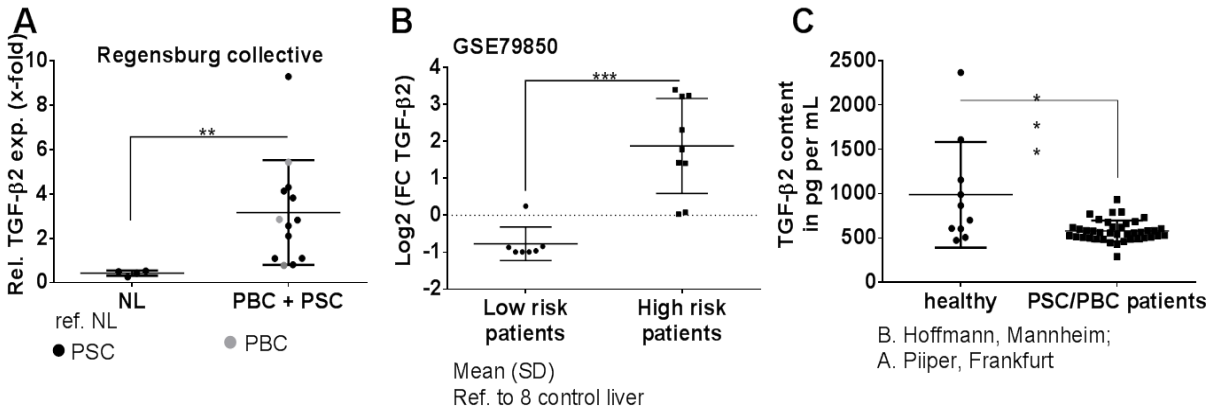

Figure 29 TGFB2 expression in the liver tissue and TGFB2 levels in the serum of human PSC and PBC patients from different collectives. Expression status of TGFB2 in the liver tissue of individual patients represented as single dots (A) in the PSC/PBC cohort from Regensburg, (B) in the GSE79850 cohort with low- and high-risk patients in comparison to non-diseased control livers. Low-risk patients responded fully to UDCA treatment. High risk was associated with the need for liver transplantation in the course of disease. (C) TGFB2 levels in the sera of matched collectives from Mannheim and Frankfurt **p ≤ 0.01, ***p ≤ 0.001; NL= normal liver .

GSE79850: Correlation of high-risk vs. low-risk expression with clinical characteristics			
	High Risk(n=)	**Low Risk (n=)**	**P**
Scheuer Grade			**0,0047**
I+II	1	6	
III+IV	7	0	
Portal Inflammation			0,1026
mild	2	5	
moderate	6	1	
Interface Hepatitis			0,5804
None-mild	5	5	
moderate	3	1	
Ductopenia			**0,0256**
(+)	7	1	
(—)	1	5	

Table 7 Correlation between TGFB2 expression and clinicopathological characteristics of 17 PBC patients analyzed and described in GSE79850. The expression levels of TGFB2 mRNA were compared between high-risk patients who underwent liver transplantation and low-risk patients displaying full response to UDCA treatment. Using Fisher's exact test, significant correlations were observed with Scheuer grade and ductopenia (p <0.05). No correlation with portal inflammation nor any diagnosis of interphase hepatitis was observed.

In one PSC and PBC patient collective (Regensburg), CD45 and PPARG mRNA expression was examined in the patients' tissue. CD45 tended to be upregulated in comparison to normal liver, while no significant elevation of PPARG expression was detected (Figure 30A). CD45 expression additionally correlated with TGFB2 expression in PSC/PBC patients from this cohort (Figure 30B, *p*=0.0255). Concurrently, high TGFB2 expression was detected in the liver tissue of patients with high CD45+ cell infiltration (Figure 30C). Thus, the data confirmed a possible mechanistic link between CD45+ cell infiltration and TGFB2 levels, as shown in mice (3.1.6.2).

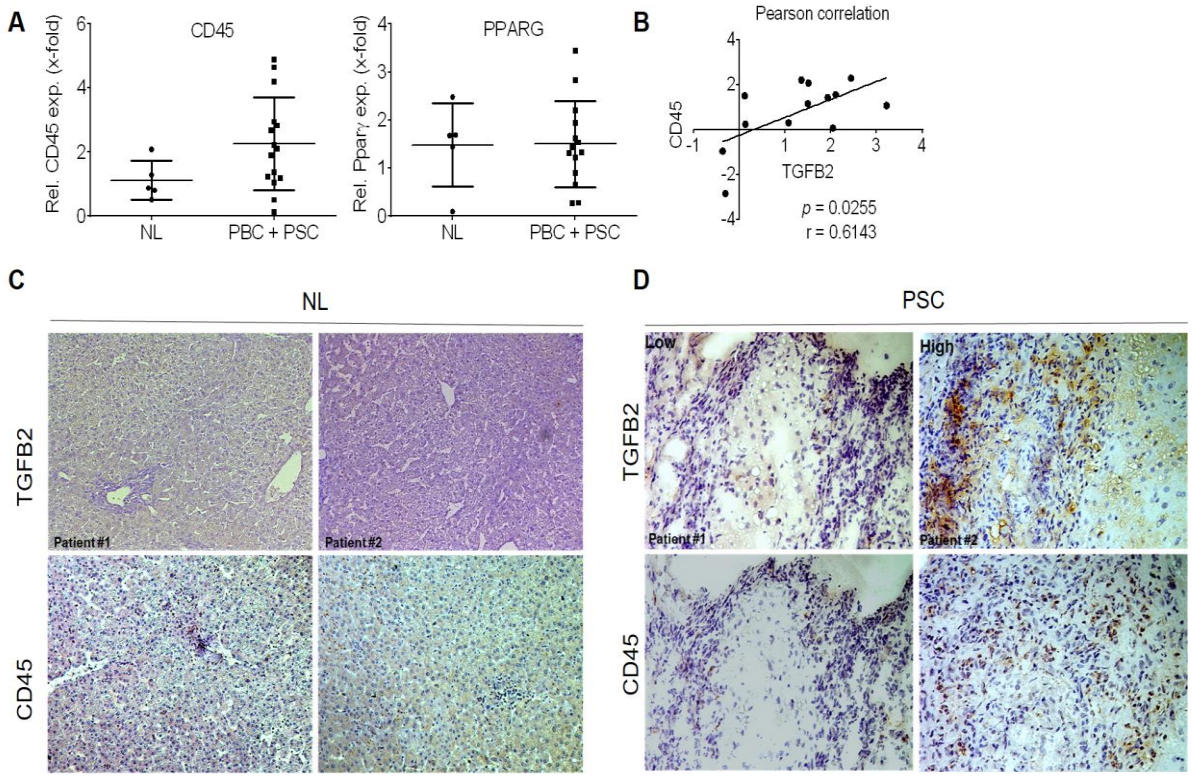

Figure 30 Analysis of two inflammation markers in the context of TGFB2 expression in PSC and PBC patients (Regensburg cohort). (A) Expression of CD45 and PPARG in PSC and PBC patients was determined. (B) CD45 expression levels correlated with TGFB2 expression levels of the same patients (pTGFB2/CD45=0.0255; rTGFB2/CD45 =0.61). (C) Immunohistochemical staining of TGF-β2 and CD45 in the liver tissue of PSC patients with low and high CD45 levels as well as healthy controls (NL).

3.1.8 Result summary

In summary, we found that TgfB2 and not, as formerly known, only TgfB1 is a key player in the onset, the progress, and the end stages of CLD. In a comparative analysis, we analyzed TgfB2 and TgfB1 expression and secretion in murine and human HSCs, hepatocytes, and HCC/hepatoblastoma cell lines. In various mouse models reflecting regeneration, acute and chronic liver disease, and human HCC sample cohorts, we demonstrated that both isoforms are expressed in different types of liver cells and that expression is elevated during the progression of CLD in mouse models in most cases. Although TgfB2 is mostly secreted at lower levels than TgfB1, its expression patterns largely follow similar profiles. However, the secretion of TgfB2 exceeded that of TgfB1 in some HCC cell lines. Our data indicates a more prominent implication of TgfB2 in biliary-derived liver disease models.

In this thesis, the anti-fibrotic and immunoregulatory effects of TgfB2 silencing in cholestatic MDR2-KO mice have been delineated for the first time. TgfB2 silencing by AONs specifically reduced collagen deposition and αSMA expression, but induced anti-fibrotic PparG expression. Accumulation of TGF-β2-specific AON was detected in macrophage-activated fibroblasts, LSEC, and activated HSCs in mice. This was in accordance with TgfB2 expression in these cell types. CD45-positive immune cell infiltration was reduced upon TGF-β2-specific AON treatment in the livers of MDR2-KO mice. Furthermore, in PSC and PBC patients, TGF-β2 levels were found to be elevated and correlated with CD45-positive immune cell infiltration.

4 Discussion

4.1 TGF-β1 and TGF-β2 co-existence in chronic liver diseases

The main findings of this study have been thouroughly discussed in the accompaying publication (Dropmann et al, Oncotarget 2016 [114]).

4.1.1 Expression in health and disease

TGF-β1 is known to be a prominent player in hepatocyte destruction, proliferation control [129] and hepatic stellate activation [130] inducing a complex process from fibrotic onset of liver disease including myofibroplast ,fibroblast activation and ECM deposition to inflammation and late stage CLD. In several cancers and diseases, TGF-β and members of its super family have been investigated with regard to their involvement and many aspects of their activity have been elucidated [59]. Interestingly, TGF-β isoforms share concordant but not redundant functions [32]. We thoroughly investigated the abundance of the TGF-β1 and TGF-β2 isoform in different liver cell types and damaged livers in different stages of disease.

Previous studies from Milani et al. [49] identified TGF-β2 occurance solely in bile duct cells along the portal tracts and liver lobular zone 1 in rat livers with ligated bile ducts and human fibrotic livers, but no expression in normal liver. Like De Bleser [50] and Bissell [48], we could confirm TGF-β2 isoform expression in Kupfer cells, LSEC and stellate cells in normal liver and in contrast to dated results from 20 years ago we additonally observed TGF-β2 expression in and secretion by hepatocytes. Recent detection methods are more sensitive and thus, low or weak signals can be detected. Being hepatocytes the most present cell type in liver, we examined TGF-β2 and TGF-β1 in both hepatocyte culture systems, CS (mimicking healthy liver tissue) and CM (mimicking diseased hepatocyte surroundings). It has been shown before by others, that significant mRNA increment of both isoforms in rat HCs and HSCs over time did not correspond to secretion levels of the cytokines suggesting an intracellular use of the newly synthesized TGF-β in the cells [131]. Our results in mouse hepatocytes confirmed these findings in both culture systems after 48h . We did not focus on cell type specific expression differences of TGF-β2 and TGF-β1 alone, but additionally investigated culture method-related behavior as well. Examinations in primary hepatic stellate cells revealed up to 10-fold higher TGF-β isoform amounts in the supernatants than in cell lysates after 8 days for both cytokines. TGF-β2 protein amounts increased from 2 days to 8 days in culture, while TGF-β1

proteins amounts reached a maximum in supernatants and cell lysates at day 2 already, indicating an intracellular cytokine specific maximum. Cytokines produced over these amounts are then continuously secreted into the supernatant as shown.

In the study described in this thesis , we could confirm previous data on TGF-β1 and its expression pattern at several stages of CLD disease in various models of liver disease including regeneration model as well as acute and chronic damage situations [48, 50]. Additionally, we we were able to significantly extent the knowledge of TGF-β2 in CLD and HCC. Previous studies have shown that TGF-β2 acts in a profibrogenic [39] and tumorigenic manner similar to TGF-β1. Participation of TGF-β2 as a profibrogenic factor could be demonstrated by Wang et al. [132] in liver and likewise in other organs when it was administered. Coadministration of TGF-β2 and CTGF, but not alone, led to profound tissue fibrosis in three murine mouse models. The effect was expressed as a fibrotic response in the abdominal cavity with parenchymal involvement. In renal fibrosis, TGF-β2 initiated EMT and induced fibrotic markers such as collagen and TGF-β1 in a renal cell line.

4.1.2 Signaling in health and disease

Canonical Smad signaling related to TGF-β2 expression was demonstrated when miR-200a treatment lead to decreased Smad3 activity and repressed TGF-β2 expression and TGF-β2 treatment to miR-200a expression reduction and enhanced Smad3 activity [133, 134]. Neutralisation of TGF-β2 using a monoclonal antibody (CAT-152) attenuated renal fibrosis and collagen deposition, further indicating its profibrogenic role [67]. First insights reflecting the impact of TGF-β2 in fibrogenic mechanisms were deduced from HCV patients. In these patients, TGF-β2 was strongly expressed in stage 3 and 4 of advanced fibrosis and correlated well with Smad2 expression [135]. With the information that the human hepatic stellate cell line LX-2 is responsive to TGF-β1 and activates the expression of typical fibrotic genes [97], we performed TGF-β isoform stimulation experiments in LX-2 cells to explore potential receptor expression changes. Although TGF-β1 is known to influence receptor expression [115], it did not alter the TGF-β receptor expression in LX-2. Interestingly, we could demonstrate that TGF-β2 stimulation remarkably induced TGF-β receptor expression after 24h. A major modulator of TGF-β signal transduction is Endoglin, which also facilitate cell's responsiveness to the TGF-β1 and TGF-β3 ligand. Our findings showed that Endoglin is significantly upregulated upon TGF-β2 stimulation in HSCs and raise the assumption that TGF-β2 may increase the HSC sensitivity to TGF-β1. Facilitated TGF-β1 binding to the receptor may more strongly induce TGF-β1-mediated stellate cell activation. We have found equal levels of Smad 1,2 and 3 after stimulation with both cytokines, but TGF-β2 pretreated LX-2 cells showed elevated Smad1 phosphorylation contrary to TGF-β1.

Finally, we could identify TGF-β2 to be differently than TGF-β1 regulated in regard to the Smad pathway. Mechanistic details of TGF-β modulation is rare so far. A study on glaucoma showed elevated TGF-β2 expression in specific Trabecular meshwork (TM) cells. Gremlin-induced TGF-β2 expression was found to modulate ECM metabolism in these cells and in tissue by increasing the expression of a variety of ECM proteins [36]. Modulation of TGF-β isoforms might be orchestrated by miR-29 members as miR-29 downregulation by TGF-β2 contributed to the induction of several ECM components as shown by Luna et al [41]. Further studies would be required to investigate the detailed mechanisms how TGF-β2 is embedded in the signaling and its consequences on gene regulation.

Whether TGF-β2 may contribute to non-Smad pathways was analyzed by different groups. Sun et al.have linked TGF-β2 to the Wnt signaling by miR-200a-mediated suppression of TGF-β2 and β-catenin in the context of experimentally induced hepatic fibrosis [136]. The Wnt/ TGF-β2 connection was also supported by findings of Biressi et al. [137] in dystrophic muscle cells. Tschaharganeh et al, as well as Dong investigated the interaction of TGF-β2 and YAP signaling. Here, YAP, as a mediator of the hippo signaling cascade, was upregulated in several cancers including liver cancer.Its modulation in transgenic mice and a liver cell line led the discovery of an universal size control mechanism in metazoa and was accompanied by strong TGF-β2 induction [138, 139].

An interdependence of the different TGF-β isoforms in the context of signaling and disease regulation was demonstrated by Oh et al. [140]. They demonstrated TGF-β3 upregulation upon suppression of TGF-β1 in human cancer cell lines, DU145 (human prostate adenocarcinoma) and A375 (human skin melanoma). Thus, both isoforms might be able to compensate for one another. They might also share some functions as TGF-β2 silencing induced downregulation of both,TGF-β1 and TGF-β3. This raises the possibilty of a common transcription factor that regulates TGF-β1 and TGF-β3 orchestrated by TGF-β2. Additional effects of specific TGF-β isoforms depletion in a given tissue type were observed by Horie et al [141]. In their study TGF-β1 and TGF-β2 showed diverse effects on target gene regulation on the behaviour of cancer cells and fibroblasts. TGF-β1-specific depletion in the context of HSC activation in vivo, still led to activation of HSCs. TGF-β2 and TGF-β3 isoforms did not compensate for the TGF-β1 deficiency [142]. Data from Shimada [143] et al. showed TGF-β1 treatment of HSCs affected the expression of TGF-β2 via Rho kinase, indicating as well that TGF-β isoforms affect one another.

4.1.3 Expression in liver regeneration (acute) and chronically induced liver damage

By defining TGF-β2 as a possible target in hepatic fibrosis and HCC, our study implies TGF-β2 involvement in processes of liver damage, regeneration and proliferation. We further identified an impact of TGF-β2 on Smad1 signaling as discussed above, nonetheless, we did not provide any mechanistical data for disease development and progression yet. In liver regeneration (acute) modeled by CCl_4 intoxification of mice, both isoforms showed similar behaviour during the regeneration process and were coincident with collagen expression. The dynamics of TGF-β1 expression during this process has been reported for a long time, but the comparison might show an analogous importance of TGF-β2. In chronic liver damage modeled by CCl_4 intoxification through repeated CCl_4 injections, synchronous dynamics were observed and suggest a congruent function of both isoforms.

4.1.4 Prominent TGF-β2 expression in biliary-derived liver damage

When investigating mouse models with biliary-derived liver damage, marked differences of both isoforms were demonstrated. TGF-β2 was considerably more induced in bile duct ligated MDR2-KO mouse livers of different ages/stages of liver disease progression. Similiary, continious TGF-β2 upregulation with advanced bile duct ligation time points was observed, accompanied by a parallel induction of fibrotic genes in a study from Abshagen et al.[144]. A link of TGF-β2 to mTOR signaling was drawn by Neef et al. [145] as TGF-β2 was downregulated in BDL after Rapamycin treatment. In contrast, TGF-β1 was not regulated in this study. Previously, Milani [49] described high TGF-β2 levels in proliferating bile ducts also emphazising a possibly role of the TGF-β2 isoform in biliary-derived liver damage. In array analyses from Shackel et al [146] including PBC patient samples, TGF-β2 was one prominently regulated gene in parallel with several other genes important for inflammation, fibrosis and proliferation. In contrast,a brief study including eight twins (E-MTAB-2347) with PBC and non-diseased siblings did not reveal TGF-β2 expression elevation in the diseased individuals.

4.1.5 Expression in cholangiocarcinoma and HCC

As a conseqence of steady liver damage, liver cancer development may occur. Intrahepatic cholangiocarcinoma (ICC) is described to be the second most common cause of liver cancer worldwide. As ICC is thought to derive from liver progenitor cells (LPC) and biliary epithial cells (BEC), there is a likelihood for deregulated TGF-β2. In line, Sulpice et al [56] analyzed 87 ICC patients and described elevated TGF-β2 expression in the stroma associated with bad survival, ICC classification, microvascular invasion, and the

presence of hilar lymph nodes. Fate tracing experiments in cholangiocarcinoma revealed that biliary cells are not the sole cell type of the disease origin as it, may also arise from differentiated hepatocytes [147]. Hepatocellular carcinoma (HCC) is thought to arise from hepatocytes .With this knowledge, we further investigated TGF-β2 expression in HCC cell lines, in an experimental HCC mouse model and in HCC patients in comparision to TGF-β1.

Our investigations on TGF-β1 expression in different HCC cell lines are in line with past studies [54, 115].Our study further showed that nearly all TGF-β1 high expressing cell lines also express high levels of TGF-β2 ($r = 0.811$; $p = 0.015$). Hep3B and HuH7 cell lines secreted remarkably more TGF-β2 than TGF-β1 implying TGF-β2-mediated tumorigenic characteristics. Involvement of TGF-β2 was also reported from Tschaharganeh et al [138] where it was downregulated in YAP-deficient HuH7 cells. Other tumorigenic features related to TGF-β2 were found in a head and neck squamous cell carcinoma model. In contrast to the effects of TGF-β1, TGF-β2 could initiate tumor cell dormancy through TGFβR-I, TGFβR-III and p38α/β induction in non-proliferative disseminated tumour cells (DTCs) of a head and neck squamous cell carcinoma (HNSCC) model. Further, TGF-β2 treatment of lymph node metastatic cells led to activation of pp38, pSmad2 and pSmad1/5 and CDK4 reduction [148]. Taken together, we and others confirm divergent and independent effects of both TGF-β isoforms in liver disease.

Our Oncomine®-based patient analyses confirmed abberant regulations of TGF-β1 and TGF-β2 in HCC and cirrhosis. In freely accessible HCC collectives, TGF-β2 upregulation was found in HCC in comparison to normal liver, while TGF-β1 was either not regulated or downregulated. Evaluation of the GSE1898 and GSE4024 data sets [149, 150], including array data of 121 HCC patients, revealed that patients with high TGF-β2 expression levels have poor survival outcome [114]. Since TGF-β2 was found highly expressed in tumor stroma by Sulpice et al. , and tumor surrounding tissue is often cirrhotically remodeled, we further investigated TGF-β2 levels in cirrhosis and precancerous stages using the datasets domiciled in Oncomine. Interestingly, we observed strong TGF-β2 expression in the transition state from normal to cirrhotic tissue. Further, TGF-β2 levels were elevated in the serum of cirrhosis patients. We also demonstrated that TGF-β2 expression in HCC patients was upregulated in comparision to normal liver tissue, while it was found to be downregulated when compared to surrounding tissue.

In our in vivo mouse model of HCC, specifically TGFα/cMyc mice, TGF-β2 expression was as well significantly affected in tumors compared to healthy liver. These specific expression changes of both isoforms seems to be context dependent and need to be taken into account for further investigations.

In summary, for the first time a direct comparision of TGF-β1 and TGF-β2 expression in the progression of liver diseases of different etiologies using cell lines, animal models and human patient samples was performed. Dependent on the origin of disease, similar (CCl_4 intoxification, expression in HCs and HSCs) and diverse regulation (MDR2-KO, BDL, human patients samples data arrays) dynamics of both isoforms were observed. Thus and in line with previous findings, our study demonstrated that TGF-β1 and TGF-β2 show equivalent, but also individual and separate functions in liver regeneration and CLD development . Thus, future studies should focus on delineating the effects and regulation of TGF-β2 signaling in liver diseases, taking into account etiologic and cell type-specific contexts.

4.2 TGF-β2 inhibition to target biliary derived liver diseases

Inhibition of TGF-β superfamily and its members has been investigated in various preclinical and clinical trials towards the treatment of liver diseases conditions ranging from fibrosis to cancer [59]. Although in some studies pan TGF-β approaches were applied that target all three isoforms, TGF-β2-directed tools focus on humanized antibodies or AONs mostly. TGF-β2 as a promising druggable target was observed in a study in which rabbits received subconjunctival injections of a TGF-β2 neutralizing antibody (CAT-152) post glaucoma surgery. CAT-152 significantly yielded in therapeutic benefit by reducing subconjunctival scarring and collagen deposition [151, 152]. This observation is line with our findings on amelioration of fibrosis upon targeting TGF-β2.

Based on our results discussed above and the finding that TGF-β2 is upregulated in PSC and PBC patients, we concluded that TGF-β2 might represent a promising new candidate to target biliary-derived liver disease. Accordingly, TGF-β2 was specifically silenced in early stage biliary disease of MDR2-KO mice by using an AON in order to diminish or reverse fibrogenesis.

AONs exert the ability to selectively target any disease causing gene and thus inhibit its translation to effective proteins. High specificity and easy application of AONs make them attractive agents for various disease target genes. Extensive therapeutic attempts have been made in in vivo animal studies and clinical trials using AONs in the last twenty years [153, 154]. Insufficient pharmacokinetic efficiency and poor cellular uptake were one of the major technical hurdles leading to further developement of next generation AONs. To optimize AONs and their biodistribution for (i.g. optimized cellular uptake, half life or binding affinity) modifications of their molecular backbone have been untertaken, thus making them to a more potent and effective therapeutic tool [155-157]. According to this state of the art requirements, we used modified AONs in our study. They were subsequently approved as being well-tolerated by the body system as examined by physiological and liver parameter in mice. Systemic application led to a selective

downregulation of TGF-β2 in the livers. The different AON uptake of wildtype and disease-activated liver cells in MDR2-KO but not in Balb/c mice might be associated with deregulation of chemokine receptors and some other genes induced by the control oligo application (placebo effect).

TGF-β2–targeting AONs were reported before in a study of malignant mesotheliomas in which in vivo and in vitro tumor growth reducing effects were reported [158]. These were in line with another cancer study that selectively targeted TGF-β2 by a specific AON in glioma tumor cells resulting in antitumor activity ex vivo [159], thus showing TGF-β2 as a drugable target. In the past, other TGF-β signaling components and fibrosis marker has been successfully targeted not only cancer stages but also in animal models for fibrotic diseases. For example, a Timp1 or Timp2-specific AON treatment reduced fibrogenesis in rats and in accordance with our data, there was a reduced collagen deposition. However, αSMA, a marker for stellate cell activation, was found not to be altered in treated compared to untreated animals [160, 161].The latter, is in contrast to our finding, showing significantly reduced αSMA levels in animals treated with TGF-β2 – targeting AON. Similarly, combinational treatment with TgfB1- and Ctgf-directed AONs reduced CCl_4-induced liver fibrosis as measured by reduced type I collagen expression [162].

Inhibition of a well-known endogenous regulatory molecule/ component of TGF-β signaling, Smad7, was utilized for the treatment of several diseases before. A result of high SMAD7 levels associated- colitis is defective TGF-β1 signaling. Colitis was successfully ameliorated and inflammation reduced in the acute phase after oral application of Smad7-directed AONs in murine models [163]. In a clinical study,in which Crohn´s disease patients received Mongersen, a Smad7-specific AON, higher remission rates and clinical response up to 72% were shown [164];(EudraCT number, 2011-002640-27. 2015) highlighting the successful usage of TgfB2-directed AON therapy.

In our study, we demonstrate that TgfB2 silencing attenuated liver fibrogenesis in MDR2-KO mice, which was accompanied by significant a reduction of CD45-positive cell infiltration and upregulation of the anti-inflammatory and anti-fibrogenic PparG. A relation between TGF-β2 and inflammation has been described in several organs and pathologies in previous studies, but not related to liver fibrosis so far. Co-stimulation of HUVEC cells with TGF-β2 and IL-1β resulted in EndMT (endothelial to mesenchymal transition) through activation of the inflammatory NFKB signaling as described by Maleszewska et al. [165]. In gastric cancer, HSC44PE-stimulated subperitoneal fibroblasts (SPFs) promoted differentiation of monocytes (THP1) into M2-like macrophages accompanied by increased expression levels of CSF1, CCL8, CXCL5, and TGFB2.This finding characterized specific fibroblasts that regulate the development of an inflammatory niche in gastric cell invasion [166]. In liver, our data suggested TGF-β2 as a pro-inflammatory component. In line, if silenced, we found a reduction of inflammatory cell infiltrates. Possibly this effect is followed by fibrosis

attenuation, although we did not analyze the existence or orientation of a causality so far. In contrast to our data, TGF-β2 suppressed LPS-induced macrophage inflammatory responses in the human intestine and appeared to have a protective role in the inflammatory injury [167]. In line with our data, Huber-Ruano et al [123] showed TgfB2 silencing effects in kidney, breast and lung tumor- derived cell lines. By usage of the same AON as used in this thesis, they revealed an inhibition of lung metastatis which might be due, at least in part, to CD68 expression induction in tumor associated macrophages (TAMs), thus influencing the inflammatory compartment. This is analogue to our data, demonstrating fibrotic and inflammatory rearrangements in MDR2-KO mice after TgfB2 depletion and hence possibly confirming regulatory function of TGF-β2 in this regard.

Whether TGF-β2 has a beneficial role on disease development or progression remains unclear and is most likely organ,cell type-specific and context-dependent. Mechanistic characterisation of TGF-β2 as a regulatory cytokine on fibrogenesis and inflammation in liver is still lacking. The data described in this thesis demonstrates a benefical health effect of TgfB2-silencing including downregulation of inflammatory cellular infiltrates leading to a reduction of inflammation-and (associated) fibrosis in cholestatitic mice. Furthermore, TGF-β2 might also be involved a modulator of the polarisation of liver-resident F4/80-positive macrophages to a non-inflammatory phenotype. TgfB2-silencing in the MDR2-KO biliary fibrosis mouse model, demonstrated a safety profile for AON application, good tolerability as well as antifibrotic effects.

In summary, the data presented, provides a strong rationale to examine anti-TgfB2-directed treatment in patients with cholestatic liver damage as applies to PSC or PBC. Unfortunately, no curative treatment for these rare but destructive diseases are available yet. In line with animal data, these patients exhibit high TGF-β2 levels associated with increased CD45 expression.

Overall, this thesis, points towards TGF-β2 as a promising therapeutic target in CLD especially of biliary origin. It further suggests the initiation of clinical trial studies on TGF-β2 inhibition in PSC and PBC patients.

5 Declaration of content

This thesis is the result of my independent investigation. Where my work is indebted to the work or ideas of others, for example from the literature or the internet, I have acknowledged this within the thesis. I am aware that a false declaration could have legal implications.

Date and signature

6 Publications

Dropmann A, Dediulia T, Breitkopf-Heinlein K, Korhonen H, Janicot M, Weber SN, Thomas M, Piiper A, Bertran E, Fabregat I, Abshagen K, Hess J, Angel P, Coulouarn C, Dooley S, Meindl-Beinker NM. „TGF-β1 and TGF-β2 abundance in liver diseases of mice and men". Oncotarget. 2016 Apr 12; 7(15):19499-518.

Anne Dropmann*, Steven Dooley*, Bedair Dewidar, Tatjana Dediulia, Julia Werle, Vanessa Hartwig, Stefanie Nittka, Hanna Korhonen, Michel Janicot, Katja Wosikowski, Albrecht Piiper, Timo Gaiser, John Brain, Dave Jones, Thomas S. Weiss, Timo Itzel, Ulrich M. Zanger, Matthias P. Ebert, Nadja M. Meindl-Beinker. "TGF-β2 silencing to target biliary derived liver diseases". Submitted to GUT (April 2018)

T Feng, J Dzieran, X Yuan, A Dropmann, T Maass, A Teufel, S Marhenke, T Gaiser, F Rückert, I Kleiter, S Kanzler, MP Ebert, A Vogel, P ten Dijke, S Dooley and NM Meindl-Beinker. "Hepatocyte-specific Smad7 deletion accelerates DEN-induced HCC via activation of STAT3 signaling in mice". Oncogenesis (2017) 6, e294; doi:10.1038/oncsis.2016.85

Seddik Hammad*, Elisabetta Cavalcanti, Julia Werle*, Maria Lucia Caruso*, Anne Dropmann, Antonia Ignazzi, Matthias Philip Ebert, Steven Dooley#, Gianluigi Giannelli#." Galunisertib modifies the liver fibrotic composition in the ABCB4-/- mouse model". Archives of Toxicology (2018), accepted, Epub, ahead of printing

7 Acknowledgments

First and foremost, I thank Professor Dr. Steven Dooley for giving me the opportunity to work in such an interesting and current field. Thank you for your guidance in my project and the various support.

I also thank PD Dr. Nadja Meindl-Beinker for her continuous support, fruitful and helpful discussions, and valuable advice regarding the design of experiments and experimental structures, in particular, but also outside of science. During the preparation of my thesis preparation, she gave me her fullest support.

I am giving my very sincere thanks to all members of Professor Dooley's laboratory who shared with me time and space and, beyond that, offered scientific support and funny discussions. I will never forget the time we spent together.

My thanks also go to those who volunteered to proofread my thesis.

I want to thank my family for their substantial support and refreshing diversions during my entire academic studies.

Last but not least, I want to express my deepest gratitude to my husband Christoph, who always gives me great support and encouragement in *dark* (scientific) times. Thank you, my dear!

8 List of Tables

9 List of Figures

10 References

1. Chen, X.P., et al., Long-term outcome of resection of large hepatocellular carcinoma. Br J Surg, 2006. 93(5): p. 600-6.
2. Matsuzaki, K., Modulation of TGF-beta signaling during progression of chronic liver diseases. Front Biosci (Landmark Ed), 2009. 14: p. 2923-34.
3. Morikawa, M., R. Derynck, and K. Miyazono, TGF-beta and the TGF-beta Family: Context-Dependent Roles in Cell and Tissue Physiology. Cold Spring Harb Perspect Biol, 2016. 8(5).
4. Anzano, M.A., et al., Sarcoma growth factor from conditioned medium of virally transformed cells is composed of both type alpha and type beta transforming growth factors. Proc Natl Acad Sci U S A, 1983. 80(20): p. 6264-8.
5. Derynck, R., R.J. Akhurst, and A. Balmain, TGF-beta signaling in tumor suppression and cancer progression. Nat Genet, 2001. 29(2): p. 117-29.
6. Gordon, K.J. and G.C. Blobe, Role of transforming growth factor-beta superfamily signaling pathways in human disease. Biochim Biophys Acta, 2008. 1782(4): p. 197-228.
7. Shi, M., et al., Latent TGF-beta structure and activation. Nature, 2011. 474(7351): p. 343-9.
8. Hyytiainen, M., C. Penttinen, and J. Keski-Oja, Latent TGF-beta binding proteins: extracellular matrix association and roles in TGF-beta activation. Crit Rev Clin Lab Sci, 2004. 41(3): p. 233-64.
9. Nishimura, S.L., Integrin-mediated transforming growth factor-beta activation, a potential therapeutic target in fibrogenic disorders. Am J Pathol, 2009. 175(4): p. 1362-70.
10. Daopin, S., et al., Crystal structure of transforming growth factor-beta 2: an unusual fold for the superfamily. Science, 1992. 257(5068): p. 369-73.
11. Marquardt, H., M.N. Lioubin, and T. Ikeda, Complete amino acid sequence of human transforming growth factor type beta 2. J Biol Chem, 1987. 262(25): p. 12127-31.
12. Massague, J., TGF-beta signal transduction. Annu Rev Biochem, 1998. 67: p. 753-91.
13. Schmierer, B. and C.S. Hill, TGFbeta-SMAD signal transduction: molecular specificity and functional flexibility. Nat Rev Mol Cell Biol, 2007. 8(12): p. 970-82.
14. Bierie, B. and H.L. Moses, Tumour microenvironment: TGFbeta: the molecular Jekyll and Hyde of cancer. Nat Rev Cancer, 2006. 6(7): p. 506-20.
15. Wrana, J.L., et al., TGF beta signals through a heteromeric protein kinase receptor complex. Cell, 1992. 71(6): p. 1003-14.
16. Huang, T., et al., TGF-beta signalling is mediated by two autonomously functioning TbetaRI:TbetaRII pairs. EMBO J, 2011. 30(7): p. 1263-76.
17. Shi, Y. and J. Massague, Mechanisms of TGF-beta signaling from cell membrane to the nucleus. Cell, 2003. 113(6): p. 685-700.
18. Zhang, Y.E., Non-Smad pathways in TGF-beta signaling. Cell Res, 2009. 19(1): p. 128-39.
19. Massague, J. and D. Wotton, Transcriptional control by the TGF-beta/Smad signaling system. EMBO J, 2000. 19(8): p. 1745-54.
20. Cheifetz, S., et al., The transforming growth factor-beta system, a complex pattern of cross-reactive ligands and receptors. Cell, 1987. 48(3): p. 409-15.
21. Cheifetz, S., et al., Distinct transforming growth factor-beta (TGF-beta) receptor subsets as determinants of cellular responsiveness to three TGF-beta isoforms. J Biol Chem, 1990. 265(33): p. 20533-8.
22. Ellingsworth, L., et al., Transforming growth factor beta 1 (TGF-beta 1) receptor expression on resting and mitogen-activated T cells. J Cell Biochem, 1989. 39(4): p. 489-500.

23. Segarini, P.R., D.M. Rosen, and S.M. Seyedin, Binding of transforming growth factor-beta to cell surface proteins varies with cell type. Mol Endocrinol, 1989. 3(2): p. 261-72.
24. Massague, J., et al., TGF-beta receptors. Mol Reprod Dev, 1992. 32(2): p. 99-104.
25. Cheifetz, S., et al., Endoglin is a component of the transforming growth factor-beta receptor system in human endothelial cells. J Biol Chem, 1992. 267(27): p. 19027-30.
26. Dickson, M.C., et al., Defective haematopoiesis and vasculogenesis in transforming growth factor-beta 1 knock out mice. Development, 1995. 121(6): p. 1845-54.
27. Shull, M.M., et al., Targeted disruption of the mouse transforming growth factor-beta 1 gene results in multifocal inflammatory disease. Nature, 1992. 359(6397): p. 693-9.
28. Kulkarni, A.B., et al., Transforming growth factor beta 1 null mutation in mice causes excessive inflammatory response and early death. Proc Natl Acad Sci U S A, 1993. 90(2): p. 770-4.
29. Williams, A.O., et al., The liver in transforming growth factor-Beta-1 (TGF-beta 1) null mutant mice. Ultrastruct Pathol, 1996. 20(5): p. 477-90.
30. Shek, F.W. and R.C. Benyon, How can transforming growth factor beta be targeted usefully to combat liver fibrosis? Eur J Gastroenterol Hepatol, 2004. 16(2): p. 123-6.
31. Akhurst, R.J. and R. Derynck, TGF-beta signaling in cancer--a double-edged sword. Trends Cell Biol, 2001. 11(11): p. S44-51.
32. Bierie, B. and H.L. Moses, TGF-beta and cancer. Cytokine Growth Factor Rev, 2006. 17(1-2): p. 29-40.
33. Levy, L. and C.S. Hill, Alterations in components of the TGF-beta superfamily signaling pathways in human cancer. Cytokine Growth Factor Rev, 2006. 17(1-2): p. 41-58.
34. Sanford, L.P., et al., TGFbeta2 knockout mice have multiple developmental defects that are non-overlapping with other TGFbeta knockout phenotypes. Development, 1997. 124(13): p. 2659-70.
35. Dunker, N. and K. Krieglstein, Tgfbeta2 -/- Tgfbeta3 -/- double knockout mice display severe midline fusion defects and early embryonic lethality. Anat Embryol (Berl), 2002. 206(1-2): p. 73-83.
36. Sethi, A., et al., Role of TGFbeta/Smad signaling in gremlin induction of human trabecular meshwork extracellular matrix proteins. Invest Ophthalmol Vis Sci, 2011. 52(8): p. 5251-9.
37. Wick, W., M. Platten, and M. Weller, Glioma cell invasion: regulation of metalloproteinase activity by TGF-beta. J Neurooncol, 2001. 53(2): p. 177-85.
38. Serini, G. and G. Gabbiana, Modulation of alpha-smooth muscle actin expression in fibroblasts by transforming growth factor-beta isoforms: an in vivo and in vitro study. Wound Repair Regen, 1996. 4(2): p. 278-87.
39. Coker, R.K., et al., Transforming growth factors-beta 1, -beta 2, and -beta 3 stimulate fibroblast procollagen production in vitro but are differentially expressed during bleomycin-induced lung fibrosis. Am J Pathol, 1997. 150(3): p. 981-91.
40. Deshiere, A., et al., Regulation of epithelial to mesenchymal transition: CK2beta on stage. Mol Cell Biochem, 2011. 356(1-2): p. 11-20.
41. Luna, C., et al., Cross-talk between miR-29 and transforming growth factor-betas in trabecular meshwork cells. Invest Ophthalmol Vis Sci, 2011. 52(6): p. 3567-72.
42. de Martin, R., et al., Complementary DNA for human glioblastoma-derived T cell suppressor factor, a novel member of the transforming growth factor-beta gene family. EMBO J, 1987. 6(12): p. 3673-7.
43. Vanky, F., et al., Human ex vivo carcinoma cells produce transforming growth factor beta and thereby can inhibit lymphocyte functions in vitro. Cancer Immunol Immunother, 1997. 43(6): p. 317-23.
44. Hau, P., et al., TGF-beta2 signaling in high-grade gliomas. Curr Pharm Biotechnol, 2011. 12(12): p. 2150-7.
45. Hinz, S., et al., Foxp3 expression in pancreatic carcinoma cells as a novel mechanism of immune evasion in cancer. Cancer Res, 2007. 67(17): p. 8344-50.
46. Kaartinen, V., et al., Abnormal lung development and cleft palate in mice lacking TGF-beta 3 indicates defects of epithelial-mesenchymal interaction. Nat Genet, 1995. 11(4): p. 415-21.
47. Dooley, S. and P. ten Dijke, TGF-beta in progression of liver disease. Cell Tissue Res, 2012. 347(1): p. 245-56.

48. Bissell, D.M., et al., Cell-specific expression of transforming growth factor-beta in rat liver. Evidence for autocrine regulation of hepatocyte proliferation. J Clin Invest, 1995. 96(1): p. 447-55.
49. Milani, S., et al., Transforming growth factors beta 1 and beta 2 are differentially expressed in fibrotic liver disease. Am J Pathol, 1991. 139(6): p. 1221-9.
50. De Bleser, P.J., et al., Transforming growth factor-beta gene expression in normal and fibrotic rat liver. J Hepatol, 1997. 26(4): p. 886-93.
51. Roth, S., K. Michel, and A.M. Gressner, (Latent) transforming growth factor beta in liver parenchymal cells, its injury-dependent release, and paracrine effects on rat hepatic stellate cells. Hepatology, 1998. 27(4): p. 1003-12.
52. Hernandez-Gea, V., et al., Role of the microenvironment in the pathogenesis and treatment of hepatocellular carcinoma. Gastroenterology, 2013. 144(3): p. 512-27.
53. Baer, H.U., et al., Transforming growth factor betas and their receptors in human liver cirrhosis. Eur J Gastroenterol Hepatol, 1998. 10(12): p. 1031-9.
54. Coulouarn, C., V.M. Factor, and S.S. Thorgeirsson, Transforming growth factor-beta gene expression signature in mouse hepatocytes predicts clinical outcome in human cancer. Hepatology, 2008. 47(6): p. 2059-67.
55. Coulouarn, C., et al., Combined hepatocellular-cholangiocarcinomas exhibit progenitor features and activation of Wnt and TGFbeta signaling pathways. Carcinogenesis, 2012. 33(9): p. 1791-6.
56. Sulpice, L., et al., Molecular profiling of stroma identifies osteopontin as an independent predictor of poor prognosis in intrahepatic cholangiocarcinoma. Hepatology, 2013. 58(6): p. 1992-2000.
57. Lee, K.T. and T.S. Liu, Expression of transforming growth factor betas and their signaling receptors in stone-containing intrahepatic bile ducts and cholangiocarcinoma. World J Surg, 2003. 27(10): p. 1143-8.
58. Hawinkels, L.J. and P. Ten Dijke, Exploring anti-TGF-beta therapies in cancer and fibrosis. Growth Factors, 2011. 29(4): p. 140-52.
59. Akhurst, R.J. and A. Hata, Targeting the TGFbeta signalling pathway in disease. Nat Rev Drug Discov, 2012. 11(10): p. 790-811.
60. Nakamura, T., et al., Inhibition of transforming growth factor beta prevents progression of liver fibrosis and enhances hepatocyte regeneration in dimethylnitrosamine-treated rats. Hepatology, 2000. 32(2): p. 247-55.
61. Qi, Z., et al., Blockade of type beta transforming growth factor signaling prevents liver fibrosis and dysfunction in the rat. Proc Natl Acad Sci U S A, 1999. 96(5): p. 2345-9.
62. Ueno, H., et al., A soluble transforming growth factor beta receptor expressed in muscle prevents liver fibrogenesis and dysfunction in rats. Hum Gene Ther, 2000. 11(1): p. 33-42.
63. Yata, Y., et al., Dose-dependent inhibition of hepatic fibrosis in mice by a TGF-beta soluble receptor: implications for antifibrotic therapy. Hepatology, 2002. 35(5): p. 1022-30.
64. Hammad, S., et al., Galunisertib modifies the liver fibrotic composition in the ABCB4-/- mouse model. Archives of Toxicology, 2018.
65. Spreafico, A., et al., A first-in-human phase I, dose-escalation, multicentre study of HSP990 administered orally in adult patients with advanced solid malignancies. Br J Cancer, 2015. 112(4): p. 650-9.
66. Denton, C.P. and D.J. Abraham, Transgenic analysis of scleroderma: understanding key pathogenic events in vivo. Autoimmun Rev, 2004. 3(4): p. 285-93.
67. Hill, C., et al., Transforming growth factor-beta2 antibody attenuates fibrosis in the experimental diabetic rat kidney. J Endocrinol, 2001. 170(3): p. 647-51.
68. Group, C.A.T.T.S., et al., Factors affecting the outcome of trabeculectomy: an analysis based on combined data from two phase III studies of an antibody to transforming growth factor beta2, CAT-152. Ophthalmology, 2007. 114(10): p. 1831-8.
69. Bogdahn, U., et al., Targeted therapy for high-grade glioma with the TGF-beta2 inhibitor trabedersen: results of a randomized and controlled phase IIb study. Neuro Oncol, 2011. 13(1): p. 132-42.

70. Schlingensiepen, K.H., et al., Transforming growth factor-beta 2 gene silencing with trabedersen (AP 12009) in pancreatic cancer. Cancer Sci, 2011. 102(6): p. 1193-200.
71. Schlingensiepen, K.H., et al., Antisense therapeutics for tumor treatment: the TGF-beta2 inhibitor AP 12009 in clinical development against malignant tumors. Recent Results Cancer Res, 2008. 177: p. 137-50.
72. Giaccone, G., et al., A phase III study of belagenpumatucel-L, an allogeneic tumour cell vaccine, as maintenance therapy for non-small cell lung cancer. Eur J Cancer, 2015. 51(16): p. 2321-9.
73. Nemunaitis, J., et al., Phase II study of belagenpumatucel-L, a transforming growth factor beta-2 antisense gene-modified allogeneic tumor cell vaccine in non-small-cell lung cancer. J Clin Oncol, 2006. 24(29): p. 4721-30.
74. Nemunaitis, J., et al., Phase II trial of Belagenpumatucel-L, a TGF-beta2 antisense gene modified allogeneic tumor vaccine in advanced non small cell lung cancer (NSCLC) patients. Cancer Gene Ther, 2009. 16(8): p. 620-4.
75. de Vries, E. and U. Beuers, Management of cholestatic disease in 2017. Liver Int, 2017. 37 Suppl 1: p. 123-129.
76. Liberal, R. and C.R. Grant, Cirrhosis and autoimmune liver disease: Current understanding. World J Hepatol, 2016. 8(28): p. 1157-1168.
77. Jepsen, P., L. Gronbaek, and H. Vilstrup, Worldwide Incidence of Autoimmune Liver Disease. Dig Dis, 2015. 33 Suppl 2: p. 2-12.
78. Beuers, U., et al., Changing Nomenclature for PBC: From 'Cirrhosis' to 'Cholangitis'. Am J Gastroenterol, 2015. 110(11): p. 1536-8.
79. Pinzani, M. and T.V. Luong, Pathogenesis of biliary fibrosis. Biochim Biophys Acta, 2018. 1864(4 Pt B): p. 1279-1283.
80. Invernizzi, P., A. Lleo, and M. Podda, Interpreting serological tests in diagnosing autoimmune liver diseases. Semin Liver Dis, 2007. 27(2): p. 161-72.
81. Lazaridis, K.N. and N.F. LaRusso, Primary Sclerosing Cholangitis. N Engl J Med, 2016. 375(12): p. 1161-70.
82. Lammers, W.J., et al., Development and Validation of a Scoring System to Predict Outcomes of Patients With Primary Biliary Cirrhosis Receiving Ursodeoxycholic Acid Therapy. Gastroenterology, 2015. 149(7): p. 1804-1812 e4.
83. Lindor, K.D., et al., High-dose ursodeoxycholic acid for the treatment of primary sclerosing cholangitis. Hepatology, 2009. 50(3): p. 808-14.
84. Hofmann, A.F., et al., Novel biotransformation and physiological properties of norursodeoxycholic acid in humans. Hepatology, 2005. 42(6): p. 1391-8.
85. Denk, G.U., et al., Conjugation is essential for the anticholestatic effect of NorUrsodeoxycholic acid in taurolithocholic acid-induced cholestasis in rat liver. Hepatology, 2010. 52(5): p. 1758-68.
86. Voumvouraki, A., et al., Increased TauGF-beta3 in primary biliary cirrhosis: an abnormality related to pathogenesis? World J Gastroenterol, 2010. 16(40): p. 5057-64.
87. Nakken, K.E., et al., Gene expression profiles reflect sclerosing cholangitis activity in abcb4 (-/-) mice. Scand J Gastroenterol, 2009. 44(2): p. 211-8.
88. Mauad, T.H., et al., Mice with homozygous disruption of the mdr2 P-glycoprotein gene. A novel animal model for studies of nonsuppurative inflammatory cholangitis and hepatocarcinogenesis. Am J Pathol, 1994. 145(5): p. 1237-45.
89. Ikenaga, N., et al., A new Mdr2(-/-) mouse model of sclerosing cholangitis with rapid fibrosis progression, early-onset portal hypertension, and liver cancer. Am J Pathol, 2015. 185(2): p. 325-34.
90. Fickert, P., et al., 24-norUrsodeoxycholic acid is superior to ursodeoxycholic acid in the treatment of sclerosing cholangitis in Mdr2 (Abcb4) knockout mice. Gastroenterology, 2006. 130(2): p. 465-81.
91. Tokiwa, T., I. Doi, and J. Sato, Preparation of single cell suspensions from hepatoma cells in culture. Acta Med Okayama, 1975. 29(2): p. 147-50.
92. Nakabayashi, H., et al., Growth of human hepatoma cells lines with differentiated functions in chemically defined medium. Cancer Res, 1982. 42(9): p. 3858-63.

93. Knowles, B.B., C.C. Howe, and D.P. Aden, Human hepatocellular carcinoma cell lines secrete the major plasma proteins and hepatitis B surface antigen. Science, 1980. 209(4455): p. 497-9.
94. Aden, D.P., et al., Controlled synthesis of HBsAg in a differentiated human liver carcinoma-derived cell line. Nature, 1979. 282(5739): p. 615-6.
95. Hasumura, S., et al., [Establishment and characterization of a human hepatocellular carcinoma cell line JHH-4]. Hum Cell, 1988. 1(1): p. 98-100.
96. Alexander, J.J., et al., Establishment of a continuously growing cell line from primary carcinoma of the liver. S Afr Med J, 1976. 50(54): p. 2124-8.
97. Xu, L., et al., Human hepatic stellate cell lines, LX-1 and LX-2: new tools for analysis of hepatic fibrosis. Gut, 2005. 54(1): p. 142-51.
98. Hengstler, J.G., et al., Cryopreserved primary hepatocytes as a constantly available in vitro model for the evaluation of human and animal drug metabolism and enzyme induction. Drug Metab Rev, 2000. 32(1): p. 81-118.
99. Bissell, D.M., Primary hepatocyte culture: substratum requirements and production of matrix components. Fed Proc, 1981. 40(10): p. 2469-73.
100. Wiercinska, E., et al., Id1 is a critical mediator in TGF-beta-induced transdifferentiation of rat hepatic stellate cells. Hepatology, 2006. 43(5): p. 1032-41.
101. Ossipow, V., U.K. Laemmli, and U. Schibler, A simple method to renature DNA-binding proteins separated by SDS-polyacrylamide gel electrophoresis. Nucleic Acids Res, 1993. 21(25): p. 6040-1.
102. Chomczynski, P. and N. Sacchi, Single-step method of RNA isolation by acid guanidinium thiocyanate-phenol-chloroform extraction. Anal Biochem, 1987. 162(1): p. 156-9.
103. Livak, K.J. and T.D. Schmittgen, Analysis of relative gene expression data using real-time quantitative PCR and the 2(-Delta Delta C(T)) Method. Methods, 2001. 25(4): p. 402-8.
104. Smith, R.D., et al., Value of noninvasive hemodynamics to achieve blood pressure control in hypertensive subjects. Hypertension, 2006. 47(4): p. 771-7.
105. Puchtler, H., F.S. Waldrop, and L.S. Valentine, Polarization microscopic studies of connective tissue stained with picro-sirius red FBA. Beitr Pathol, 1973. 150(2): p. 174-87.
106. Junqueira, L.C., G. Bignolas, and R.R. Brentani, Picrosirius staining plus polarization microscopy, a specific method for collagen detection in tissue sections. Histochem J, 1979. 11(4): p. 447-55.
107. Jamall, I.S., V.N. Finelli, and S.S. Que Hee, A simple method to determine nanogram levels of 4-hydroxyproline in biological tissues. Anal Biochem, 1981. 112(1): p. 70-5.
108. Boigk, G., et al., Silymarin retards collagen accumulation in early and advanced biliary fibrosis secondary to complete bile duct obliteration in rats. Hepatology, 1997. 26(3): p. 643-9.
109. Sigal, M., et al., Darbepoetin-alpha inhibits the perpetuation of necro-inflammation and delays the progression of cholestatic fibrosis in mice. Lab Invest, 2010. 90(10): p. 1447-56.
110. Abshagen, K., et al., Foxf1 siRNA delivery to hepatic stellate cells by DBTC lipoplex formulations ameliorates fibrosis in livers of bile duct ligated mice. Curr Gene Ther, 2015. 15(3): p. 215-27.
111. Murakami, H., et al., Transgenic mouse model for synergistic effects of nuclear oncogenes and growth factors in tumorigenesis: interaction of c-myc and transforming growth factor alpha in hepatic oncogenesis. Cancer Res, 1993. 53(8): p. 1719-23.
112. Haupenthal, J., et al., Reduced efficacy of the Plk1 inhibitor BI 2536 on the progression of hepatocellular carcinoma due to low intratumoral drug levels. Neoplasia, 2012. 14(5): p. 410-9.
113. Reid, L.M. and D.M. Jefferson, Culturing hepatocytes and other differentiated cells. Hepatology, 1984. 4(3): p. 548-59.
114. Dropmann, A., et al., TGF-beta1 and TGF-beta2 abundance in liver diseases of mice and men. Oncotarget, 2016. 7(15): p. 19499-518.
115. Dzieran, J., et al., Comparative Analysis of TGF-beta/Smad Signaling Dependent Cytostasis in Human Hepatocellular Carcinoma Cell Lines. PLoS One, 2013. 8(8): p. e72252.

116. Mas, V.R., et al., Genes involved in viral carcinogenesis and tumor initiation in hepatitis C virus-induced hepatocellular carcinoma. Mol Med, 2009. 15(3-4): p. 85-94.
117. Wurmbach, E., et al., Genome-wide molecular profiles of HCV-induced dysplasia and hepatocellular carcinoma. Hepatology, 2007. 45(4): p. 938-47.
118. Chiang, D.Y., et al., Focal gains of VEGFA and molecular classification of hepatocellular carcinoma. Cancer Res, 2008. 68(16): p. 6779-88.
119. Archer, K.J., et al., Identifying genes for establishing a multigenic test for hepatocellular carcinoma surveillance in hepatitis C virus-positive cirrhotic patients. Cancer Epidemiol Biomarkers Prev, 2009. 18(11): p. 2929-32.
120. Chen, X., et al., Gene expression patterns in human liver cancers. Mol Biol Cell, 2002. 13(6): p. 1929-39.
121. Guichard, C., et al., Integrated analysis of somatic mutations and focal copy-number changes identifies key genes and pathways in hepatocellular carcinoma. Nat Genet, 2012. 44(6): p. 694-8.
122. Roessler, S., et al., A unique metastasis gene signature enables prediction of tumor relapse in early-stage hepatocellular carcinoma patients. Cancer Res, 2010. 70(24): p. 10202-12.
123. Huber-Ruano, I., et al., An antisense oligonucleotide targeting TGF-beta2 inhibits lung metastasis and induces CD86 expression in tumor-associated macrophages. Ann Oncol, 2017. 28(9): p. 2278-2285.
124. Fickert, P., et al., Regurgitation of bile acids from leaky bile ducts causes sclerosing cholangitis in Mdr2 (Abcb4) knockout mice. Gastroenterology, 2004. 127(1): p. 261-74.
125. Pascual, G., et al., A SUMOylation-dependent pathway mediates transrepression of inflammatory response genes by PPAR-gamma. Nature, 2005. 437(7059): p. 759-63.
126. Martin, H., Role of PPAR-gamma in inflammation. Prospects for therapeutic intervention by food components. Mutat Res, 2009. 669(1-2): p. 1-7.
127. Kaplan, M.M. and M.E. Gershwin, Primary biliary cirrhosis. N Engl J Med, 2005. 353(12): p. 1261-73.
128. Molodecky, N.A., et al., Increasing incidence and prevalence of the inflammatory bowel diseases with time, based on systematic review. Gastroenterology, 2012. 142(1): p. 46-54 e42; quiz e30.
129. Michalopoulos, G.K., Liver regeneration. J Cell Physiol, 2007. 213(2): p. 286-300.
130. Friedman, S.L., Mechanisms of hepatic fibrogenesis. Gastroenterology, 2008. 134(6): p. 1655-69.
131. Roth-Eichhorn, S., K. Kuhl, and A.M. Gressner, Subcellular localization of (latent) transforming growth factor beta and the latent TGF-beta binding protein in rat hepatocytes and hepatic stellate cells. Hepatology, 1998. 28(6): p. 1588-96.
132. Wang, Q., et al., Cooperative interaction of CTGF and TGF-beta in animal models of fibrotic disease. Fibrogenesis Tissue Repair, 2011. 4(1): p. 4.
133. Wang, B., et al., miR-200a Prevents renal fibrogenesis through repression of TGF-beta2 expression. Diabetes, 2011. 60(1): p. 280-7.
134. Lu, R., et al., Tumor suppressive microRNA-200a inhibits renal cell carcinoma development by directly targeting TGFB2. Tumour Biol, 2015. 36(9): p. 6691-700.
135. Shirasaki, T., et al., Impaired interferon signaling in chronic hepatitis C patients with advanced fibrosis via the transforming growth factor beta signaling pathway. Hepatology, 2014. 60(5): p. 1519-30.
136. Sun, X., et al., Participation of miR-200a in TGF-beta1-mediated hepatic stellate cell activation. Mol Cell Biochem, 2014. 388(1-2): p. 11-23.
137. Biressi, S., et al., A Wnt-TGFbeta2 axis induces a fibrogenic program in muscle stem cells from dystrophic mice. Sci Transl Med, 2014. 6(267): p. 267ra176.
138. Tschaharganeh, D.F., et al., Yes-associated protein up-regulates Jagged-1 and activates the Notch pathway in human hepatocellular carcinoma. Gastroenterology, 2013. 144(7): p. 1530-1542 e12.
139. Dong, J., et al., Elucidation of a universal size-control mechanism in Drosophila and mammals. Cell, 2007. 130(6): p. 1120-33.
140. Oh, S., et al., Transforming growth factor-beta gene silencing using adenovirus expressing TGF-beta1 or TGF-beta2 shRNA. Cancer Gene Ther, 2013. 20(2): p. 94-100.

141. Horie, M., et al., Differential knockdown of TGF-beta ligands in a three-dimensional co-culture tumor-stromal interaction model of lung cancer. BMC Cancer, 2014. 14: p. 580.
142. Hellerbrand, C., et al., The role of TGFbeta1 in initiating hepatic stellate cell activation in vivo. J Hepatol, 1999. 30(1): p. 77-87.
143. Shimada, H., N.R. Staten, and L.E. Rajagopalan, TGF-beta1 mediated activation of Rho kinase induces TGF-beta2 and endothelin-1 expression in human hepatic stellate cells. J Hepatol, 2011. 54(3): p. 521-8.
144. Abshagen, K., et al., Pathobiochemical signatures of cholestatic liver disease in bile duct ligated mice. BMC Syst Biol, 2015. 9: p. 83.
145. Neef, M., et al., Low-dose oral rapamycin treatment reduces fibrogenesis, improves liver function, and prolongs survival in rats with established liver cirrhosis. J Hepatol, 2006. 45(6): p. 786-96.
146. Shackel, N.A., et al., Identification of novel molecules and pathogenic pathways in primary biliary cirrhosis: cDNA array analysis of intrahepatic differential gene expression. Gut, 2001. 49(4): p. 565-76.
147. Fan, B., et al., Cholangiocarcinomas can originate from hepatocytes in mice. J Clin Invest, 2012. 122(8): p. 2911-5.
148. Bragado, P., et al., TGF-beta2 dictates disseminated tumour cell fate in target organs through TGF-beta-RIII and p38alpha/beta signalling. Nat Cell Biol, 2013. 15(11): p. 1351-61.
149. Lee, J.S., et al., Application of comparative functional genomics to identify best-fit mouse models to study human cancer. Nat Genet, 2004. 36(12): p. 1306-11.
150. Lee, J.S., et al., A novel prognostic subtype of human hepatocellular carcinoma derived from hepatic progenitor cells. Nat Med, 2006. 12(4): p. 410-6.
151. Mead, A.L., et al., Evaluation of anti-TGF-beta2 antibody as a new postoperative anti-scarring agent in glaucoma surgery. Invest Ophthalmol Vis Sci, 2003. 44(8): p. 3394-401.
152. Group, C.A.T.T.S., et al., A phase III study of subconjunctival human anti-transforming growth factor beta(2) monoclonal antibody (CAT-152) to prevent scarring after first-time trabeculectomy. Ophthalmology, 2007. 114(10): p. 1822-30.
153. Agrawal, S., Antisense oligonucleotides: towards clinical trials. Trends Biotechnol, 1996. 14(10): p. 376-87.
154. Sharma, H.W. and R. Narayanan, The therapeutic potential of antisense oligonucleotides. Bioessays, 1995. 17(12): p. 1055-63.
155. Akhtar, S. and S. Agrawal, In vivo studies with antisense oligonucleotides. Trends Pharmacol Sci, 1997. 18(1): p. 12-8.
156. Fluiter, K., et al., In vivo tumor growth inhibition and biodistribution studies of locked nucleic acid (LNA) antisense oligonucleotides. Nucleic Acids Res, 2003. 31(3): p. 953-62.
157. Lorenzer, C., et al., Going beyond the liver: progress and challenges of targeted delivery of siRNA therapeutics. J Control Release, 2015. 203: p. 1-15.
158. Marzo, A.L., et al., Antisense oligonucleotides specific for transforming growth factor beta2 inhibit the growth of malignant mesothelioma both in vitro and in vivo. Cancer Res, 1997. 57(15): p. 3200-7.
159. Vallieres, L., Trabedersen, a TGFbeta2-specific antisense oligonucleotide for the treatment of malignant gliomas and other tumors overexpressing TGFbeta2. IDrugs, 2009. 12(7): p. 445-53.
160. Nie, Q.H., et al., Inhibiting effect of antisense oligonucleotides phosphorthioate on gene expression of TIMP-1 in rat liver fibrosis. World J Gastroenterol, 2001. 7(3): p. 363-9.
161. Nie, Q.H., et al., Inhibitory effect of antisense oligonucleotide targeting TIMP-2 on immune-induced liver fibrosis. Dig Dis Sci, 2010. 55(5): p. 1286-95.
162. Uchio, K., et al., Down-regulation of connective tissue growth factor and type I collagen mRNA expression by connective tissue growth factor antisense oligonucleotide during experimental liver fibrosis. Wound Repair Regen, 2004. 12(1): p. 60-6.
163. Boirivant, M., et al., Inhibition of Smad7 with a specific antisense oligonucleotide facilitates TGF-beta1-mediated suppression of colitis. Gastroenterology, 2006. 131(6): p. 1786-98.

164. Monteleone, G., et al., Mongersen, an oral SMAD7 antisense oligonucleotide, and Crohn's disease. N Engl J Med, 2015. 372(12): p. 1104-13.
165. Maleszewska, M., et al., IL-1beta and TGFbeta2 synergistically induce endothelial to mesenchymal transition in an NFkappaB-dependent manner. Immunobiology, 2013. 218(4): p. 443-54.
166. Abe, A., et al., Site-specific fibroblasts regulate site-specific inflammatory niche formation in gastric cancer. Gastric Cancer, 2017. 20(1): p. 92-103.
167. Maheshwari, A., et al., TGF-beta2 suppresses macrophage cytokine production and mucosal inflammatory responses in the developing intestine. Gastroenterology, 2011. 140(1): p. 242-53.